Application of bulk nanobubbles in ultrafiltration and spray drying of dairy concentrates

by

Karthik Sajith Babu

B.Tech., National Institute of Food Technology, Entrepreneurship and Management - Thanjavur, 2015
M.S., Kansas State University, 2018

AN ABSTRACT OF A DISSERTATION

submitted in partial fulfillment of the requirements for the degree

DOCTOR OF PHILOSOPHY

Food Science

KANSAS STATE UNIVERSITY
Manhattan, Kansas

2022

Abstract

Milk protein concentrates (MPC) are ideal dairy ingredient to provide nutritional and functional benefits in high-protein dairy and food products. However, one of the key challenges encountered by the MPC manufacturers during the spray drying is the high viscosity after ultrafiltration and evaporation. Reducing viscosity and aiding an increase in the solid levels before spray drying can offer significant savings on the overall energy cost during spray drying. On the other side, it is also a challenge for the end-user to incorporate the MPC powders in a formulation due to their poor rehydration properties. Therefore, simple and innovative strategies to reduce viscosity before spray drying while also improving final powder properties are of critical consideration for the dairy industry. Moreover, the dairy industry's eco-efficiency strategy focuses on manufacturing high-quality dairy products at a low cost with minimal environmental impact are gaining more attention. For instance, reduced energy usage while keeping high permeation flux values is critical for eco-efficiency. In this research, application of bulk nanobubbles (NBs) for improving the processability and functionality of various dairy concentrates were evaluated.

The chapter 3, 4, and 5 investigated the use of NBs generated by hydrodynamic and acoustic cavitation for improving the processability of dairy concentrates, rehydration/flow properties of MPCs. Control and NB-MPC dispersions were evaluated in terms of rheological behavior and microstructure. Additionally, MPC dispersions were spray dried after the NB treatment and the resultant NB-MPC powders were characterized and compared with the control MPCs in terms of rehydration characteristics and microstructure. NB-MPC powders exhibited better rehydration properties than the control MPC powders. Overall, these studies therefore,

recommends the possibility of using NB treatment for more efficient drying while improving the functional properties of the resultant MPC powders.

The chapter 6 evaluated the influence of NB incorporation during the UF process of skim milk. Both lab and pilot-scale UF experiments were conducted to evaluate the effect of NB incorporation on UF process by evaluating permeate flux, membrane microstructure, fouling resistance, energy consumption, and skim milk concentrate characteristics. For both the lab/pilot-scale runs, after the initial water flux measurements, the membrane was fouled with the skim milk concentrate dispersions operated at 20°C under a constant transmembrane pressure 30 psi in constant concentration mode (the permeate was returned to the feed tank at regular 10-min intervals) and the total run time was fixed for 1 hour. The results revealed that NB treatment had a significant effect on permeate flux in both the lab and pilot-scale runs. Overall, the NB treatment helped to improve UF membrane performance and therefore this study suggests the potential of using NB treatment for a more efficient UF processing.

Application of bulk nanobubbles in ultrafiltration and spray drying of dairy concentrates

by

Karthik Sajith Babu

B.Tech., National Institute of Food Technology, Entrepreneurship and Management - Thanjavur, 2015
M.S., Kansas State University, 2018

A DISSERTATION

submitted in partial fulfillment of the requirements for the degree

DOCTOR OF PHILOSOPHY

Food Science

KANSAS STATE UNIVERSITY
Manhattan, Kansas

2022

Approved by:

Major Professor
Jayendra K. Amamcharla

Copyright

Abstract

Milk protein concentrates (MPC) are ideal dairy ingredient to provide nutritional and functional benefits in high-protein dairy and food products. However, one of the key challenges encountered by the MPC manufacturers during the spray drying is the high viscosity after ultrafiltration and evaporation. Reducing viscosity and aiding an increase in the solid levels before spray drying can offer significant savings on the overall energy cost during spray drying. On the other side, it is also a challenge for the end-user to incorporate the MPC powders in a formulation due to their poor rehydration properties. Therefore, simple and innovative strategies to reduce viscosity before spray drying while also improving final powder properties are of critical consideration for the dairy industry. Moreover, the dairy industry's eco-efficiency strategy focuses on manufacturing high-quality dairy products at a low cost with minimal environmental impact are gaining more attention. For instance, reduced energy usage while keeping high permeation flux values is critical for eco-efficiency. In this research, application of bulk nanobubbles (NBs) for improving the processability and functionality of various dairy concentrates were evaluated.

The chapter 3, 4, and 5 investigated the use of NBs generated by hydrodynamic and acoustic cavitation for improving the processability of dairy concentrates, rehydration/flow properties of MPCs. Control and NB-MPC dispersions were evaluated in terms of rheological behavior and microstructure. Additionally, MPC dispersions were spray dried after the NB treatment and the resultant NB-MPC powders were characterized and compared with the control MPCs in terms of rehydration characteristics and microstructure. NB-MPC powders exhibited better rehydration properties than the control MPC powders. Overall, these studies therefore,

recommends the possibility of using NB treatment for more efficient drying while improving the functional properties of the resultant MPC powders.

The chapter 6 evaluated the influence of NB incorporation during the UF process of skim milk. Both lab and pilot-scale UF experiments were conducted to evaluate the effect of NB incorporation on UF process by evaluating permeate flux, membrane microstructure, fouling resistance, energy consumption, and skim milk concentrate characteristics. For both the lab/pilot-scale runs, after the initial water flux measurements, the membrane was fouled with the skim milk concentrate dispersions operated at 20°C under a constant transmembrane pressure 30 psi in constant concentration mode (the permeate was returned to the feed tank at regular 10-min intervals) and the total run time was fixed for 1 hour. The results revealed that NB treatment had a significant effect on permeate flux in both the lab and pilot-scale runs. Overall, the NB treatment helped to improve UF membrane performance and therefore this study suggests the potential of using NB treatment for a more efficient UF processing.

Table of Contents

List of Figures

List of Tables

Acknowledgements

I would like to thank my advisor Dr. Jayendra K Amamcharla for his support and guidance throughout during my doctoral program. I also would like to express my gratitude to my committee members, Dr. Scott Smith, Dr. Karen Schmidt, and Dr. Yonghui Li for serving on my committee.

I am thankful to National Dairy Council and Midwest Dairy Foods Research Center (St. Paul, MN) for their financial support. I am also thankful to Ravi Thakkar for scanning electron micrography support, Dr. Tej Shrestha for nanoparticle tracking analysis support, and Dr. Dan Boyle for his help with confocal laser scanning microscopy and transmission electron microscopy analysis. I am also very grateful to all of my lab mates and fellow graduate students (2016-2022).

I would like to express my sincere gratitude to my Papa, Amma, and my wife. They unconditionally loved me and endlessly supported me throughout my graduate studies.

Dedication

To my beloved advisor, late Dr. Shiby Varghese. Thank you for being the best advisor I have had in my life. You have constantly helped me put things into perspective and have prepared me for great things for the future.

Chapter 1 - Introduction

The global milk powder market is predicted to reach ~13 million tons by 2023 and to a value of ~71 billion USD by 2027. Dairy powders are manufactured using unit operations like evaporation and spray drying. Spray drying is a widely used technology for the manufacture of dairy powders; however, it is very energy-intensive, contributing mainly to the total energy consumption. For example, skim milk is concentrated in a multiple effect evaporator (MEE) to a concentration of approximately 50% TS and subsequently spray-dried in a spray dryer. The energy consumption in a typical MEE is 260-330 kJ/kg water removal. On the other hand, energy consumption in a typical spray dryer is approximately 4,000 kJ/kg water removal which is 10 times more compared to a MEE. It is logical to remove as much water as possible in a MEE to reduce the operating cost of milk powder manufacture. Therefore, any technological approaches that can be coupled with spray drying to optimize the process better are critical from a sustainability perspective. One of the major concerns for the manufacture of dairy powders is the energy-associated environmental footprint. There have been findings that state that the energy footprint for milk powders is seven times more than packaged milk; therefore, to meet the future need for a significant reduction in energy consumption, innovative technologies are needed (Flysjö, 2012; Moejes et al., 2018). This could be attributed to the high-water content in milk and the energy-intensive thermal processing required for this water removal. Thus, ideally, for an energy-efficient process minimizing thermal inputs is the key. This could be achieved by pre-concentration and pre-treatments of the liquid before spray drying. Chamberland et al. (2020) reported that pre-concentrating cheese whey and milk ultrafiltered permeate to 20% and 22% w/w dry matter, respectively, by reverse osmosis prior to evaporation reduced the natural gas and electricity consumption by 36% and 10%, respectively. Pre-treatments such as high solids

content drying could also help with energy efficiency. Remarkably, Fox et al. (2010) reported that an increase in just 2% dry matter could achieve 6% energy reduction. However, high-solids drying is challenged by equipment performance constraints and product quality due to feed concentrate physical properties. Particularly viscosity is a significant concern while increasing dry matter content in the feed concentrate. Reducing viscosity also translates to reduced fouling of heat exchangers, improved heat transfer during evaporation, and a reduced amount of blocking in the spray drying nozzles. It is important for the dairy industry to adapt new technologies and strategies to reduce the viscosity of spray dryer feed even at higher total solids; this can offer significant savings on the overall energy cost of powder production. Therefore, any innovative approaches for reducing the viscosity of high solids concentrate could be a promising step to higher energy savings. Many processing strategies have been investigated to reduce the viscosity of the feed concentrates. This can be achieved either by altering the protein-protein interactions and/or by employing techniques like hydrodynamic/acoustic cavitation, high-pressure homogenization, carbon dioxide injection, etc.

Milk protein concentrate (MPC) is an ideal dairy ingredient to provide nutritional and functional benefits in high protein dairy and food products. However, one of the key challenges encountered by the MPC manufacturers during the processing is the high viscosity after ultrafiltration and evaporation. Reducing viscosity and aiding an increase in the solid levels before spray drying can offer significant savings on the overall energy cost of powder production. On the other side, it is also a challenge for the end-user to incorporate the MPC powders in a formulation due to their poor rehydration properties. Therefore, simple and innovative strategies to reduce viscosity before spray drying while also improving final powder properties are of critical consideration for the dairy industry producing MPCs. In the present

work, we are exploring the possibility of utilizing micro-and nano-bubbles (MNBs) for improving the processability and rehydration properties of MPCs. One of the common methods that are reported to produce bulk MNBs are based on hydrodynamic and acoustic cavitation. Several types of generators have been developed using the principles of the venture effect, swirl liquid flow, and pressurized dissolution. The size of bubbles generated can be governed by controlling pressure, temperature, flow rate applied to the flowing fluid. However, applied studies on MNBs in the food matrix are relatively nascent. Despite the theoretical challenges in understanding the existence of NBs in a complex matrix, they are being applied in various areas, and there is a constant surge for more innovation using the MNBs. In recent years, ultrasound has been widely investigated at a laboratory scale to reduce the viscosity of skim milk concentrate. High-intensity ultrasound (>20 kHz) employs mechanical waves at a frequency to generate acoustic cavitation. The bubbles expand to full size and then collapse violently generating a shock wave formation that is able to consequently reduce the viscosity of the feed.

Ultrafiltration (UF) is one of the most often utilized membrane processes in the dairy industry, particularly for fractionation and concentration of milk components. Several products, including milk concentrate for cheese manufacturing, low-lactose dairy products, milk protein concentrate, and serum proteins for dietary supplements, may be made using this method. The permeate flow (the phase moving through the membrane), the rate of fouling, and the fraction of soluble components rejected determine the efficiency and cost of a membrane process. As a result, the effectiveness of the membrane process and the changes in milk components throughout this process are important considerations when employing concentrated milk produced by UF in the manufacturing of various dairy products. The decline in membrane effectiveness caused by concentration polarization and fouling events is the most significant

constraint of the practical application of ultrafiltration for intricate fluids. In the present work, we have also explored the possibility of utilizing NBs for improving the processability and rehydration properties of MPCs.

Research on nano-scaled materials is constantly evolving as they show significant practical advantages in various manufacturing sectors. Nanostructured materials are defined to be of diameter in the range of 1 to 100 nm. However, a single internationally accepted definition for nanomaterials does not exist. The last two decades have seen substantial academic and industrial interest in investigations on the unique properties of both microbubbles and ultrafine bubbles or nanobubbles (NBs). Generally, microbubbles range from 10 – 50 μm, and bubbles with a particle size of <200 nm are typically referred to as NBs (Temesgen et al., 2017). Previously, Agarwal et al. (2011) presented the name micro-nano bubbles (MNBs), although an explicit category for NBs and MNBs are still unclear. MNBs are tiny bubbles with diameters ranging from hundreds of nanometers to several tens of micrometers. MNBs are gaining interest due to their wide range of applications in many fields of science and technology. MNBs exhibit high internal pressures, high gas solubility, and large surface-to-volume ratio. The physical properties of MNBs are different from those of milli-scaled bubbles, and the MNBs are stable for considerably long periods. MNBs have shown stability even for two weeks, and clusters of NBs could further increase their stability up to months (Azevedo et al., 2016). NBs clearly have unique from macro gas–liquid systems due to their incredibly tiny size. NBs have a prolonged existence period, a slow rising speed in water, extremely high internal pressure, a strong negative charge, and the ability to rupture and create hydroxyl radicals, among other properties. Although there is currently a lack of theoretical study on bulk NBs, multiple applications of bulk NBs have been

described in a variety of fields, including surface cleaning, agro-food industries, water pollution remediation, etc.

References

Agarwal, A., Ng, W. J., & Liu, Y. (2011). Principle and applications of microbubble and nanobubble technology for water treatment. Chemosphere, 84(9), 1175-1180.

Azevedo, A., Etchepare, R., Calgaroto, S., & Rubio, J. (2016). Aqueous dispersions of nanobubbles: Generation, properties and features. Minerals Engineering, 94, 29-37.

Chamberland, J., Benoit, S., Doyen, A., & Pouliot, Y. (2020). Integrating reverse osmosis to reduce water and energy consumption in dairy processing: a predictive analysis for Cheddar cheese manufacturing plants. Journal of Water Process Engineering, 38, 101606.

Flysjö, A. M. 2012. Greenhouse gas emissions in milk and dairy product chains: Improving the carbon footprint of dairy products.

Fox, M., Akkerman, C., Straatsma, H., & De Jong, P. (2010). Energy reduction by high dry matter concentration and drying. New Food, 60-63.

Moejes, S. N., & Van Boxtel, A. J. B. (2017). Energy saving potential of emerging technologies in milk powder production. Trends in Food Science & Technology, 60, 31-42.

Temesgen, T., Bui, T. T., Han, M., Kim, T. I., & Park, H. (2017). Micro and nanobubble technologies as a new horizon for water-treatment techniques: A review. Advances in colloid and interface science, 246, 40-51.

Chapter 2 - Generation methods and applications of bulk nanobubbles in the dairy and food processing industry[1]

Abstract

Nanobubble (NB) technologies have received considerable attention for various applications due to their low cost, eco-friendliness, scale-up potential, process control, and unique physical characteristics. NB stands for nanoscopic gaseous cavities, which are typically < 1 μm in diameter. NBs can exist on surfaces (surface or interfacial NBs) and be dispersed in a bulk liquid phase (bulk NBs). In comparison with the microbubbles, NBs exhibit high specific surface area, negative surface charge, and better adsorption. Bulk NBs can be generated by hydrodynamic/acoustic cavitation, electrolysis, water-solvent mixing, nano-membrane filtration, etc. NBs exhibit extraordinary longevity compared to microbubbles, prompting the interest of the scientific community aiming for potential applications including medicine, agriculture, food, wastewater treatment, surface cleaning, etc. Based on the limited amount of research work available regarding the influence of NBs on food matrices, further research, however, needs to be done to provide more insights into its applications in food industries. This review provides an overview of the generation methods for NBs, techniques to evaluate them, and a discussion of their stability and several applications in various fields of science were discussed. However, recent studies have revealed that, despite the many benefits of NB technologies, several of the NB generating approaches are still limited in their application in specific food processing industries. Further study should focus on process optimization, integrating various NB generation techniques, and cost control in order to achieve rapid technical progress and industrialization of NB-based technologies.

---

[1]Submitted for publication: Critical Reviews in Food Science and Nutrition

Introduction

Nanomaterials are of great technological and commercial significance, with a considerable influence on a variety of sectors. The word “nano,” meaning “dwarf,” comes from the Greek language. In 1974, Norio Taniguchi coined the term “nanotechnology,” and it involves the application of any nanoscale material in a variety of industrial/biomedical applications. Nanomaterials are referred to by the FDA as “materials that have at least one dimension in the range of approximately 1-100 nm and exhibit dimension-dependent phenomena”. The nanostructured materials and nanoparticles are categorized into four groups based on the materials: carbon, inorganic, organic, and composite-based nanomaterials. Additionally, based on dimensions, nanomaterials are classified as zero, one, two, and three dimensions. Nanomaterials are categorized as natural or engineered depending on their origin. (Jeevanandam et al. 2018). Since the nanomaterials are naturally present, for example, nanoscale components like casein micelles in milk. More than 4,500 years ago, humans took advantage of strengthening of ceramic matrixes by using natural asbestos nanofibers (Schaming and Remita 2015). The worldwide market for nanomaterials, which was anticipated to be worth USD 7.1 billion in 2020, is expected to expand to USD 12.1 billion by 2026. The U.S. nanomaterials market is estimated at USD 2.1 for the year 2021 (Global Industry Analysts, 2021).

Nanomaterials have risen to prominence in technological breakthroughs as a result of their adaptable physical, chemical, and biological characteristics, as well as their superior performance over other materials. Medicine, agriculture, food science and technology, electronics, cosmetics, and civil engineering are just a few of the sectors where nanotechnology is widely used. Several researchers are still investigating a variety of unique ways for using nanotechnology in the various food products. In food processing, nanostructures can be utilized

as antimicrobials, nanocomposites, nano additives, anticaking agents, nanocarriers as well as nano sensors in food packaging to assure food properties (Ezhilarasi et al. 2000). Edible nano-coatings (~5 nm) are used in meat processing, agriculture other food industries and offer flavor, color, and other added benefits (Nile et al. 2020). Furthermore, because of their mechanical, thermal, and barrier qualities, as well as their low cost, nano-clays are widely utilized and explored for food packaging (Gabr et al. 2015). The food and dairy processing industries demand new robust technologies, which are critical to producing fresh, safe, and flavorful products with improved quality. Presently, the food industry is enabling a variety of engineered nanomaterials in food product development, providing solutions for current problems associated with processing/functionality while offering long-term economic benefits. Due to an ever-increasing demand for high-quality and consumers' perception of processed foods, convenient and natural taste/flavor foods that lacks chemical additives and preservatives are gaining attention. As a result, the food and dairy industries are looking at ways to reformulate existing formulations with components that are believed to be healthy/familiar or by modifying processing with safe mechanical pretreatments, thus offering clean label solutions. Moreover, innovative technologies that significantly minimize the environmental footprint in dairy production are also gaining attention (Patil et al. 2021).

Recently, researchers have been concentrating their efforts on micro-and nanoscale gas bubble technologies. Bubbles of various sizes are commonly observed in everyday life, such as the tiny gas bubbles created when air is mixed with cold tap water or air bubbles in a carbonated drink. Ordinary bubbles have greater diameters, leading them to rise swiftly to the surface of an aqueous solution, collapse, or burst, and vanish. Nanobubbles (NBs), on the other hand, have been demonstrated to remain in bulk liquids for long periods of time. Typically, for an entity to

be classified as nanomaterial, ≥ 50% of particles in the material should have one or more of its external dimensions ranging from 1-100 nm (Mech et al. 2020); however, to date, ambiguity still exists in describing the size ranges of nano-sized bubbles. NBs are gas-filled cavities with a diameter of less than 1 μm in liquids. Ultrafine bubbles are another name for the NBs (ISO 20480-1:2017). In contrast, the term micro- and nano-bubbles (MNBs) include all diameters ranging from hundreds of nanometers to several tens of micrometers. Despite the fact that a recognizable community of scientists working on NBs has only been active for a short time. This field of study has gradually gained growing attention in recent years, with more than half of all relevant publications and patents produced in a previous couple of years. NB technologies have received substantial attention for industrial applications such as wastewater purification, cleaning, disinfection, and other agriculture and food-related applications in recent years due to the low cost, eco-friendliness, and scale-up ease (Agarwal, Ng, and Liu 2013; Ahmed et al. 2018). The essential features of NBs and their applications in the bulk liquid media are highlighted in this review. The NBs' creation, stability, measurement, and uses are all discussed. It is intended that this review will add to the growing body of knowledge about NB technologies.

Bulk and surface nanobubbles

NBs in the bulk liquid have recently been studied (Alheshibri et al. 2016), and the presence of these gas-filled NBs is still controversial (Jadhav and Barigou 2020b; Rak and Sedlák 2020). In recent years, two new types of NBs have been widely studied: (i) surface NBs, which form at solid-liquid interfaces, and (ii) bulk NBs, which exist in bulk liquid with a typical diameter of 100-200 nm. Due to their nano-sized diameter, NBs have distinct physical properties that attract more attention than macro-sized bubbles with bigger bubble diameters. Surface NBs were first put forward by Parker, Claesson, and Attard (1994), and they suggested that bubbles of

size 10-100nm formed from dissolved gases might be attached to the surfaces. The most widely used methods to generate surface NBs include direct water deposition (Borkent et al. 2010), temperature change (Guan et al. 2012), electrolysis (Luo and White 2013), and solvent-water exchange (Lou et al. 2000), etc. The purpose of this review is to give an overview of the fundamental features and stability of NBs in bulk liquid media, and in-depth details on surface NBs can be found elsewhere (Che and Theodorakis 2017; Fang et al. 2018; Theodorakis and Che 2019). Compared to surface NBs, bulk NBs have a vivid outlook in many applications, such as surface cleaning (Yang and Duisterwinkel 2011) and water treatment (Agarwal, Ng, and Liu 2011). The physicochemical properties of the liquid phase like the viscosity, surface tension, density along with bubble size, bubble rise velocity controls the hydrodynamics as well as flow pattern in the gas-liquid system. Figure 2.1 depicts the critical characteristics of bubbles. Compared to ordinary bubbles, the longevity, high gas dissolution rate, and large surface-to-volume ratio are the key features of NBs (Gurung, Dahl, and Jansson 2016), enabling its use in the field of science. However, applied studies on NBs in the food matrix are relatively nascent. Despite the theoretical challenges in understanding the exitance of NBs in a complex matrix, they are being applied in various areas, and there is a constant surge for more innovation using the NBs. NB technologies attract significant interest in various areas of food processing (Phan et al. 2020a; 2021a), promoting development of animals/plants (Ebina et al. 2013), wastewater treatment (Temesgen et al. 2017), medical field (Alshwali et al. 2020), gasoline engine (Oh et al. 2013), and cleaning (Zhu et al. 2016). Figure 2.2 illustrates the prominent unique physicochemical characteristics of NBs. To generate NBs, numerous generator types have been developed. It is required to design and develop NB generators that are portable, easy to use, and can produce NBs quickly. Though the presence of bulk NBs was first perceived in 1981 by

Johnson and Cooke (bubbles were stable ~22 h owing to natural surfactants found in saltwater forming films on bubble-water contact), the existence of bubbles with a size <1um surrounded by liquid remains a contentious issue because it contradicts conventional theories. Many researchers reported that NBs showed an extremely long lifetime, ranging from several weeks to months. Besides the investigations regarding the existence and generation of surface NBs, there is a strong interest in bulk NBs during the past five years (Azevedo et al. 2016; Oh and Kim 2017). The internal pressure inside of a NB is calculated using Young-Laplace equation (Liu and Cao 2016) as $2\gamma/r$ (γ: interfacial tension and r: bubble radius); for a 100 nm NB, internal pressure must be around 1.4 MPa (surface tension of pure water at atmospheric condition: 72 mN/m). Because of Henry's law, this necessitates a very high gas concentration in solution to achieve equilibrium with the extremely high gas pressure in the interior of the NBs. Bulk NBs' long-term stability is related to their low buoyancy force and their colloidal stability, which is attributed to Brownian motion alone, as shown by Nirmalkar, Pacek, and Barigou (2018b), and their interfacial stability against dissolution. As bulk NBs shrink, their radius decreases, and the Laplace pressure driving dissolution accelerates. whereas, for surface NBs, the radius of curvature increases (Tan, An, and Ohl 2020). Ohgaki et al. (2010) generated the bulk NBs by the incorporation of various gas (CH_4, N_2, and Ar) into the water solution. They observed a concentration of up to $1.9x10^{16}$ bubbles/dm^3 with a lifetime of up to 2 weeks. Yasui, Tuziuti, and Kanematsu (2018) previously reviewed several models for bulk NBs stability. In another study, bulk NBs were generated by ultrasound cavitation (Nirmalkar, Pacek, and Barigou 2018a) and observed the generated bulk NBs were stable for more than ten months and noted no significant change in the mean bubble diameter. Recently, bulk NBs (190 and 680 nm) with O_2 and air were produced in water using counterflow HC (Michailidi et al. 2020). Bulk NBs produced by this

method was remarkably stable in size and showed a lifetime of three months. Jadhav and Barigou (2020a) used three different techniques to generate bulk NBs and demonstrated they are gas-filled domains in solutions. Bulk NBs can be stabilized by charges anchored to the gas/water contact, according to Tan et al. (2020). The most startling evidence for bulk NBs were showcased in this study. The stability of bulk NBs is theoretically determined by the intensity of their surface charge and the electrostatic interaction between two charged surfaces. Despite the fact that there are countless published publications on the subject, the existence of bulk NBs is always a point of contention due to their exceptional stability. Despite this, a full physical model describing the stability of bulk NBs has yet to be developed. Recently, experimental data and molecular dynamic computations have been offered as a potential tool for exploring interactions in bulk phase and interface areas (Michailidi et al. 2020).

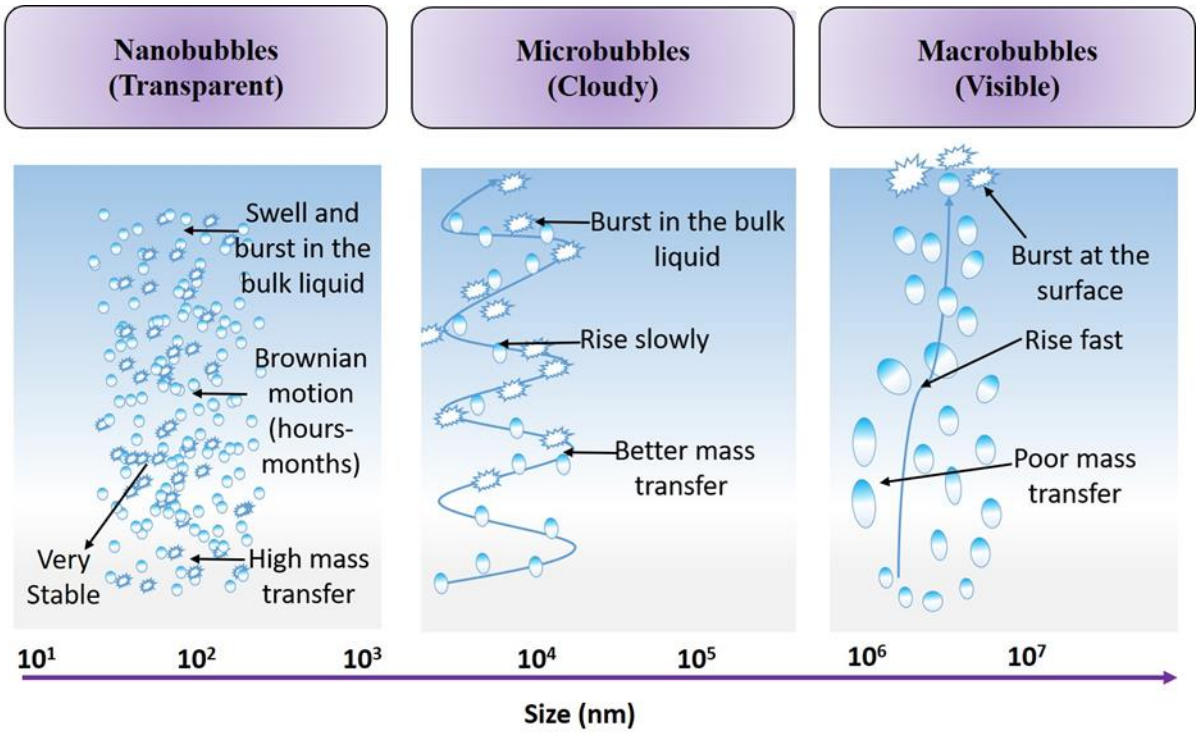

Figure 2.1 Prominent bubble characteristics alongside size adapted and modified from Temesgen et al (2017).

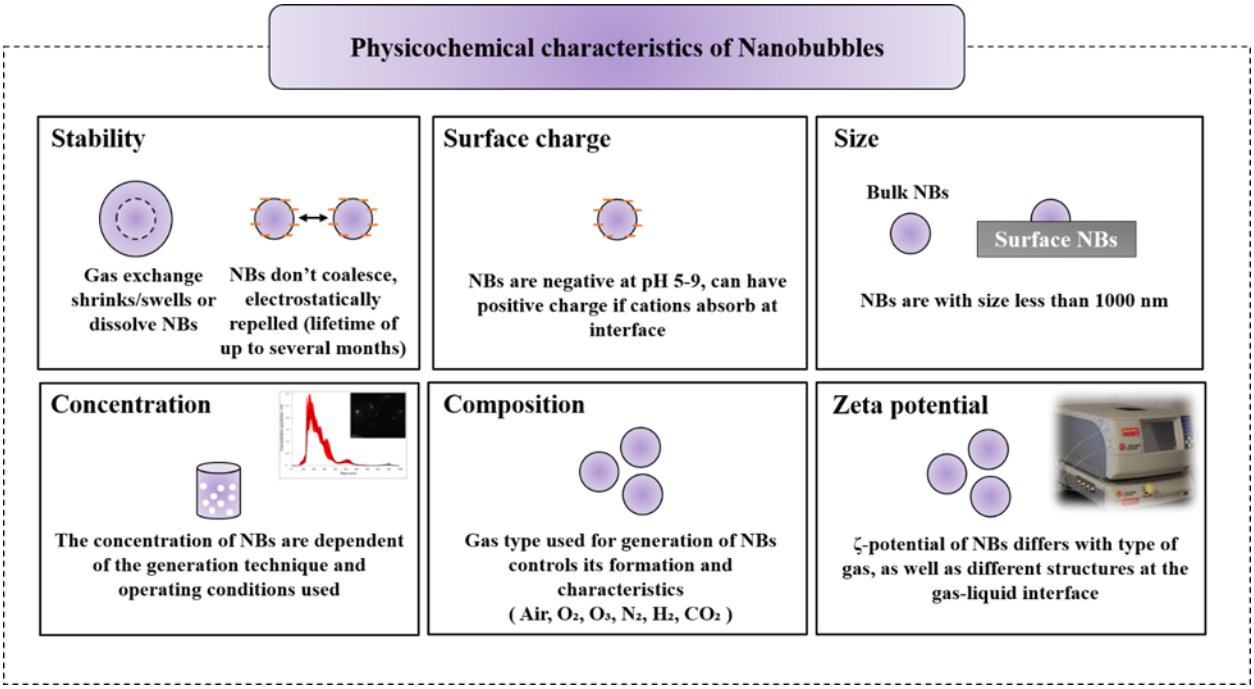

Figure 2.2 A generic illustration summarizing the nanobubble characteristics.

Generation of bulk nanobubbles

Different techniques are available for the generation of bulk NBs, including water-solvent mixing, acoustic cavitation, HC, nano-membrane filtration, compression/decompression of gas, electrolysis, fluidic oscillation, periodic pressure changes, chemical reactions, vibrations, electric fields, etc. Figure 2.3 shows the schematic diagram for some of the widely used NB generation techniques. Each method has its advantages, and the selection is application-specific. Methods like HC/acoustic cavitation and membranes are the most used NB generation methods and can be operated with a broad range of gases and for custom-designed setups for research purposes. On the other hand, methods like electrolysis are applicable only with specific gases, and electrolysis of water can only generate H_2 and O_2 NBs. However, the current NB generators may have drawbacks, such as the requirement to inject liquid at high pressures, liquid-gas mix up within the NB generators, contamination from gas-liquid recirculation, and a lack of control over bubble size. As a result, the hunt for NBs production techniques that can create significant

concentrations of bulk NBs, cost-effective, easy to scale up, and have process control continues to meet specific industrial demands are continued. Some of the commercially available devices for NB generation are shown in Table 1.

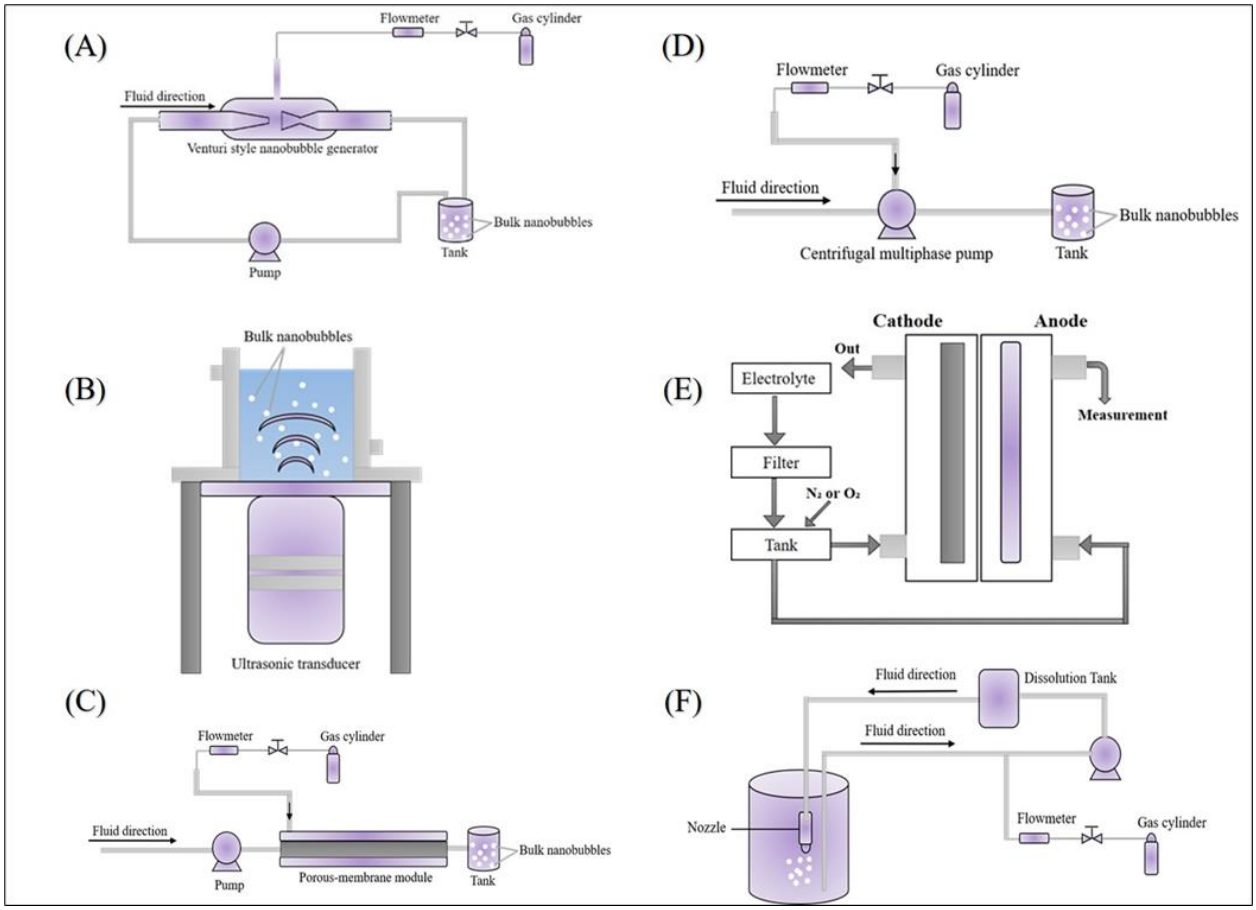

Figure 2.3 Schematic diagram showing various nanobubble generation techniques: A - hydrodynamic cavitation using venturi system (Xiong and Peng 2015), B - acoustic cavitation (Yasuda, Matsushima, and Asakura 2019), C - Membrane system (Ulatowski and Sobieszuk 2018), D - Centrifugal multiphase pump (Etchepare et al. 2017), E - electrolytic cell (Kikuchi et al. 2006), F - micro- and nano-sized nozzle (Meegoda et al.2018).

Cavitation

Cavitation is one of the most common processes for producing bulk NBs. The cavitation phenomenon arises from the violent collapse of bubbles generated as a result of pressure differences. When the hydrodynamic motion of the liquid is the cause for the decrease in liquid pressure due to liquid flow through a constriction like venturi systems, the related cavitation is called HC. Instead, when the reduction in liquid pressure is due to intense ultrasonic waves, the resulting cavitation is called acoustic cavitation. Very recently, Khaire and Gogate (2021) have reviewed the various applications of HC in food processing. Generation of NBs by cavitation can be categorized as (1) HC by a fluid flow; (2) acoustic cavitation from ultrasonic waves passing via the bulk liquid; (3) optical cavitation from high-intensity laser beam; and (4) particle-induced cavitation (passing particles like protons in the liquid causing particle-induced cavitation).

Many researchers have developed methods for generating bulk NBs by HC using a centrifugal multiphase pump, venturi style cavitation, orifice plate, and throttling valve. Li et al. (2015) studied the generation of MNBs by HC of deionized water to characterize homogeneous nucleation. They reported that the HC could generate MNBs with a diameter of <50 μm and learned that the bubble sizes weren't affected by increasing fluid velocity but influenced the concentration of the bubbles generated. Etchepare et al. (2017) developed a new method for generating HC using a needle valve and centrifugal multiphase pump for deionized water at room temperature. They obtained the highest concentration of 4×10^9 bubbles per mL at 5 bar. The surface tension and size were 49 mN/m and 60-70, respectively. They also reported that the bubbles obtained showed high stability as the size/concentration did not change substantially for up to two months. Previously, HC was also used by Tao et al. (2008) to create bubbles with an average diameter of 900 nm. Azevedo, Etchepare, and Rubio (2017) generated MBs and NBs by

injecting air into a suction chamber of a multiphase pump, producing bubbles due to the shearing of impellers and hydrodynamic pressure, thereby generating a concentration of 1×10^8 NBs per mL with mean diameter 220 nm. Oliveira, Azevedo, and Rubio (2018) generated NBs in a fully controllable HC tube with concentrations ranging between 4.2 and 6.4×10^8 NBs per mL with the size of the bubbles ranging from 100 to 550 nm. Maoming et al. (2010) developed an NB generator and studied the properties, uniformity, and stability of the NBs generated. They reported that the increase in temperature and dissolved CO_2 concentration had a positive effect on the NB size. They also noted that the median size of the NBs had a positive impact on time and dissolved CO_2 concentration and thus affecting the stability of the NBs. Wu et al. (2012) used a baffled high-intensity agitation via HC to generate bubbles of a mean diameter of approximately 500 nm. In 1 mM KCl solution, they found that increasing the agitation speed had a positive effect in producing NBs; however, they also noted that the agitation time had a minor impact on the number of bubbles produced.

Acoustic bubbles or acoustic cavitation bubbles are the bubbles that result from acoustic cavitation. Acoustic cavitation produces NBs larger than 200 nm when the acoustic pressure-amplitude is quite high. Bubble nuclei develop to cavitation bubbles with expansion and compression before collapsing when ultrasound is irradiated to water. Very recently, Singla and Sit (2021) have reviewed the various applications of acoustic cavitation in combination with other available technologies in food processing. According to Jadhav and Barigou (2020a), the collapse of microbubbles (MBs) after the acoustic cavitation results in the production of bulk NBs that were previously undetected. The ultrasonic power, frequency, and exposure time influence the NB concentration and diameter; thus, controlling it is critical. Very recently, Bu and Alheshibri (2021) reviewed the behavior of NBs under various ultrasonic settings. They have

noted that in acoustic domains, there is no broadly established clarification for the formation and high longevity of NBs. In another study, Yasuda, Matsushima, and Asakura (2019) generated NBs using ultrasonic irradiation at frequency of 22 kHz and power at 15 W and noted NBs of 50-220 nm in diameter. The concentration of bubbles rises with irradiation duration, and NBs were found to be in the concentration of about 1.2×10^9 per mL. Interestingly, Tanaka et al. (2021) found that 30 minutes of indirect ultrasonic irradiation reduced the number of preexisting nanobubbles generated by pressured dissolution and swirling liquid flow by ~90%. Rak, Ovadova, and Sedlak (2019) investigated the role of acoustic cavitation in the production of bulk NBs. The authors were interested in distinguishing whether the nano entities formed after cavitation is indeed nanoparticles or NBs. They used nanoparticle tracking analysis (NTA), density measurements, and inductively coupled plasma mass spectrometry for providing this distinctive evidence. They revealed that the nanoparticles in the fluid were solid titanium and vanadium nanoparticles and not bulk NBs. The concentrations of the titanium in the liquid were measured at a sonication time of 60 minutes, and it was found to be 8.76 μg/mL. Furthermore, they have queried the results reported by Jadhav and Barigou (2020a) and argued that the nano entities observed weren't NBs instead were nanoparticles. However, Jadhav and Barigou (2020b) responded that the generation of massive amounts of titanium particles was due to their longer periods of sonication time. It is to be noted that Jadhav and Barigou (2020b) used a shorter exposure of 100 s, the temperature during the acoustic cavitation was maintained at 20°C using a flow-cell. Likewise, the authors of this review also have observed results similar to that reported by Jadhav and Barigou (2020a). We have generated bulk NBs by continuous acoustic cavitation employing a 20 kHz ultrasonic processor (VCX 1500, Sonics & Materials, USA) and with a flow cell design (temperature controlled at 20ºC). A new and clean probe was used to acoustically

cavitate the bulk liquid (10 mL/min) using a peristaltic pump (Watson Marlow, USA). The non-existence/traces of titanium nanoparticles were determined using inductively coupled plasma mass spectrometry. The sample was then transferred to the Perkin Elmer NexIon 350 inductive coupled plasma-mass spectrometry for analyzing titanium concentration in bulk NB suspensions. Treated water samples had the presence of titanium in trace amount (0.00017 μg/mL), implying the presence of titanium contamination could not be blamed for the detected nano-entities using NTA (concentration: 1.19×10^9 particles/mL). This observation further confirms the presence of bulk NBs generated via acoustic cavitation. In contrast, Rak, Ovadova, and Sedlak (2019) reported the concentrations of titanium as 4.97 μg/mL at an exposure time of 30 mins and have argued about the non-existence of bulk NBs. Furthermore, our findings are in line with Jadhav and Barigou (2020b). They also have noticed traces of titanium; however, the concentrations were exceptionally low due to the optimized acoustic cavitation treatment applied. Additionally, (Nirmalkar, Pacek, and Barigou 2018a) examined the effects of sonication time at 20 kHz and 750 W power on bulk NBs suspension. They noted that with the increase in sonication time, the bubble concentration increased from 1.76×10^6 to 2.69×10^6 NBs/mL, and further increased to ~8×10^6 NBs/mL when the sonication time was increased. On the other hand, Mo et al. (2018) examined the effects of ultrasound exposure at 40 kHz and 300W power and reported that the NB concentration first increased and then decreased gradually. Overall, the NB generation employing acoustic cavitation is easier to operate and takes less time for its generation.

Membrane

Membranes with nano pores have been recognized to generate NBs (Kukizaki and Goto 2006; Kukizaki 2009). A gas phase is typically driven through a membrane into a water phase. Subsequently, size-controlled bubbles are generated at the interface between the water phase and

the membrane surface. NB formation via this method comprises two steps: expansion of bubbles and its detachment. The surface tension between air and water retains NBs near the pore opening, while the drag force produced by the water phase pulls them away and detaches them from the pore opening. (Kukizaki and Goto 2006). The reduction of the pore diameter is deemed critical in obtaining NBs. Notably, Fujikawa et al. (2003) noted the smallest bubbles noted were ~10 μm (the membrane pores were ~130 μm). Very recently, Dhungana and Bhandari (2021) outlined the use of a ceramic membrane to generate gaseous NBs and its applications in liquid food processing. Compared to the ceramic membrane-based method, when the air and CO_2 MNBs were generated by HC (venturi-style), the authors noticed a lot of foaming in their dairy protein dispersion systems. The authors also pointed out that the operating mechanism of cavitation-based techniques is complicated, and they lack control over bubble size and consistency; and suggests continuous membrane nanobubble generation method as a simple approach that may be integrated into a continuous system. Kukizaki and Goto (2006) generated MNBs from shirasu-porous-glass membranes, and they have noted that the diameter of NBs may also be regulated by the membrane pore size. Membranes can be successfully used to make monodispersed NBs with a diameter of 360-720 nm. (diameters of pore ranging from 43-85 nm). Ahmed et al. (2018) explored the influence of two different pore sizes (100 and 1000 nm) on the NB size and zeta potential. The diameters of O_2 and N_2 NBs were around 150 and 300 nm, respectively. The zeta potential of O_2 and N_2 NBs (60 psi) were -38 mV and -45 mV, respectively.

Ethanol-water exchange

The mixing of ethanol-water as a simple approach for creating NBs in bulk has been widely researched (Zhang, Maeda, and Craig 2006; Qiu et al. 2017; Alheshibri and Craig 2019;

Millare and Basilia 2018) and on surfaces (Lou et al. 2000). NBs are produced by displacing (pre-distilled) ethanol with purified water. As a result of combining equilibrated solvents with ambient gases, the dissolved gases in the mixture become supersaturated, potentially resulting in the nucleation of bulk NBs (Qiu et al. 2017). Zhang et al. (2006) noted warm ethanol and water (45°C) were shown to be more efficient in the production of NBs. They studied the morphology of NBs using TM-AFM and reported the NBs had an average height of 26 nm and a lateral dimension of 591 nm. Recently, Qiu et al. (2017) used ethanol-water exchange to generate NBs having a diameter of 100 to 200 nm. They observed that the concentration of NBs was 4.5×10^8 bubbles/mL and had a lifetime of up to 4.5 h. The concentrations of bulk NBs at 30, 35, 40, and 45°C were also studied; the authors noted that higher temperatures could produce more NBs. For the NBs generated at 45°C, the concentration of NBs was around 13×10^8 bubbles/mL. More recently, Alheshibri and Craig (2019) used ethanol-water exchange to generate NBs with a diameter of 200 nm and remarkably, increasing the ethanol content resulted in less particles.

Electrolysis

Electrolytic generation is distinct from the generation techniques based on cavitation, as gas NBs are formed because of electrochemical reaction occurring on electrodes through the electrolysis of different salts. Besides, electrolysis of water in the presence of acid/base results in the creation of H_2 and O_2 NBs. The generation of bubbles during electrolysis at the electrode surface has been widely reported (Zhu et al. 2016). Both gas concentration at the electrode surface and the behavior of desired gas NBs are essential for obtaining a high concentration of gas with electrolysis. Kikuchi et al. (2001) and Kikuchi et al. (2007) produced H_2 and O_2 NBs using electrolysis. It was noted that H_2 NBs have a lifetime of a few hours while O_2 NBs have a lifetime of a few days. In another study, Zhu et al. (2016) reported stable NBs for approximately

24 h with ~90 nm in diameter, and ~5×10^8 NBs per mL were reported. Likewise, Kikuchi et al. (2009) generated NBs via electrolysis water (O_2), and the bubble diameter size of the control, day two and day three, was 30, 180, and 250 nm, respectively). Previously, Postnikov et al. (2018) used alternating polarity electrolysis to generate bulk NBs. Measurements were done at 150 kHz and 325 kHz when electrical pulses were switched on and 3 minutes later after turning off pulses. When the pulses were switched on, the bubble size was ~60 and ~80 nm at 325 and 150 kHz, respectively. Whereas, when pulses were turned off, the bubble size was ~240 and ~260 nm at 325 and 150 kHz, respectively. The size of created NBs is noticeably smaller when the pulses are applied at a higher frequency; nonetheless, when the pulses were turned off, coalescence occurs.

Miscellaneous techniques

In the decompression-type and gas-water circulation-type method of generation, the gas incorporation in the bulk liquid is enhanced at high pressure, resulting in supersaturation. After that, a mixed gas water solution is decompressed to atmospheric pressure, causing NBs to form. (Ikeura, Kobayashi, and Tamaki 2011). Likewise, Calgaroto, Wilberg, and Rubio (2014) produced NBs from depressurized gas-saturated solution via needle valve (2mm) to with diameters ranging from 130 to 720 nm. Very recently, Ghaani, Kusalik, and English (2020) investigated surface-electrostatic NB formation and stabilization using external electric fields in gas-liquid systems. In another study, Fang et al. (2020) generated bulk NBs by vibration (frequency: 900 r/min); the NB concentration noted was 8.1×10^7 per mL. They noted that the sizes of most NBs generated were below 400 nm. After 24 h, the concentration of bulk NBs reduced, but it kept around 68% of its initial concentration, indicating adequate stability for vibration-generated NBs. Previously, Jin, Feng, Yang, and Gu (2019) employed periodically

compression of gas into water, a pressure-driven technique for preparing bulk NBs, and over the course of 48 h, the development of the NB size and zeta potential was investigated. They have noted the highest NB concentration of 1.92×10^{10} particles/mL was obtained at the compression times of 600. The diameter and zeta potential were around 248 nm and −40 mV, respectively at 48 h. Their findings revealed that NBs have stable for days to months. Uchida, Yamazaki, and Gohara (2016) researched the MNBs formation in water by the dissociation of gas hydrates. Gas hydrates are solid, crystalline substances, and when they are dissociated in solution after saturation is reached, it forms bubbles. CH_4 hydrate dissociation observed MNBs of diameters 300-400 nm and with 10^9 NBs per mL of bubble concentration. In another study, Wang et al. (2019) produced bulk NBs using periodic pressure change. They achieved NB production using internal pressure changes periodically in a U-tube. The N_2 NBs generated were observed to be stable for 48 h. Initial diameters were less than 100 nm, whereas, after 48 h, diameters were 115 nm and 500 nm. Recently, Ferraro et al. (2020) presented a novel approach for creating bulk NB suspensions by consecutive expansion/compression strokes within a sealed syringe based on Henry's theory of vacuum degasification and also gave evidence that the observed nano-entities must be gas-filled NBs. NB concentration at 45 cycles was noted to be $\sim 1.0 \times 10^9$ per mL, with NB diameter noted as 125 nm. The NBs produced by baffled high-intensity agitation are stable for 5 h in a surfactant-free solution and ~24 h in a surfactant-containing solution. (Wu et al. 2012). Oh and Kim (2017) generated CO_2 NBs by gas-liquid mixing method and observed a higher NB concentration over 24 h (2.94×10^8 particles per mL with size 110 nm). The O_2 NBs with a mean size of 137 nm measured by dynamic light scattering (DLS) was observed to be stable until day six in the absence of additives (Ushikubo et al. 2010). Compared to pure water, the generated MNBs in 100 mM NaCl solution remained in bulk for at least a week, by the ionic

shielding effect. However, higher NaCl concentrations resulted in lower bubble concentrations, which steadily declined over time (Uchida et al. 2016). The most important properties of NBs in various industrial applications depend on the kinetics of NB generation, and bubble size, surface charge, and hydrophobicity are among its physicochemical features. Properties of NBs have relied mainly on temperature, pressure, salt, surfactant, storage condition, dissolved gases, etc.

Table 2.1 Commercially available nanobubble generating systems*

Nanobubble generating systems	Descriptions	Company/lab testing using pure water**	References
Moleaer Inc.	They have a range of generators available. For example, Moleaer XTB NB generator can be integrated into existing plants, and it comes with a flow rate of 25 gallons per minute and with a gas flow range of 0-2.5 cubic feet per hour.	Mean size: 115.9 nm Concentration: 9.81×10^8 particles/mL	(https://www.moleaer.com/)
Continuous high-shear rotor-stator device (Silverson Machines Ltd, UK)	Bulk NBs generated using hydrodynamic cavitation by high shear, intense turbulence, and collision effects. The device equipped with a single 4-blade rotor of 26 mm inner diameter and 38 mm outer diameter, located inside a stator of 39 mm inner diameter and 41 mm outer diameter having 8 holes of 10 mm diameter with a 0.75 kW motor.	Mean size: ~110 nm Concentration: ~2.4×10^8 particles/mL	(Jadhav and Barigou 2020)
Asuplus Nanobubble Technology (Japan)	NB cylinder type available with various configurations and capable for in-line applications with custom designed systems.	Mean size: 128.5 nm Concentration: 5.1×10^8 particles/mL	(https://www.airywater.com/)
VCX 1500 HV Model (Sonics and Materials, USA)	Bulk nanobubbles can be generated by acoustic cavitation using ultrasonic processor (20 kHz probe-type) and high-volume continuous flow cell.	Mean size: ~230 nm Concentration: ~1.19×10^9 particles/mL	(Babu and Amamcharla 2021)
Venturi-type bubble generators (Hydra-Flex venturi injector, USA)	Venturi injectors work by creating a pressure difference between the inlet and outlet. The constricted flow at the injector's core creates a vacuum, which pushes the air in. The air flow via the injector may be adjusted to manage the injection rate and size of the injected bubbles, which can be monitored by the air flow meter.	Mean size: 249.8 nm Concentration: 3.76×10^8 particles/mL	(Babu and Amamcharla 2020)

*The authors declare they have no conflict of interest.

**The size and concentration of nanobubbles were measured using NanoSight instrument.

Existence and stability of bulk nanobubbles

Several researchers characterized NB properties and debated paradoxes between theory and experimental NB existence and stability. New models and methods are developed to explain the unique NB stability phenomena. The applications of NBs are primarily based on their longevity, which can range from several days to months. In contradiction, the prolonged stability of NBs does not align with classical thermodynamic theories. Future research is needed to completely comprehend the basics of NBs and how they interact with complicated food matrices. Internal pressure is inversely proportional to diameter according to the Young-Laplace law; hence NBs should be dissolved as soon as possible. For example, NBs of diameter 10-100 nm should have an internal gas pressure of hundreds or tens of atmospheres, and it should dissolve within milliseconds. Bulk NBs have a long shelf life because of their low buoyancy force, which keeps them from rising to the surface, colloidal stability, and interfacial stability against dissolution. The Hadamard–Rybczynski equation may be used to calculate the bubble's ascensional velocity. (Ruckenstein 2013). In water, NBs with a diameter of 100 nm have an extremely low ascensional velocity (8.2×10^{-9} m/s) (Ohgaki et al. 2010). Recently, by coupling DLS and zeta potential measurements, Tan et al. (2020) proposed a model that suggests bulk NBs can potentially be stabilized by a mechanism of accumulating surface charge density. The skin model, particle crevice model, electrostatic repulsion model, "armored" bubble model, many-body model, and dynamic equilibrium model are amongst the notable models for the stability of NBs. According to the skin model, a bubble is entirely coated with organic materials/surfactants, and the skin stops gas loss by diffusion. The gas pressure is lower than the liquid pressure, according to the particle crevice model. As a result, the gas does not dissolve in

the liquid, resulting in a longer lifetime. A microscopic bubble is negatively charged and has an extremely high zeta potential value, according to an electrostatic repulsion model. The Laplace pressure owing to surface tension may be balanced by electrostatic repulsion of a bubble's negatively charged surface. The "armored" bubble concept argues that a surfactant and solid nanoparticles deposited onto the bubble surface stabilize the bubble. Another scenario is the many-body effect, in which NBs in a group of NBs shelter each other from diffusion through shielding effect (Yasui et al. 2018).

Characterization of bulk nanobubbles

To prove the presence of bulk NBs, many imaging, physical and chemical analytical approaches are applied. In recent articles, these measuring methodologies and processes are described in greater depth (Nirmalkar, Pacek, and Barigou 2018a; Jadhav and Barigou 2020a). NTA is commonly employed technique to determine the concentration and size of bulk NBs. Zeta potential values may also be used to describe NBs, and they are given as a measure of the electrostatic repulsion or attraction among particles and NBs. The longer lifespan of NBs is thought to be owing to negative-charge accumulation at the gas-water interface. The pH and dissolved salt concentrations is known to have a big impact on the NB surface charge. Very recently, NB stability in various salt solutions and effects of electrolytes and surfactants on NB formation and stability have been investigated and evaluated (Phan et al. 2021c; Hewage, Kewalramani, and Meegoda 2021). The impact of bubble size on zeta potential is an interesting topic; remarkably, Takahashi (2005) measured zeta potential on MBs and demonstrated no correlation between zeta potential and the diameter of the bubble. In contrast to changes in bulk NB concentration and mean diameter, Kanematsu, Tuziuti, and Yasui (2020) found that zeta potential did not change much and ranged from -35 to -20 mV, even for samples held for more

>9 months. Several measuring methods, like resonant mass measurement and DLS methods, were previously utilized to investigate bulk and surface NBs. (Ushikubo 2010; Kobayashi et al. 2014; Zhang and Seddon 2016; Ahmed 2018). Since DLS is incapable of resolving binary particle systems with nearly identical diameters (Filipe, Hawe and Jiskoot 2010; Panchal et al. 2014) and resonant mass measurement can't tell the difference between surface-attached, and bulk NBs in a sample, more accurate methods are required. Several researchers have used the NMR technique to establish evidence of NBs (Liu et al. 2013; Liu et al. 2012; Ushikubo et al. 2010). Furthermore, microscopy techniques (transmission electron microscopy and cryogenic scanning electron microscopy) and chemical analytical methods can give proof of bulk NBs' presence and stability. Jadhav and Barigou (2020a) have analyzed pure water and bulk NBs, and the organic contamination was detected using gas chromatography mass spectroscopy, whereas the inorganic contamination was detected using inductive coupled plasma mass spectroscopy. Details of this work have been described elsewhere (Jadhav and Barigou 2020a). Various currently available and widely used techniques to characterize the bulk NBs are discussed below.

Nanoparticle tracking analysis

The average size distribution of particles in bulk can be determined using traditional DLS; however, has a limited resolution. They may also account for contamination, resulting in erroneous results. NTA using Nanosight, on the other hand, has the benefit of providing particle number distribution by default, as opposed to DLS. The NTA principle has already been discussed by Patois et al. (2012). The NB size is calculated by documenting the 2-D Brownian motion of the particular light-scattering entities and using the Einstein-Stokes equation to calculate the hydrodynamic diameters. The number concentration is computed by counting the number of light-scattering centers in the microscope's focus plane. The NTA approach is

extensively employed by many researchers since it can discriminate between different kinds of particles of similar size when used in conjunction with multidimensional parameter measurement (Alheshibri and Craig 2019; Kanematsu, Tuziuti, and Yasui 2020).

Atomic force microscopy

The morphology and stability of NBs can be studied by atomic force microscopy (AFM). The ethanol-water exchange generated NBs were used by Lou et al. (2000), who carried out one of the earliest surface NB AFM studies. Circular features with hemispherical cross-sections seen with the AFM on solid surfaces under water were interpreted as individual NBs. Previously, Tyrrell and Attard (2001) used tapping mode AFM images of NBs adsorbed on the hydrophobic surface and reported that in cross-section, NBs are densely packed and uneven with a curvature radius of 100 nm and height of 30 nm. Walczyk et al. (2014) used and compared three different measurement modes in AFM measurements of argon NBs. Several imaging experiments using AFM were done mainly in tapping mode, contact mode, peak force tapping, frequency modulation, force spectroscopy, noncontact mode, and lift mode (Ishida et al. 2000; Yang, Lu, and Hwang 2013; Lu, Yang, and Hwang 2012; Seddon, Zandvliet, and Lohse 2011; Walczyk, Hain, and Schönherr 2014; Peng, Hampton, and Nguyen 2013; Lou et al. 2000). Understanding the unique data acquisition methods, scanning protocols, and parameters involved, on the other hand, is critical, making it challenging to compare findings acquired in different AFM modes. The tip shape, the amplitude of the cantilever oscillations, and the peak force in peak force tapping all influence the height and size of the NB in AFM.

Spectroscopy techniques

Fourier transform infrared spectroscopy (FTIR) is also seen as a tool to identify NBs in bulk solutions. The gas within the NBs must be infrared active in order to use attenuated total

reflectance (ATR) spectroscopy. Very recently, Jadhav and Barigou (2020a) have used ATR-FTIR with a spectral range from 400-4000 cm^{-1} to study the purity of bulk NBs produced by water-ethanol mixing, HC, and acoustic cavitation. The FTIR spectra of the NBs formed in pure water match that of pure water perfectly, indicating that the nano-entities detected aren't solid or liquid contaminants. Oh and Kim (2017) studied CO_2 generated NBs using ATR-FTIR because dissolved and gaseous CO_2 has very distinct infrared spectra. They investigated bulk NBs using an ATR-FTIR spectroscopy instrument, with scans from 650-4000 cm^{-1}. The NBs in bulk liquid were with gaseous CO_2 molecules, according to the infrared spectra. Furthermore, Ohgaki et al. (2010), using ATR-IR noted the surface of bulk NBs has strong hydrogen bonds, which may limit gas diffusivity across the interfacial layer. Raman spectroscopy is another technique that could shed light on the existence of NBs. Raman spectroscopy, like FTIR, uses molecular vibrations to evaluate a sample's chemical structure and identify the chemical compounds it contains. Recently, Jadhav and Barigou (2020a) have also used Raman spectroscopy to examine bulk NB suspensions. Ferraro et al. (2020) compared the functional groups present in pure water and bulk NB solutions created by sequential expansion/compression strokes using FT-IR and Raman spectroscopy.

Application of bulk nanobubbles

Dairy applications

Researchers at Kansas State University are actively investigating possible dairy applications of MNBs. Previously, a patent application (WO2017127636 Al) on the use of MNBs in liquid processing was filed (Amamcharla, Li, and Liu 2017). The application of MNBs in liquid dairy products are proven to reduce its viscosity and enhance processability, eventually decreasing processing costs. Previously, Amamcharla et al. (2017) demonstrated that the

viscosity of the MNB incorporated Greek-style yogurt (GSY) samples showed significantly lower viscosity and remained lower throughout the 3-day test period, demonstrating that the MNBs remained stable within the GSY product. Additionally, incorporating MNBs has been shown to increase ultrafiltration flux, and thereby decrease overall processing costs. For the dairy manufacturers producing MPCs, simple and creative techniques before spray drying are key considerations. The applications of MPC powders include high-protein beverage/bar, infant milk formula, cheese, yogurt, etc.; however, its end-use applications are limited by its poor solubility and flowability (Babu et al. 2018a; Babu and Amamcharla 2018b). The high viscosity after ultrafiltration and evaporation is one of the main problems faced by MPC producers during the processing. Reducing viscosity and assisting in the rise of solid levels prior to spray drying can result in considerable energy savings in powder manufacturing. Indeed, due to their poor rehydration capabilities, it is difficult for the end-user to incorporate MPC powders into a formulation. Process and functionality improvement of MPCs can be achieved by various methods; however, these methods have practical or economic concerns for many manufacturers. Recently, Babu and Amamcharla (2020) explored the use MNBs as a pre-treatment for the improvement of rheological and functional properties of MPCs. The resultant MNB treated powders exhibited highly beneficial characteristics as compared to control powders. MNB treatment showed a decrease in viscosity of 70-80 % when processed at specific operational parameters compared to the control retentates. This lower viscosity improves the efficiency and performance of downstream process technologies, such as higher total solids in spray drying and less fouling in evaporators. Also, the MNB treated powders were noticed to be free-flowing with significantly lower ($P < 0.05$) basic flow energy values when compared to the untreated MPC powders. Very recently, Babu and Amamcharla (2021a) have evaluated the influence of bulk

NBs generated via acoustic cavitation during spray drying on the rehydration, flow, and morphological characteristics of the MPC powders. The flow curve in Figure 2.4 demonstrates the rheological differences upon NB treatment. The apparent viscosity of the control MPC dispersion at total solids of 19% was 203.84 mPa·s at 100 s^{-1}. Whereas the viscosity decreased to16.81 mPa·s, after the NB treatment at 90% amplitude using bulk NBs were produced by continuous acoustic cavitation by a 20 kHz ultrasonic processor (VCX 1500, Sonics & Materials, USA) along with a flow cell design. This was further supported by visual observations in the microstructure. The CLSM micrographs in Figure 2.4 showed a more aggregated microstructure for C-MPC, whereas bulk NB treated MPC has a fine uniform structure. The focused beam reflectance measurement of the NB treated MPC powders had higher fine particles counts during dissolution, indicating these powders were more soluble than control powders (Figure 2.5). The rate of water transfer during rehydration was supported by the presence of these large air voids and pores throughout the particle-matrix (Figure 2.5). McSweeney et al. (2021) previously observed better solubility of MPC powders injected with N_2 (control: 83.6 % and N_2 treated: 96.2 %). NB treated MPC powder particles have porous shape, and the existence of significant air spaces between them helps increasing the physical space between casein micelles and decrease protein-protein interactions (McSweeney et. 2021). From the findings of these studies, NB incorporation before spray drying signifies a prospective to a less energy-intense drying process, with superior final powder properties.

Very recently, Khaira et al. (2020) evaluated the impact of NB liquid in enhancing the physical quality of ice cream. The NB liquid in the ice cream was compared with the one made using normal water. It was noted that ice cream made with NB liquids were able to hold the ice cream body better than the control made with normal water with higher density (0.77 g/mL) and

firmness (34.80 gram-force) values. They also reported an evident decrease in the apparent viscosity (0.15 Pa.s, 30 % lower than the one made using normal water) of ice cream made with NB liquid were also reported. Previously, Adhikari et al. (2020) reported that ice-cream treated with CO_2 (2000 ppm) and subsequent 60 s of acoustic cavitation had significantly greater overrun values in comparison to the untreated sample. An attempt was made by Babu, Lui, and Amamcharla (2018) to investigate the application of MNBs for enhancing the rheological and functional properties GSY. Significant rheological differences have been observed between the control (C-GSY) and MNB treated GSY (MNB-GSY) during storage. Before storage, the apparent viscosity at $100s^{-1}$ (η_{100}) was 1.09 Pa.s for C-GSY and 0.71 Pa·s for MNB-GSY. Injection of GSY with MNBs significantly ($P < 0.05$) decreased the η_{100} by 30% on one week of storage. Additionally, the η_{100} of MNB-GSY was lesser than C-GSY on weeks 2, 3, and 4 of storage. The number of grains of MNB-GSY was 37 grains/g of yogurt and was lower than 143 grains/g observed in C-CGY. Differences were also noticed in syneresis, which was lower for the MNB-GSY compared with the control. Overall, Nb treatment is a simple, cost-effective process to implement in existing production plants and has no labeling issues. The economic benefit of NB application can minimize or replace the use of mechanical and chemical pre/post-processing.

With the advent of membrane technology, milk fractionation became a crucial dairy industry procedure to make several dairy products/ingredients, initially with tubular ceramic membranes and then with the introduction of spiral-wound polymer membranes. Membrane fouling reduces the effectiveness of milk filtration, but it appears to be unavoidable given the variety of foulant-foulant and membrane-foulant interactions that may occur. Presently, Babu and Amamcharla (2021b) are testing the potential of bulk NBs for improving the efficiency of ultrafiltration membrane processing in the dairy industry. The skim milk concentrate of 25%

total solids was used to evaluate the influence of NBs during ultrafiltration. A 25% reduction in viscosity was seen in the NB treated dispersions compared to the control dispersions. The lower viscosity of the NB retentates could positively affect the performance of ultrafiltration. The initial flux was about ~50% lower for control, compared to NB treated sample. Furthermore, it was noted that the deposit layer on the polyethersulfone membrane with NB incorporated skim milk concentrates had a thickness of the fouled layer of ~19 um; however, the untreated samples had a thickness of the fouled layer of ~45 um.

Food applications

Barker, Jefferson, and Judd (2002) reported that smaller bubbles are favored in beverages, as it is believed that they positively affect the texture and mouthfeel of the drink. Also, in this study, a sensory taste test was conducted using volunteer tasters on carbonated water, and tasters were asked to select the one with more carbonation among the two drinks (regular and small bubbles, both after 5 min of carbonation). The results indicated that 87% of the tasters were able to distinguish the more carbonated sample, and 73% indicated that the sample containing small bubbles was more carbonated than the other. Saint-Eve et al. (2010) studied the taste and aroma perceptions in carbonated mint beverages. They reported that CO_2 addition can suppress the sweet perception irrespective of the flavoring and can impact the sourness perception. However, considerable research is still needed to bring NB applications to different food systems to study possible sensory enhancements.

Gel-based foods incorporated with bubbles result in improved textural properties due to its high internal surface area. The incorporation of the CO_2 gaseous phase in hydrocolloid gels could alter the textural properties (Nussinovitch, Velez-Silvestre, and Peleg 1992). Zúñiga and Aguilera (2009) studied gelatin gel which are gas-filled and reported the size of the bubbles

increased with higher protein contents (5, 7, and 9%) for air, nitrogen, and helium bubbles. They found that for air-filled gels with the lowest gelatin content, around 70% of the bubbles were less than 100 um, whereas, for the greatest gelatin concentration, only 23% were less than 100 um. For nitrogen and helium gas-filled gels, this was 81-54 % and 71-35 %, respectively. MNBs influence the crystal development and nucleation of sucrose/maltodextrin dispersions during the ultrasound aided freezing process, according to Zhu et al. (2018). Remarkably, ultrasound treatment and the incorporation of MNBs influence the initiation of nucleation. The high-pressure caused from the collapsing of MNBs in fact acts as catalyst for nucleation (Zhu et al. 2018). Furthermore, under the identical sonication and MNB treatment, the freezing rate of sucrose liquid was greater than that of maltodextrin liquid sample, indicating that Newtonian fluid was even more susceptible to the cavitation. Previously, Adhikari et al. (2018) investigated the impact of adding N_2 and CO_2 to a supersaturated lactose solution. MNBs were thought to promote lactose crystal nucleation by providing additional nucleating sites. At 30 mL per min of gas addition, the yield was 21.8% and 17.4% in CO_2 and N_2 addition, respectively. However, the yield of control was 14.7%. The higher yield obtained from CO_2 addition was attributed to the better CO_2 solubility. Furthermore, The CO_2 MNB addition lowered the particle size of the lactose crystals by increasing the number of nuclei and reducing the amount of solute depositing on those nuclei (Adhikari et al. 2018). The viscosity dropping effect of NB treatment for a 7-day test period (at 23 and 4ºC) in apple juice concentrate and canola oil was demonstrated by Phan et al. (2021b) and it was attributed to the NB size and concentration. The authors also reported the lowering effect on viscosities with NB treatment declines over time as the size of the NBs grew larger, and the concentration of dissolved gas decreased.

Because of its surfactant characteristics, interest in NB technology has grown over the years; nevertheless, its antimicrobial effectiveness in food-related applications is still evolving. When compared to standard ozone disinfection, ozonated NBs have been shown to lower *E. coli* by two log cycles (Agarwal et al. 2011). NB treatment has been tested against norovirus surrogates in oysters and was reported to inactivate more than 99 % of the active virus after 12 h (Tsuge 2014). Furthermore, HC-produced NBs were found to have a high inactivation ability against *E. coli* (Agarwal et al. 2011). In comparison to pre-treatments without MBs, Soli et al. (2010) found that the pre-treatment on MBs assisted in diminishing natural flora by 1 log CFU on lettuce. In a model beef processing system, Wilder (2016) investigated the efficiency of chlorinated NB solutions in controlling various pathogenic microbes. After 60 min, all microbial populations studies were decreased by > 6 log CFU/mL (5.23 ppm free available chlorine). Kobayashi et al. (2010) used CO_2 MNBs to reduce the coliform counts in cut wakegi at a temperature of 20-30°C and exposure time of 10-30 mins and reported significant reductions in the coliform bacteria counts. They have suggested the inactivation of microbes by MNB-CO_2 as an alternative to washing cut vegetables with sodium hypochlorite. Very recently, Singh et al. (2020) reported CO_2 MNBs in chlorine, and peracetic acid significantly increased the potency of antimicrobial solutions against *E. coli* and *L. monocytogenes*.

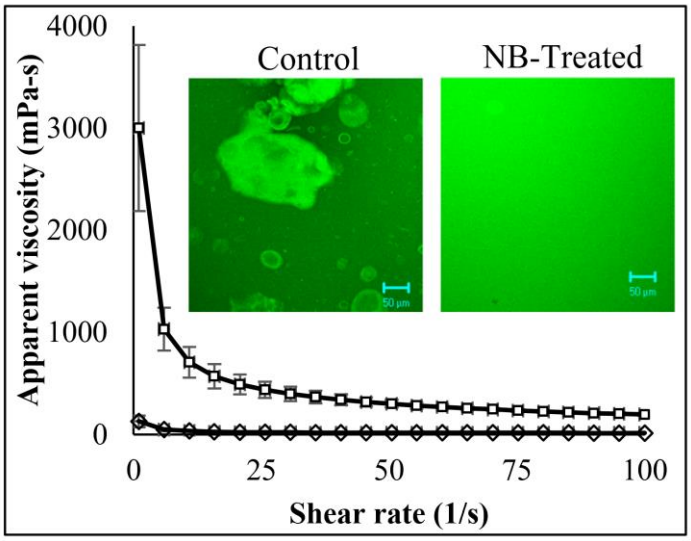

Figure 2.4 Viscosity as a function of shear rate (flow curves) (A) Milk Protein Concentrate (MPC) dispersions: control (□) and nanobubble treated (◊) MPC dispersions with their microstructure from confocal laser scanning microscopy (Babu and Amamcharla 2021a).

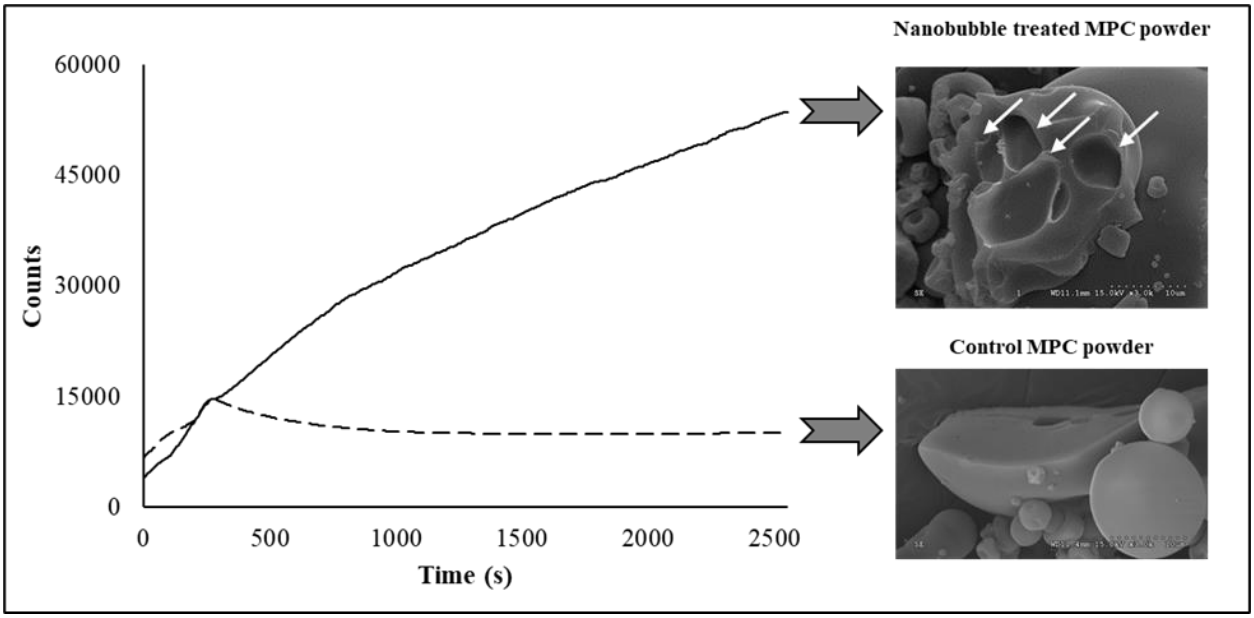

Figure 2.5 Changes in fine (<10 μm) counts obtained from data collected using the focused beam reflectance measurement for the spray dried control (--) and nanobubble treated (-) milk protein concentrate powders at a dissolution temperature of 20ºC. Scanning electron micrographs (× 3000) of spray dried milk protein concentrate powders: control and nanobubble treated (Babu and Amamcharla 2021a).

Fouling control

Because of their excellent mass transfer efficiency, NBs cab be helpful to prevent membrane fouling. (Wu et al. 2008; Ghadimkhani, Zhang, and Marhaba 2016). Cleaning chemicals containing NBs can be used to prevent surface fouling as well as to defoul surfaces. Recent studies show that NBs as a cleaning agent are gaining popularity. Wu et al. (2008) reported that NBs generated via electric current were used to clean fouled surfaces and it minimized fouling of surfaces. The NBs produced on pyrolytic graphite surfaces electrochemically were employed to remove proteins which were previously been adsorbed to the surface. In the first treatment cycle, NBs removed 20% of the of bovine serum albumin from the stainless-steel surface, and by the fourth cycle, >60% of the of bovine serum albumin had been removed. The NBs, they reported, act out as a physical barrier to adsorption, thereby reducing the coverage of bovine serum albumin. Chen et al. (2009) evaluated the use of NBs generated by electrodialysis as cleaning agents for stainless-steel surfaces and found that when NBs were added to the cleaning water, protein removal increased by more than 7%. Liu, Wu, and Craig (2008) observed that the electrochemically generated NBs were effective in cleaning the adsorbed bovine serum albumin effectively on both the hydrophilic and hydrophobic surfaces. When compared to the hydrophilic surface, the NBs were more effective for the hydrophobic surface, requiring only two cycles to remove bovine serum albumin from the hydrophobic surface. The removal of bovine serum albumin from the hydrophilic surface, however, took four cycles. In ceramic membrane filtration, air NBs were utilized to prevent fouling. This was accomplished because the hydroxyl radicals bonded to the organic materials and broke them down into minute fragments, cleansing the membranes with no side effects and restoring the permeate flow to its original level (Ghadimkhani et al. 2016). Previously, Gandhi (2018) studied

the efficiency of MNB aqueous ozone as a disinfectant in the removal of *B. licheniformis* and *B. cereus* biofilm from stainless-steel surfaces. MNB aqueous ozone application had a significant log reduction of 2.43 and 3.03 $\log_{10}$ CFU/cm^2 for *B. cereus* and *B. licheniformis*, respectively.

Water treatment

Several researchers have investigated different methods for generating MBs and NBs for water treatment as it is gaining popularity. However, the complex composition of the liquid phase makes its applications challenging. Due to their large specific surface area, MNBs have a substantial potential for pollutant adsorption on the bubble surface, which has been demonstrated previously (Yoshida et al. 2008). The key reasons for MNBs' application in surface water treatment are their key properties, including negatively charged surfaces, large mass transfer efficiency, and large specific surface area. Another study used the MB ozonation under semi-batch system operation for water disinfection. It was observed that with higher ozone concentration, there was a more significant log reduction caused by the effect of inlet ozone concentration for the generated of MBs on the inactivation of *B. subtilis* spores (for an exposure time of 2 min it was 0.3 to 5-log reduction). The researchers also noted that higher solubility of ozone than oxygen resulted in a reduction in the diameter of MBs generated (Zhang, Xi, Huang, and Hu 2013). In another study, heavy metal removal was investigated using NB enriched de-ionized water by adsorption with activated carbon. This could be achieved as the NBs can act as carriers to transfer the lead ions to the activated carbon's negatively charged surface. Interestingly, it was noted that the NBs only influenced the adsorption rate but did not affect the ability of the absorbent (Kyzas et al. 2019). The potential to decontaminate water using MBs and NBs have been studied and reportedly improves the efficacy of the chemical treatment process by catalyzing the reactions of chemicals (Agarwal et al. 2011). The MNBs were also employed

for the water detoxification (Yamasaki, Sakata, and Chuhjoh 2010). Besides, the MBs and NBs with air and nitrogen can improve the activity of the anaerobic and aerobic microorganisms in a submerged membrane bioreactor. The NBs assist in the removal of pollutants such as nanoparticles, colloids, and organic or inorganic precipitates (Azevedo, Etchepare, and Rubio 2017; Etchepare et al. 2017; Calgaroto, Azevedo, and Rubio 2016). NBs coupled with the ultraviolet process significantly increased the removal efficacy of organic matter (Gao et al. 2019).

Challenges and future perspectives

Extended longevity, low rising velocity, and extremely high pressure inside the NBs are all unique characteristics of NBs. However, there is no data in many studies on whether various experimental setups were similar or different from each other. For example, in HC, the dimensions of the pipes vary between designs; the causes of such differences reflected in bubble sizes acquired by the same study team cannot be established accurately simply on data supplied in their research articles. Despite the positive results regarding the usability of NBs for food/dairy processing, the ongoing implementation of these NB technologies throughout the numerous food processing sectors must be further investigated due to the complexity of the food matrices. Furthermore, a successful NB-assisted technique demands engineering computations and method optimization, making the process more complex than traditional methods for improving processability/product performance. Strategizing NB applications by adjusting system geometry or combining different hydrodynamic/membrane NB generation approaches for specific applications might be another potential study path. Overall, the lower capital expenditures associated with replacing other methods with NB technology may be the most crucial benefit for the industrial adoption of this methodology. Further economic and engineering

research, on the other hand, may be able to solve the transitions and lead to the utilization of large-scale NB units in the food/dairy industries. Furthermore, knowledge on the possible advantages of NB integration in food systems is currently limited, but it is hoped that this will be addressed shortly. The majority of earlier studies were undertaken on the benchtop, which might explain why NB applications in many food/dairy industries have been sluggish to develop. As a result, more academic-industrial cooperation for commercial NB applications is required, as well as research into how these approaches may improve the food business must be addressed (sustainability and energy efficiency). Advances in the manufacture of NB machines can help to develop portable NB systems with the same efficacy as stationary or lab scale NB systems. In food/dairy processing plants, it is hoped that these NB generating systems will be simple to integrate into a variety of in-line applications.

Conclusion

While certain NB technologies are well-established and have been actively employed in industries for over a decade, substantial advances in understanding the principles responsible for their generation and stability have happened in recent years. Numerous NB generating methods, such as hydrodynamic cavitation, ultrasonication, electrolysis, and membrane systems, have been shown to create sufficient NBs for various purposes. Each generation process, in particular, has advantages and disadvantages. In an industrial context, their selection is divided into two categories: usefulness and cost. NBs can be monitored using a variety of techniques, including NTA in bulk aqueous media, atomic force microscope, nuclear magnetic resonance, transmission electron microscopy, and a variety of spectroscopic and analytical methods. A complete understanding of the properties of the material to be NB integrated is required in addition to monitoring the process. Rheological behavior is one of these properties, and the potential for the

temperature to alter the stability of NBs should be further examined. Microbial inactivation, dairy/food processing, product performance, fouling management, and wastewater treatment might all benefit from NB treatment in the food and dairy industries. Although significant progress has been made in understanding the NB stability and integration processes of a range of NB technologies, most of this knowledge is still confined to the lab scale. Only a few pilot studies are being carried out; however, further study is needed to completely comprehend the interaction between temperature, applied pressure, type/concentration of gas used. In addition, a more thorough research of newer NB generator designs might lead to novel uses when the systems are scaled up to an industrial scale.

Acknowledgments

This project was conducted under Kansas State Research and Extension contribution number 20-358-J.

Disclosure statement

The authors state that they have no known competing financial interests or personal ties that may have influenced the work presented in this review paper. The authors and Kansas State University do not promote the use of any specific instrumentation, and the use of company names is entirely for scientific clarification.

References

Adhikari, B. M., T. Truong, N. Bansal, and B. Bhandari. 2018. Influence of gas addition on crystallisation behaviour of lactose from supersaturated solution. *Food and Bioproducts Processing* 109:86-97.

Adhikari, B. M., T. Truong, S. Prakash, N. Bansal, and B. Bhandari. 2020. Impact of incorporation of CO2 on the melting, texture and sensory attributes of soft-serve ice cream. *International Dairy Journal* 109:104789.

Agarwal, A., W. J. Ng, and Y. Liu. 2011. Principle and applications of microbubble and nanobubble technology for water treatment. *Chemosphere* 84 (9):1175-1180.

Agarwal, A., W. J. Ng, and Y. Liu. 2013. Cleaning of biologically fouled membranes with self-collapsing microbubbles. *Biofouling* 29 (1): 69-76.

Ahmed, A. K. A., C. Sun, L. Hua, Z. Zhang, Y. Zhang, W. Zhang, and T. Marhaba. 2018. Generation of nanobubbles by ceramic membrane filters: The dependence of bubble size and zeta potential on surface coating, pore size and injected gas pressure. *Chemosphere* 203:327-335.

Alheshibri, M., and V. S. Craig. 2019. Generation of nanoparticles upon mixing ethanol and water; Nanobubbles or Not?. *Journal of Colloid and Interface Science*, 542:136-143.

Alheshibri, M., J. Qian, M. Jehannin, and V. S. Craig. 2016. A history of nanobubbles. *Langmuir* 32 (43):11086-11100.

Alshwali, H., K. Iohara, M. Taroush, G. T. J. Huang, M. Nakashima, and A. A. Azim. 2020. Nanobubble-enhanced antimicrobial agents: a promising approach for regenerative endodontics. *Journal of Endodontics*.

Amamcharla, J., B. Li, and Z. Liu. 2017. Use of micro- and nanobubbles in liquid processing. US Patent WO 2017/127636 Al filed July 27, 2017.

Azevedo, A., R. Etchepare, and J. Rubio. 2017. Raw water clarification by flotation with microbubbles and nanobubbles generated with a multiphase pump. *Water Science and Technology* 75 (10):2342-2349.

Azevedo, A., R. Etchepare, S. Calgaroto, and J. Rubio. 2016. Aqueous dispersions of nanobubbles: Generation, properties and features. *Minerals Engineering* 94:29-37.

Babu, K. S., and J. K. Amamcharla. 2018. Application of front-face fluorescence spectroscopy as a tool for monitoring changes in milk protein concentrate powders during storage. *Journal of Dairy Science*, 101 (12): 10844-10859.

Babu, K. S., and J. K. Amamcharla. 2020. Application of micro-nano-bubbles to improve the processability of milk protein concentrates. Poster presented at the American Dairy Science Association Virtual Annual Meeting, June 22–24.

Babu, K. S., and J. K. Amamcharla. 2021a. Application of bulk nanobubbles generated by acoustic cavitation to improve the processability of milk protein concentrates. Paper presented at the American Dairy Science Association Virtual Annual Meeting, July 11–14.

Babu, K. S., and J. K. Amamcharla. 2021b. Effect of bulk nanobubbles on ultrafiltration membrane performance and energy efficiency: Physiochemical properties and microstructure of the resulting retentates. (unpublished)

Babu, K. S., K. Siliveru, J. K. Amamcharla, P. V. Vadlani, and R. K. Ambrose. 2018. Influence of protein content and storage temperature on the particle morphology and flowability

characteristics of milk protein concentrate powders. *Journal of Dairy Science* 101 (8):7013-7026.

Babu, K. S., Z. Liu, and J. K. Amamcharla. 2018. Use of micro- and nano-bubbles for improving the functional properties of Greek-style yogurt. Poster presented at the American Dairy Science Association Annual Meeting, Knoxville, TN, June 24–27.

Barker, G. S., B. Jefferson, and S. J. Judd. 2002. The control of bubble size in carbonated beverages. *Chemical Engineering Science* 57 (4):565-573.

Borkent, B. M., S. de Beer, F. Mugele, and D. Lohse. 2010. On the shape of surface nanobubbles. *Langmuir* 26 (1):260-268.

Bu, X., & M. Alheshibri 2021. The effect of ultrasound on bulk and surface nanobubbles: a review of the current status. *Ultrasonics Sonochemistry* 76: 105629.

Calgaroto, S., A. Azevedo, and J. Rubio. 2016. Separation of amine-insoluble species by flotation with nano and microbubbles. *Minerals Engineering* 89:24-29.

Calgaroto, S., K. Q. Wilberg, and J. Rubio. 2014. On the nanobubbles interfacial properties and future applications in flotation. *Minerals Engineering*, 60:33-40.

Che, Z., and P. E. Theodorakis. 2017. Formation, dissolution and properties of surface nanobubbles. *Journal of Colloid and Interface Science* 487:123-129.

Chen, H., H. Mao, L. Wu, J. Zhang, Y. Dong, Z. Wu, and J. Hu. 2009. Defouling and cleaning using nanobubbles on stainless steel. *Biofouling* 25 (4):353-357.

Dhungana, P., and B. Bhandari. 2021. Development of a continuous membrane nanobubble generation method applicable in liquid food processing. *International Journal of Food Science & Technology* 56 (9):4268-4277.

Ebina, K., K. Shi, M. Hirao, J. Hashimoto, Y. Kawato, S. Kaneshiro, T. Morimoto, K. Koizumi, and H. Yoshikawa. 2013. Oxygen and air nanobubble water solution promote the growth of plants, fishes, and mice. *PLoS One* 8 (6):e65339.

Etchepare, R., A. Azevedo, S. Calgaroto, and J. Rubio. 2017. Removal of ferric hydroxide by flotation with micro and nanobubbles. *Separation and Purification Technology* 184:347-353.

Etchepare, R., H. Oliveira, M. Nicknig, A. Azevedo, and J. Rubio. 2017. Nanobubbles: Generation using a multiphase pump, properties and features in flotation. *Minerals Engineering* 112:19-26.

Ezhilarasi, P. N., Karthik, P., Chhanwal, N., & Anandharamakrishnan, C. (2013). Nanoencapsulation techniques for food bioactive components: a review. *Food and Bioprocess Technology* 6(3): 628-647.

Fang, Z., L. Wang, X. Wang, L. Zhou, S. Wang, Z. Zou, R. Tai, L. Zhang, and J. Hu. 2018. Formation and stability of surface/bulk nanobubbles produced by decompression at lower gas concentration. *The Journal of Physical Chemistry C* 122 (39):22418-22423.

Fang, Z., X. Wang, L. Zhou, L. Zhang, and J. Hu. 2020. Formation and Stability of Bulk Nanobubbles by Vibration. *Langmuir* 36 (9):2264-2270.

Ferraro, G., A. J. Jadhav, and M. Barigou. 2020. A Henry's law method for generating bulk nanobubbles. *Nanoscale* 12 (29):15869-15879.

Filipe, V., A. Hawe, and W. Jiskoot. 2010. Critical evaluation of Nanoparticle Tracking Analysis (NTA) by NanoSight for the measurement of nanoparticles and protein aggregates. *Pharmaceutical Research* 27 (5):796-810.

Fujikawa, S., R. Zhang, S. Hayama, and G. Peng. 2003. The control of micro-air-bubble generation by a rotational porous plate. *International Journal of Multiphase Flow* 29 (8):1221-1236.

Gabr, M. H., W. Okumura, H. Ueda, W. Kuriyama, K. Uzawa, and I. Kimpara. 2015. Mechanical and thermal properties of carbon fiber/polypropylene composite filled with nano-clay. *Composites Part B: Engineering* 69:94-100.

Gandhi, G. 2018. Study of high protein dairy powder (MPC80) susceptibility to fouling and efficacy of micro-nano-bubble aqueous ozone in removal of Bacillus spp. biofilms on stainless steel surfaces. Last Modified May 1, 2018. Accessed October 1, 2021. https://krex.k-state.edu/dspace/bitstream/handle/2097/38842/GaganGandhi2018.pdf?sequence=1&isAllowed=y

Gao, Y., Y. Duan, W. Fan, T. Guo, M. Huo, W. Yang, S. Zhu, and W. An. 2019. Intensifying ozonation treatment of municipal secondary effluent using a combination of microbubbles and ultraviolet irradiation. *Environmental Science and Pollution Research* 26 (21):21915-21924.

Ghaani, M. R., P. G. Kusalik, and N. J. English. 2020. Massive generation of metastable bulk nanobubbles in water by external electric fields. *Science Advances* 6 (14):eaaz0094.

Ghadimkhani, A., W. Zhang, and T. Marhaba. 2016. Ceramic membrane defouling (cleaning) by air Nano Bubbles. *Chemosphere* 146:379-384.

Global Industry Analysts. 2021. Nanomaterials - Global Market Trajectory & Analytics. Research and Markets. Accessed November 11, 2021. https://www.strategyr.com/market-report-nanomaterials-forecasts-global-industry-analysts-inc.asp

Guan, M., W. Guo, L. Gao, Y. Tang, J. Hu, and Y. Dong. 2012. Investigation on the temperature difference method for producing nanobubbles and their physical properties. *ChemPhysChem* 13 (8):2115-2118.

Guidance, D. 2011. Considering Whether an FDA-Regulated Product Involves the Application of Nanotechnology. Accessed November 11, 2021. http://www.food-label-compliance.com/Sites/5/Downloads/003-FDA-Draft-Industry-Guidance-CONSIDERING-NANOTECHNOLOGY-APPLICATIONS-14-June-2011.pdf

Gurung, A., O. Dahl, and K. Jansson. 2016. The fundamental phenomena of nanobubbles and their behavior in wastewater treatment technologies. *Geosystem Engineering* 19 (3):133-142.

Hewage, S. A., J. Kewalramani, and J. N. Meegoda. 2021. Stability of nanobubbles in different salts solutions. *Colloids and Surfaces A: Physicochemical and Engineering Aspects* 609: 125669.

Ikeura, H., F. Kobayashi, and M. Tamaki. 2011. Removal of residual pesticide, fenitrothion, in vegetables by using ozone microbubbles generated by different methods. *Journal of Food Engineering* 103 (3):345-349.

Ishida, N., T. Inoue, M. Miyahara, and K. Higashitani. 2000. Nano bubbles on a hydrophobic surface in water observed by tapping-mode atomic force microscopy. *Langmuir* 16 (16):6377-6380.

Jadhav, A. J., and M. Barigou. 2020a. Bulk Nanobubbles or Not Nanobubbles: That is the Question. *Langmuir* 36 (7):1699-1708.

Jadhav, A. J., and M. Barigou. 2020b. Response to "Comment on Bulk Nanobubbles or Not Nanobubbles: That is the Question". *Langmuir* 37 (1):596-601.

Jeevanandam, J., A. Barhoum, Y. S. Chan, A. Dufresne, and M. K. Danquah. 2018. Review on nanoparticles and nanostructured materials: history, sources, toxicity and regulations. *Beilstein journal of nanotechnology*, 9(1):1050-1074.

Jin, J., Z. Feng, F. Yang, and N. Gu. 2019. Bulk nanobubbles fabricated by repeated compression of microbubbles. *Langmuir* 35 (12):4238-4245.

Johnson, B. D., and R. C. Cooke. 1981. Generation of stabilized microbubbles in seawater. *Science* 213 (4504):209-211.

Kanematsu, W., T. Tuziuti, and K. Yasui. 2020. The influence of storage conditions and container materials on the long term stability of bulk nanobubbles—Consideration from a

perspective of interactions between bubbles and surroundings. *Chemical Engineering Science* 219:115594.

Khaira, N. M., N. A. Abd Rahmana, A. S. Baharuddina, H. S. Hafidb, and M. Wakisakab. 2020. Capturing the impact of nanobubble liquid in enhancing the physical quality of ice cream. *Journal of Agricultural and Food Engineering*. 2:0012.

Khaire, R. A., and P. R. Gogate. 2021. Application of hydrodynamic cavitation in food processing. *In Design and Optimization of Innovative Food Processing Techniques Assisted by Ultrasound*. Academic Press.

Kikuchi, K., A. Ioka, T. Oku, Y. Tanaka, Y. Saihara, and Z. Ogumi. 2009. Concentration determination of oxygen nanobubbles in electrolyzed water. *Journal of Colloid and Interface Science* 329 (2):306-309.

Kikuchi, K., S. Nagata, Y. Tanaka, Y. Saihara, and Z. Ogumi. 2007. Characteristics of hydrogen nanobubbles in solutions obtained with water electrolysis. *Journal of Electroanalytical Chemistry*, 600(2), 303-310.

Kikuchi, K., Y. Tanaka, Y. Saihara, M. Maeda, M. Kawamura, and Z. Ogumi. 2006. Concentration of hydrogen nanobubbles in electrolyzed water. *Journal of Colloid and Interface Science* 298 (2):914-919.

Kim, J. Y., M. G. Song, and J. D. Kim. 2000. Zeta potential of nanobubbles generated by ultrasonication in aqueous alkyl polyglycoside solutions. *Journal of Colloid and Interface Science* 223 (2):285-291.

Kobayashi, F., H. Ikeura, M. Tamaki, and Y. Hayata. 2009. Application of CO_2 micro-and nano-bubbles at lower pressure and room temperature to inactivate microorganisms in Cut wakegi (Allium wakegi Araki). In Southeast Asia Symposium on Quality and Safety of Fresh and Fresh-Cut Produce 875 (pp. 417-424).

Kobayashi, H., S. Maeda, M. Kashiwa, and T. Fujita. 2014. Measurement and identification of ultrafine bubbles by resonant mass measurement method. *In OPC '14: Proc. SPIE 9232, International Conference on Optical Particle Characterization* (9232): 92320S.

Kukizaki, M. 2009. Microbubble formation using asymmetric Shirasu porous glass (SPG) membranes and porous ceramic membranes—A comparative study. *Colloids and Surfaces A: Physicochemical and Engineering Aspects* 340 (1-3):20-32.

Kukizaki, M., and M. Goto. 2006. Size control of nanobubbles generated from Shirasu-porous-glass (SPG) membranes. *Journal of Membrane Science* 281 (1-2):386-396.

Kyzas, G. Z., G. Bomis, R. I. Kosheleva, E. K. Efthimiadou, E. P. Favvas, M. Kostoglou, and A. C. Mitropoulos. 2019. Nanobubbles effect on heavy metal ions adsorption by activated carbon. *Chemical Engineering Journal* 356:91-97.

Li, H., A. Afacan, Q. Liu, and Z. Xu. 2015. Study interactions between fine particles and micron size bubbles generated by hydrodynamic cavitation. *Minerals Engineering* 84:106-115.

Liu, G., Z. Wu, and V. S. Craig. 2008. Cleaning of protein-coated surfaces using nanobubbles: an investigation using a quartz crystal microbalance. *The Journal of Physical Chemistry C*, 112 (43):16748-16753.

Liu, H., and G. Cao. 2016. Effectiveness of the Young-Laplace equation at nanoscale. *Scientific Reports* 6:23936.

Liu, S., M. Enari, Y. Kawagoe, Y. Makino, and S. Oshita. 2012. Properties of the water containing nanobubbles as a new technology of the acceleration of physiological activity. *Chemical Engineering Science* 93:250-256.

Liu, S., Y. Kawagoe, Y. Makino, and S. Oshita. 2013. Effects of nanobubbles on the physicochemical properties of water: The basis for peculiar properties of water containing nanobubbles. *Chemical Engineering Science* 93:250-256.

Lou, S. T., Z. Q. Ouyang, Y. Zhang, X. J. Li, J. Hu, M. Q. Li, and F. J. Yang. 2000. Nanobubbles on solid surface imaged by atomic force microscopy. *Journal of Vacuum Science and Technology B: Microelectronics and Nanometer Structures Processing, Measurement, and Phenomena* 18 (5):2573-2575.

Lu, Y. H., C. W. Yang, and I. S. Hwang. 2012. Molecular layer of gas like domains at a hydrophobic–water interface observed by frequency-modulation atomic force microscopy. *Langmuir* 28 (35):12691-12695.

Luo, L., and H. S. White. 2013. Electrogeneration of single nanobubbles at sub-50-nm-radius platinum nanodisk electrodes. *Langmuir* 29 (35):11169-11175.

Maoming, F. A. N., T. A. O. Daniel, R. Honaker, and L. U. O. Zhenfu. 2010. Nanobubble generation and its application in froth flotation (part I): nanobubble generation and its effects on properties of microbubble and millimeter scale bubble solutions. *Mining Science and Technology (China)* 20 (1):1-19.

McSweeney, D. J., V.Maidannyk, J. A O'Mahony, and N. A. McCarthy. 2021. Influence of nitrogen gas injection and agglomeration during spray drying on the physical and bulk handling properties of milk protein concentrate powders. *Journal of Food Engineering* 293: 110399.

Mech, A., W. Wohlleben, A. Ghanem, V. D. Hodoroaba, S. Weigel, F. Babick, R. Brüngel, C.M. Friedrich, K. Rasmussen, and H. Rauscher. 2020. Nano or Not Nano? A Structured Approach for Identifying Nanomaterials According to the European Commission's Definition. *Small* 16 (36):2002228.

Meegoda, J. N., S. Aluthgun Hewage, and J. H. Batagoda. 2018. Stability of nanobubbles. *Environmental Engineering Science* 35 (11):1216-1227.

Michailidi, E. D., G. Bomis, A. Varoutoglou, G. Z. Kyzas, G. Mitrikas, A. C. Mitropoulos, E. K. Efthimiadou, and E. P. Favvas. 2020. Bulk nanobubbles: Production and investigation of their formation/stability mechanism. *Journal of Colloid and Interface Science* 564:371-380.

Millare, J. C., and B. A. Basilia 2018. Nanobubbles from Ethanol-Water Mixtures: Generation and Solute Effects via Solvent Replacement Method. *ChemistrySelect* 3 (32):9268-9275.

Mo, C. R., J. Wang, Z. Fang, L. M. Zhou, L. J. Zhang, and J. Hu. 2018. Formation and stability of ultrasonic generated bulk nanobubbles. *Chinese Physics B 27*(11): 118104.

Moejes, S. N., and A. J. B. Van Boxtel. 2017. Energy saving potential of emerging technologies in milk powder production. *Trends in Food Science & Technology* 60 :31-42.

Nile, S.H., V. Baskar, D. Selvaraj, A. Nile, J. Xiao, and G. Kai. 2020. Nanotechnologies in food science: Applications, recent trends, and future perspectives. *Nano-Micro Letters* 12:45.

Nirmalkar, N., A. W. Pacek, and M. Barigou. 2018a. On the existence and stability of bulk nanobubbles. *Langmuir* 34 (37):10964-10973.

Nirmalkar, N., A. W. Pacek, and M. Barigou. 2018b. Interpreting the interfacial and colloidal stability of bulk nanobubbles. *Soft Matter* 14 (47):9643-9656.

Nussinovitch, A., R. Velez-Silvestre, and M. Peleg. 1992. Mechanical properties of hydrocolloid gels filled with internally produced CO_2 gas bubbles. *Biotechnology Progress* 8 (5):424-428.

Oh, S. H., and J. M. Kim. 2017. Generation and stability of bulk nanobubbles. *Langmuir* 33 (15):3818-3823.

Oh, S. H., S. H. Yoon, H. Song, J. G. Han, and J. M. Kim. 2013. Effect of hydrogen nanobubble addition on combustion characteristics of gasoline engine. *International Journal of Hdrogen Energy* 38 (34):14849-14853.

Ohgaki, K., N. Q. Khanh, Y. Joden, A. Tsuji, and T. Nakagawa. 2010. Physicochemical approach to nanobubble solutions. *Chemical Engineering Science* 65 (3):1296-1300.

Oliveira, H., A. Azevedo, and J. Rubio. 2018. Nanobubbles generation in a high-rate hydrodynamic cavitation tube. *Minerals Engineering* 116:32-34.

Panchal, J., J. Kotarek, E. Marszal, and E. M. Topp. 2014. Analyzing subvisible particles in protein drug products: a comparison of dynamic light scattering (DLS) and resonant mass measurement (RMM). *The AAPS Journal* 16 (3):440-451.

Parker, J. L., P. M. Claesson, and P. Attard. 1994. Bubbles, cavities, and the long-ranged attraction between hydrophobic surfaces. *The Journal of Physical Chemistry* 98 (34):8468-8480.

Patil, M. H., G. Tanguy, C. L. Floch-Fouéré, R. Jeantet, and E. G. Murphy. 2021. Energy usage in the manufacture of dairy powders: Advances in conventional processing and disruptive technologies. *Drying Technology* 1-19.

Patois, E., M. A. H. Capelle, C. Palais, R. Gurny, and T. Arvinte. 2012. Evaluation of nanoparticle tracking analysis (NTA) in the characterization of therapeutic antibodies and seasonal influenza vaccines: pros and cons. *Journal of Drug Delivery Science and Technology* 22 (5):427-433.

Peng, H., M. A. Hampton, and A. V. Nguyen. 2013. Nanobubbles do not sit alone at the solid–liquid interface. *Langmuir* 29 (20):6123-6130.

Phan, K. K. T., T. Truong, Y. Wang, and B. Bhandari. 2020. Nanobubbles: Fundamental characteristics and applications in food processing. *Trends in Food Science and Technology* 95:118-130.

Phan, K. K. T., T. Truong, Y. Wang, and B. Bhandari. 2021a. Formation and Stability of Carbon Dioxide Nanobubbles for Potential Applications in Food Processing. *Food Engineering Reviews* 13 (1):3-14.

Phan, K., T. Truong, Y. Wang, and B. Bhandari. 2021b. Effect of CO_2 nanobubbles incorporation on the viscosity reduction of fruit juice concentrate and vegetable oil. *International Journal of Food Science & Technology* 56 (9):4278-4286.

Phan, K., T. Truong, Y. Wang, and B. Bhandari. 2021c. Effect of electrolytes and surfactants on generation and longevity of carbon dioxide nanobubbles. *Food Chemistry* 363: 130299.

Postnikov, A. V., I. V. Uvarov, N. V. Penkov, and V. B. Svetovoy. 2018. Collective behavior of bulk nanobubbles produced by alternating polarity electrolysis. *Nanoscale* 10 (1):428-435.

Qiu, J., Z. Zou, S. Wang, X. Wang, L. Wang, Y. Dong, H. Zhao, L. Zhang, and J. Hu. 2017. Formation and Stability of Bulk Nanobubbles Generated by Ethanol–Water Exchange. *ChemPhysChem* 18 (10):1345-1350.

Rak, D., and M. Sedlák. 2020. Comment on "Bulk Nanobubbles or Not Nanobubbles: That is the Question". *Langmuir* 36 (51):15618-15621.

Rak, D., M. Ovadová, and M. Sedlák. 2019. (Non) existence of bulk nanobubbles: the role of ultrasonic cavitation and organic solutes in water. *The journal of physical chemistry letters* 10 (15):4215-4221.

Ruckenstein, E. 2013. Nanodispersions of bubbles and oil drops in water. *Colloids and Surfaces A: Physicochemical and Engineering Aspects*, 423:112-114.

Saint-Eve, A., I. Déléris, G. Feron, D. Ibarra, E. Guichard, and I. Souchon. 2010. How trigeminal, taste and aroma perceptions are affected in mint-flavored carbonated beverages. *Food Quality and Preference* 21 (8):1026-1033.

Schaming, D., and H. Remita. 2015. Nanotechnology: from the ancient time to nowadays. *Foundations of Chemistry* 17 (3):187-205.

Seddon, J. R., H. J. Zandvliet, and D. Lohse. 2011. Knudsen gas provides nanobubble stability. *Physical Review Letters* 107 (11):116101.

Singh, A., A. S. Sekhon, P. Unger, M. Babb, Y. Yang, and M. Michael. 2020. Impact of gas micro-nano-bubbles on the efficacy of commonly used antimicrobials in the food industry. *Journal of Applied Microbiology* 130 (4):1092-1105.

Singla, M., and N. Sit. 2021. Application of ultrasound in combination with other technologies in food processing: A review. *Ultrasonics Sonochemistry* 105506.

Soli, K. W., A. Yoshizumi, A. Motomatsu, M. Yamakawa, M. Yamasaki, T. Mishima, N. Miyaji, K.I. Honjoh, and T. Miyamoto. 2010. Decontamination of fresh produce by the use of slightly acidic hypochlorous water following pre-treatment with sucrose fatty acid ester under microbubble generation. *Food Control* 21 (9):1240-1244.

Takahashi, M. 2005. ζ potential of microbubbles in aqueous solutions: electrical properties of the gas− water interface. *The Journal of Physical Chemistry B* 109 (46):21858-21864.

Tan, B. H., H. An, and C. D. Ohl. 2020. How Bulk Nanobubbles Might Survive. *Physical Review Letters*, 124 (13):134503.

Tanaka, S., H. Kobayashi, S. Ohuchi, K. Terasaka, and S. Fujioka. 2021. Destabilization of ultrafine bubbles in water using indirect ultrasonic irradiation. *Ultrasonics Sonochemistry 71*: 105366.

Tao, D., Yu, S., Zhou, X., Honaker, R. Q., and B. K. Parekh. 2008. Picobubble column flotation of fine coal. *International Journal of Coal Preparation and Utilization* 28 (1):1-14.

Temesgen, T., T. T. Bui, M. Han, T. I. Kim, and H. Park. 2017. Micro and nanobubble technologies as a new horizon for water-treatment techniques: A review. *Advances in Colloid and Interface Science* 246:40-51.

Theodorakis, P. E., and Z. Che. 2019. Surface nanobubbles: Theory, simulation, and experiment. A review. *Advances in colloid and interface science* 272:101995.

Tsuge, H. 2014. Micro-and Nanobubbles: Fundamentals and Applications. CRC press.

Tyrrell, J. W., and P. Attard. 2001. Images of nanobubbles on hydrophobic surfaces and their interactions. *Physical Review Letters* 87 (17):176104.

Uchida, T. K. Yamazaki, and K. Gohara. 2016. Generation of micro-and nano-bubbles in water by dissociation of gas hydrates. *Korean Journal of Chemical Engineering* 33 (5):1749-1755.

Uchida, T., S. Liu, M. Enari, S. Oshita, K. Yamazaki, and K. Gohara. 2016. Effect of NaCl on the lifetime of micro-and nanobubbles. *Nanomaterials* 6 (2):31.

Ulatowski, K., and P. Sobieszuk. 2018. Influence of liquid flowrate on size of nanobubbles generated by porous-membrane modules. *Chemical and Process Engineering* 39 (3):335-345.

Ushikubo, F. Y., T. Furukawa, R. Nakagawa, M. Enari, Y. Makino, Y. Kawagoe, T. Shiina, and S. Oshita. 2010. Evidence of the existence and the stability of nano-bubbles in water. *Colloids and Surfaces A: Physicochemical and Engineering Aspects* 361 (1-3):31-37.

Walczyk, W., N. Hain, and H. Schönherr. 2014. Hydrodynamic effects of the tip movement on surface nanobubbles: a combined tapping mode, lift mode and force volume mode AFM study. *Soft Matter* 10 (32):5945-5954.

Wang, Q., H. Zhao, N. Qi, Y. Qin, X. Zhang, and Y. Li. 2019. Generation and stability of size-Adjustable Bulk Nanobubbles Based on periodic pressure Change. *Scientific Reports* 9 (1):1-9.

Wilder, A. J. 2016. Evaluation of a novel commercial ground beef production system using a chlorinated nanobubble antimicrobial technology to control Shiga toxin-producing Escherichia coli and Salmonella spp. surrogates. Last Modified December 1, 2016. Accessed October 1, 2021. https://krex.k-state.edu/dspace/bitstream/handle/2097/34534/AmandaWilder2016.pdf?sequence=1

Wu, C., K. Nesset, J. Masliyah, and Z. Xu. 2012. Generation and characterization of submicron size bubbles. *Advances in Colloid and Interface Science* 179:123-132.

Wu, Z., H. Chen, Y. Dong, H. Mao, J. Sun, S. Chen, V.S. Craig, and J. Hu. 2008. Cleaning using nanobubbles: defouling by electrochemical generation of bubbles. *Journal of Colloid and Interface Science* 328 (1): 10-14.

Xiong, Y., and F. Peng. 2015. Optimization of cavitation venturi tube design for pico and nano bubbles generation. *International Journal of Mining Science and Technology* 25 (4):523-529.

Yamasaki, K., K. Sakata, and K. Chuhjoh. 2010. Water treatment method and water treatment system. US Patent 7,662,288 filed September 28, 2006, and issued February 16, 2010.

Yang, C. W., Y. H. Lu, and S. Hwang. 2013. Imaging surface nanobubbles at graphite–water interfaces with different atomic force microscopy modes. *Journal of Physics: Condensed Matter* 25 (18):184010.

Yang, S., and A. Duisterwinkel. 2011. Removal of nanoparticles from plain and patterned surfaces using nanobubbles. *Langmuir* 27 (18):11430-11435.

Yasuda, K., H. Matsushima, and Y. Asakura. 2019. Generation and reduction of bulk nanobubbles by ultrasonic irradiation. *Chemical Engineering Science* 195:455-461.

Yasui, K., T. Tuziuti, and W. Kanematsu. 2018. Mysteries of bulk nanobubbles (ultrafine bubbles); stability and radical formation. *Ultrasonics Sonochemistry* 48:259-266.

Yoshida, A., O. Takahashi, Y. Ishii, Y. Sekimoto, and Y. Kurata. 2008. Water purification using the adsorption characteristics of microbubbles. *Japanese Journal of Applied Physics* 47(8R):6574.

Zhang, F., J. Xi, J. J. Huang, and H. Y. Hu. 2013. Effect of inlet ozone concentration on the performance of a micro-bubble ozonation system for inactivation of Bacillus subtilis spores. *Separation and Purification Technology*, 114:126-133.

Zhang, M., and J. R. Seddon. 2016. Nanobubble–nanoparticle interactions in bulk solutions. *Langmuir* 32 (43):11280-11286.

Zhang, X. H., N. Maeda, and V. S. Craig. 2006. Physical properties of nanobubbles on hydrophobic surfaces in water and aqueous solutions. *Langmuir* 22 (11):5025-5035.

Zhu, J., H. An, M. Alheshibri, L. Liu, P. M. Terpstra, G. Liu, and V. S. Craig. 2016. Cleaning with bulk nanobubbles. *Langmuir* 32 (43):11203-11211.

Zhu, Z., D. W. Sun, Z. Zhang, Y. Li, and L. Cheng. 2018. Effects of micro-nano bubbles on the nucleation and crystal growth of sucrose and maltodextrin solutions during ultrasound-assisted freezing process. *LWT- Food Science and Technology* 92:404-411.

Zúñiga, R. N., and J. M. Aguilera. 2009. Structure–fracture relationships in gas-filled gelatin gels. *Food Hydrocolloids* 23 (5):1351-1357.

Chapter 3 - Application of micro- and nano-bubbles to improve the processability of milk protein concentrates[1]

Abstract

Micro- and nano-bubbles (MNB) have unique properties and have attracted great attention in the past two decades, offering prospective applications in various disciplines. The first objective of this study was to confirm the venturi-style MNB generation is capable of producing sufficient bulk MNBs. Nanoparticle tracking system was used to measure the bubble concentration and particle size of MNB-treated deionized water. MNB-treated deionized water had a bubble concentration of 3.76×10^8 particles/mL (~350 million bubbles/mL more compared to control) and a mean particle size of 249.8 nm. The second objective of this study was to investigate the effect of MNB treatment on the microstructure and functional properties of milk protein concentrate (MPC) dispersions. Reconstituted MPC dispersions (21%, w/w) without air injection was considered as control (C-MPC) and MPC dispersions passed through the MNB system was considered as MNB-treated (MNB-MPC) dispersions. C-MPC and MNB-MPC dispersions were evaluated in terms of rheological behavior and microstructure. The microscopic observations of MNB-MPC dispersions showed less aggregated microstructures and greater structural differences when compared to C-MPC dispersions, therefore lowering the viscosity. The viscosity of MNB-MPC at a shear rate of 100 s^{-1} significantly decreased ($P < 0.05$) to 57.58 mPa·s (C-MPC: 162.40 mPa·s), a net decrease in viscosity by ~65% after MNB treatment. Additionally, MPC dispersions were spray dried after the MNB treatment and the resultant MNB-MPC powders were characterized and compared with the control MPCs in terms of

[1]Published: Journal of Dairy Science (https://doi.org/10.3168/jds.2021-21341)

rehydration characteristics and microstructure. Focused beam reflectance measurement of the MNB-MPC powders indicated lower counts of large particles (150-300 μm) during dissolution, signifying MNB-MPC powders exhibited better rehydration properties than the C-MPC powders. This study, therefore, recommends the possibility of using MNB treatment for more efficient drying while improving the functional properties of the resultant MPC powders.

Introduction

Application of micro- and nano-scaled materials are constantly evolving, and they have the outstanding possibility of bringing significant advantages in various manufacturing sectors. Nanostructured materials are defined to be of diameters in the range of 1 to 100 nm. However, a single internationally accepted definition for nanomaterials does not exist (Jeevanandam et al., 2018). The last two decades have seen substantial academic and industrial interest in investigations on the unique properties of both microbubbles and ultrafine bubbles or nanobubbles (NBs). Generally, microbubbles range from 10-50 μm and bubbles with a particle size of <200 nm are typically referred to as NBs (Temesgen et al., 2017). Previously, Agarwal et al. (2011) presented the name micro- and nano-bubbles (MNBs), although a clear category for NBs and MNBs is still unclear. MNBs are tiny bubbles with diameters ranging from hundreds of nanometers to several tens of micrometers. MNBs are gaining interest due to their wide range of applications in many fields of science and technology. MNBs exhibit high internal pressures, high gas solubility, and large surface-to-volume ratio. The physical properties of MNBs are different from those of milli-scaled bubbles and the MNBs are stable for considerably long periods. MNBs have shown stability even for two weeks, and clusters of NBs could further increase their stability (Azevedo et al., 2016; Weijs et al., 2011). The core application areas of MNBs include wastewater treatment, agriculture, aquaculture, and medical application. Recently,

Amamcharla et al. (2017) and Phan et al. (2020) have outlined applications of MNBs in various food and dairy processing applications. There are various techniques available for the generation of MNBs, including venturi-style MNB generator. The venturi-style generator has attracted much attention industrially as well as in research fields due to its simplicity, high efficiency, low energy consumption, and the ease of scale up (Fan et al., 2010; Agarwal et al., 2011; Ahmadi et al., 2014). Overall, there is only limited literature available on the effect of MNBs on the performance and structural properties of different food and dairy systems. Spray drying is a widely used unit operation for the manufacture of dairy powders; however, it is very energy-intensive process. Therefore, technological approaches to better optimize the process are critical from a sustainability standpoint. Chamberland et al. (2020) reported that pre-concentrating cheese whey and milk ultrafiltered permeate to 20% and 22% w/w dry matter, respectively, by reverse osmosis prior to evaporation reduced the natural gas and electricity consumption by 36% and 10%, respectively. Remarkably, Fox et al. (2010) reported that an increase in just 2% dry matter could achieve 6% energy reduction. However, viscosity is a significant concern while increasing dry matter content in spray drying feed concentrate. Therefore, an innovative approach to reduce the viscosity of high-solid milk concentrates could be a promising step to higher energy savings.

Milk protein concentrate (MPC) powders are ideal ingredients for a wide range of applications, such as in beverages, yogurt, cheeses, nutritional formulations, and protein bars due to their high protein content, low lactose content, high buffering capacity, pleasant milk flavor profile, and other functional properties (Agarwal et al., 2015). However, rehydration characteristics in MPC powders are influenced by protein contents (Babu and Amamcharla, 2021) and powder properties, such as surface and bulk composition (Crowley et al., 2014),

rehydration conditions (Crowley et al., 2015), particle morphology (Babu et al., 2018a), and storage (Babu and Amamcharla 2018). Several studies demonstrated that MPC powders exhibit poor solubility over extended storage time due to changes in the physicochemical interactions of the proteins (Anema et al., 2006; Havea, 2006). Numerous studies have investigated ways to improve its rehydration behavior via tailoring the behavior of milk components, through alteration of the ionic environment of the MPC dispersions (Marella et al., 2015), addition of whey proteins (Gaiani et al., 2007), and using lecithin nanovesicles (Bansal et al., 2017). Additionally, employing various engineering techniques have also shown to improve the solubility of MPC powders: static high-pressure treatment (Udabage et al., 2012), high-intensity ultrasonication (McCarthy et al., 2014), high-shear treatment (Augustin et al., 2012), extrusion porosification (Bouvier et al., 2013), hydrodynamic cavitation (Li et al., 2018), and nitrogen gas injection (McSweeney et al., 2021). Kosasih et al. (2016) studied the influence of CO_2 on the physical and functional properties of whole milk powder and reported increased dispersibility, powder porosity, and occluded air content. Application of CO_2 MNBs significantly decreased the scooping hardness and melting rate of soft-serve ice cream, and also enhanced the overall acceptability of soft-serve ice cream (Adhikari et al., 2020). Previously, McSweeney et al. (2021) observed better rehydration behavior of N_2 injected MPC powders. The influence of CO_2 injection on the physical and functional properties of whole milk powder has been described by Kosasih et al. (2016). They noted that CO_2 injection prior to spray drying increased powder dispersibility, porosity, and occluded air content. Hanrahan et al. (1962) examined the impact of N_2 injection into whole milk concentrate before spray drying and described an increase in dispersibility and powder particle size. However, limited research has been implemented regarding the use of gas injection to modify powder particle structure and improve the

subsequent flow properties of high-protein dairy ingredients. The effect of MNBs on the physical properties of high-protein powders has not been previously investigated but may assist the manufacture of MPC powders with improved flow behavior.

In the present work, we are exploring the possibility of MNB treatment to improve the processability and rehydration properties of MPCs. This study aims to i) characterize the MNBs generated by venturi-based air injection method in deionized (DI) water in terms of bubble concentration and mean diameter; ii) evaluate the effect of MNB on rheology and microstructure of MPC dispersions; and iii) investigate the rehydration, microstructure, morphology, and flow properties of MNB-treated MPC powders.

Materials and Methods

Development of MNB generation system

A laboratory scale MNB generation system was designed and assembled at Kansas State University and a schematic diagram of the experimental set-up is shown in Figure 3.1. A venturi injector (Hydra-Flex, Savage, MN) was used to generate bulk MNBs. The custom-built MNB system was connected to a Flowjet duplex diaphragm pump (Xylem, Model: D3835H5011A, Irvine, CA) with a flow rate of 2 gallons/min. The size of the bubbles was controlled by adjusting the airflow through the MNB injector using the air flow meter 4140 (TSI, Shoreview, MN).

Characterization of bulk MNBs in water

The existence of MNB remains as a puzzling and trending topic mainly due to their exceptional longevity and other extraordinary properties that are investigated by many research groups worldwide (Jadhav and Barigou, 2020). In this study, a nanoparticle tracking analyzer (NTA) was used to measure MNB concentration and MNB mean diameter. NTA measurements

were carried out using the Malvern NanoSight LM10 (NanoSight, Amesbury, United Kingdom) equipped with a sample chamber with a 640 nm laser. Before experimentation, control DI water was initially examined for any nanoscale entities using the NTA. The Control- and MNB-incorporated DI water was characterized in terms of size and concentration using the NTA system. The samples were then injected into the chamber until the sample reached the tip of the nozzle using sterile syringes (BD Discardit II, Franklin Lakes, NJ). All measurements were done at room temperature. NTA software tracks the particles individually and uses the Stokes-Einstein equation to calculate the hydrodynamic diameter of the particles. The NTA software also records a video file to visualize the differences in the dispersion of particles and simultaneously identifies and tracks each particle on a frame-by-frame basis.

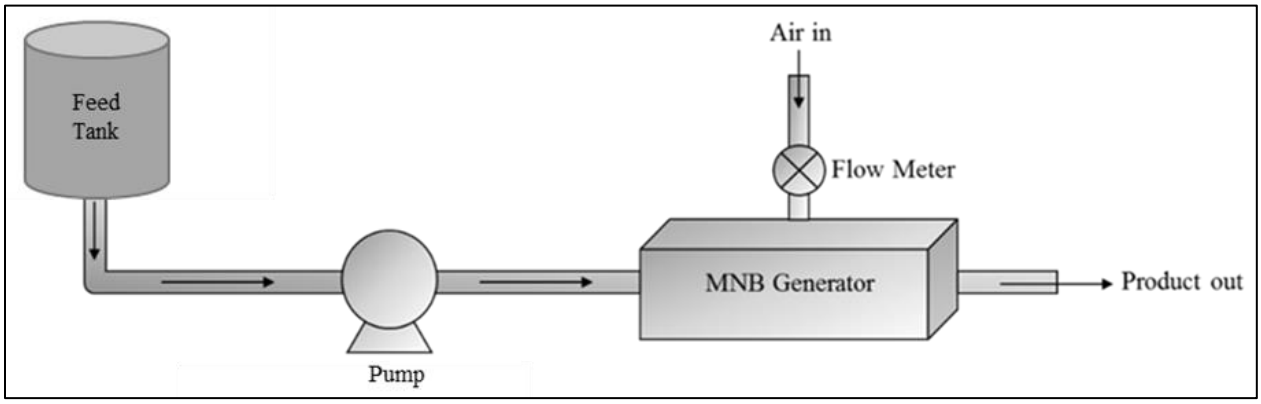

Figure 3.1 Schematic diagram of the experimental set-up.

Characterization of MPC dispersions containing bulk MNBs

The MPC dispersions were prepared in the laboratory using two lots of MPC powder with 85% protein content (MPC85) obtained from a commercial dairy ingredient supplier within the USA. The average protein, moisture, fat, lactose, and ash content of the MPC85 used for this study was 86.85% (w/w), 5.25% (w/w), 0.93% (w/w), 4.79% (w/w) and 6.68% (w/w), respectively. MPC dispersions of 21% (w/w) total solids were prepared by gradually adding 420

g of MPC powder to 1580 g DI water maintained at 45ºC using a water bath (Fisher Scientific, Pittsburgh, PA, USA). Subsequently, the MPC dispersions were stored overnight at 4°C to ensure complete rehydration. After overnight hydration, the MPC dispersions were taken out and all the treatments were done at room temperature. Control MPC dispersions (C-MPC; pumped through the diaphragm pump without MNB treatment) and MNB-treated MPC dispersions (MNB-MPC; MNB-treated using the custom-built MNB system with an air injection at 0.008L/min) were characterized using the NTA, rheological measurements, and microstructure. C-MPC and MNB-MPC dispersions contained 21.58 ± 1.07 and 21.61 ± 0.20% (w/w) total solids content, respectively. Additionally, the C-MPC and MNB-MPC dispersions were spray dried and characterized using the rehydration behavior and microstructure.

NTA analysis. Casein micelles in the MPC dispersions can interfere with the measurement and in the similar size to MNBs, making the quantification of MNBs in the MPC system in terms of size and concentration less realistic. The C-MPC and MNB-MPC dispersions were characterized in terms of concentration and size using the NTA system. Since a greater dilution was required to test it using the NanoSight, C-MPC and MNB-MPC dispersions were serially diluted to achieve 1: 50,000 dilution.

Rheological measurements. The viscosity of C-MPC and MNB-MPC dispersions were measured at 20ºC using a stress-strain-controlled rheometer (MCR-92 Anton Paar, Vernon Hills, IL) equipped with a 50 mm diameter stainless steel cone with angle 1° and 101 μm gap. Flow curves were analyzed at shear rates between 0.1 and 100 s^{-1}. The data obtained were fitted to the power-law model to obtain the consistency coefficient and flow behavior index.

Microstructure. The microstructure of C-MPC and MNB-MPC dispersions were studied using confocal laser scanning microscopy (CLSM), following the method described by Gandhi et

al. (2017). Samples were prepared for CLSM by diluting 1:100 using DI water before measurements. Proteins were stained using the Fast green FCF (Sigma-Aldrich, St. Louis, MO) stain. Stock solution of Fast green (5 mg dye in 5 mL water) was applied to the sample for 5-10 min. The stained samples were analyzed in LSM 5 Pa (Zeiss, Thornwood, NY). Three-dimensional images were obtained by scanning the sample across a defined section along the z-axis.

Transmission electron microscopy (TEM) was also used to image C-MPC and MNB-MPC dispersions in order to illustrate the differences in microstructure. Samples were analyzed using negative-staining technique. The dispersions were diluted at 1:100 with DI water. One drop of the diluted sample was mounted on Formvar/carbon-coated 200-mesh copper grids (Electron Microscopy Sciences, Fort Washington, PA) for 2 min. Subsequently, it was combined with a drop of 2% uranyl acetate, left for 30 s, the excess liquid was wiped off with a filter paper, and was examined using a CM 100 TEM (FEI Company, Hillsboro, OR) operating at 100 kV and images captured with a digital camera (model C8484, Hamamatsu, Bridgewater, NJ) using the AMT software (Advanced Microscopy Techniques, Chazy, NY).

Characterization of MPC powders

The prepared C-MPC and MNB-MPC dispersions were spray dried in a lab-scale spray dryer (YC-015, Shanghai China). The inlet temperature was set at 180ºC, and the outlet temperature ranged between 60-65ºC. The spray pressure was maintained at 30 psi, and the relative humidity of the room was periodically recorded using a digital humidity meter (Traceable Humidity Meter, Fisher Scientific, Hampton, NH). The spray-dried MPC powders were collected and sealed in Whirl-Pak bags (Nasco, Fort Atkinson, WI) for further analysis.

Rehydration behavior. The C-MPC and MNB-MPC powders were reconstituted at 5% (w/w) powder concentration in DI water, and the solubility of the powders were estimated based on the TS in the spernetant obtained by centrifugation at 700 × g for 10 min at 25°C as described by Anema et al. (2006). The amount of soluble material (σ) in the MPC was calculated using Equation 1.

$$\sigma = \frac{weight\ of\ dry\ material}{weight\ of\ solution} \times 100 \qquad (1)$$

The dissolution characteristics of the C-MPC and MNB-MPC powders were evaluated using the focused beam reflectance measurement method (Babu and Amamcharla, 2018).

Particle size analysis. The average particle size of reconstituted C-MPC and MNB-MPC powders were measured by dynamic laser light scattering using a particle size analyzer (DelsaMax PRO; Beckman Coulter, Brea, CA). C-MPC and MNB-MPC powders were reconstituted to 5% solution using DI water and were kept overnight for complete rehydration before the analysis. Samples diluted with DI water (1:100, v/v) were used to measure the particle size. Samples were equilibrated inside the instrument for 2 min and then analysis were carried out at 20ºC. Zeta potential was measured by the phase analysis light scattering method in the DelsaMax PRO.

Microstructure. The microstructure of C-MPC and MNB-MPC powders were examined using a scanning electron micrography (SEM) according to the method described by Mimouni et al. (2010). The MPC powders were directly mounted onto a carbon double-sided adhesive tape on microscopy stubs and sputter-coated with palladium using a Denton Vacuum Desk II sputter coater (Denton Vacuum, Moorestown, NJ) for 15 min to avoid the charge buildup under the electron beam. The imaging was performed using a S-3500N (Hitachi Science Systems Ltd.,

Tokyo, Japan) and was examined by a secondary electron detector operating at 10 kV. For imaging of reconstituted C-MPC and MNB-MPC powders, 5% solutions were prepared and TEM analysis were done following the same method as that of MPC dispersions.

Statistical Analysis

The MPC85 powders were procured form two lots and was treated as independent replicates. The MNB treatment trials were conducted in duplicates, with new samples prepared for each replicate. Statistical analysis of the C-MPC and MNB-MPC dispersions and resultant C-MPC and MNB-MPC powders were analyzed using PROC GLMMIX procedure of SAS (Version 9.4, SAS Institute Inc., Cary, NC). Statistical differences among means were determined with a significance level of $\alpha = 0.05$.

Results and Discussion

Characterization of bulk MNBs in water

NTA was used to test the efficiency of the custom-built MNB generation system. Figure 3.2 shows the NTA results obtained from control (not treated) and MNB-treated DI water. The Nanosight showed a significant increase in particle concentration upon MNB treatment, suggesting that the venturi injector was efficient in generating MNBs. The concentration-weighted size distribution of DI water from NTA was observed with a mode of 94.7 nm, a mean of 174.4 nm, and SD of 127 nm. The particle size distribution was D10-86.5; D50-135.6; D90-321.7 nm. Whereas, MNB-treated DI water had a mode of 170.1 nm, a mean of 249.8 nm, and SD of 115.8 nm. The particle size distribution was D10-149.2; D50-220.7; D90-388.3 nm. The concentration was found to be 1.72×10^7 and 3.76×10^8 particles/mL for DI water and MNB-treated DI water, respectively, suggesting MNB-treated DI water had ~350 Million /mL more bubbles compared to control. Ahmadi and Darban (2013) used venturi-type MNB generation

technique to generate air MNBs (gas flow rate of 0.3 L/min) and have noted a size of 130 nm, whereas Fan et al. (2010), used the venturi-style generation using CO_2 (gas concentration of 6.1 ppm) and have noted a bubble size of 529 nm. In previous studies on bulk NBs, it is proven that NBs exist and exhibits high longevity (Jadhav and Barigou, 2020). However, the lack of definite evidence whether they are indeed gaseous-bulk NBs or non-gaseous nanoparticles possesses skepticism (Alheshibri et al., 2021).

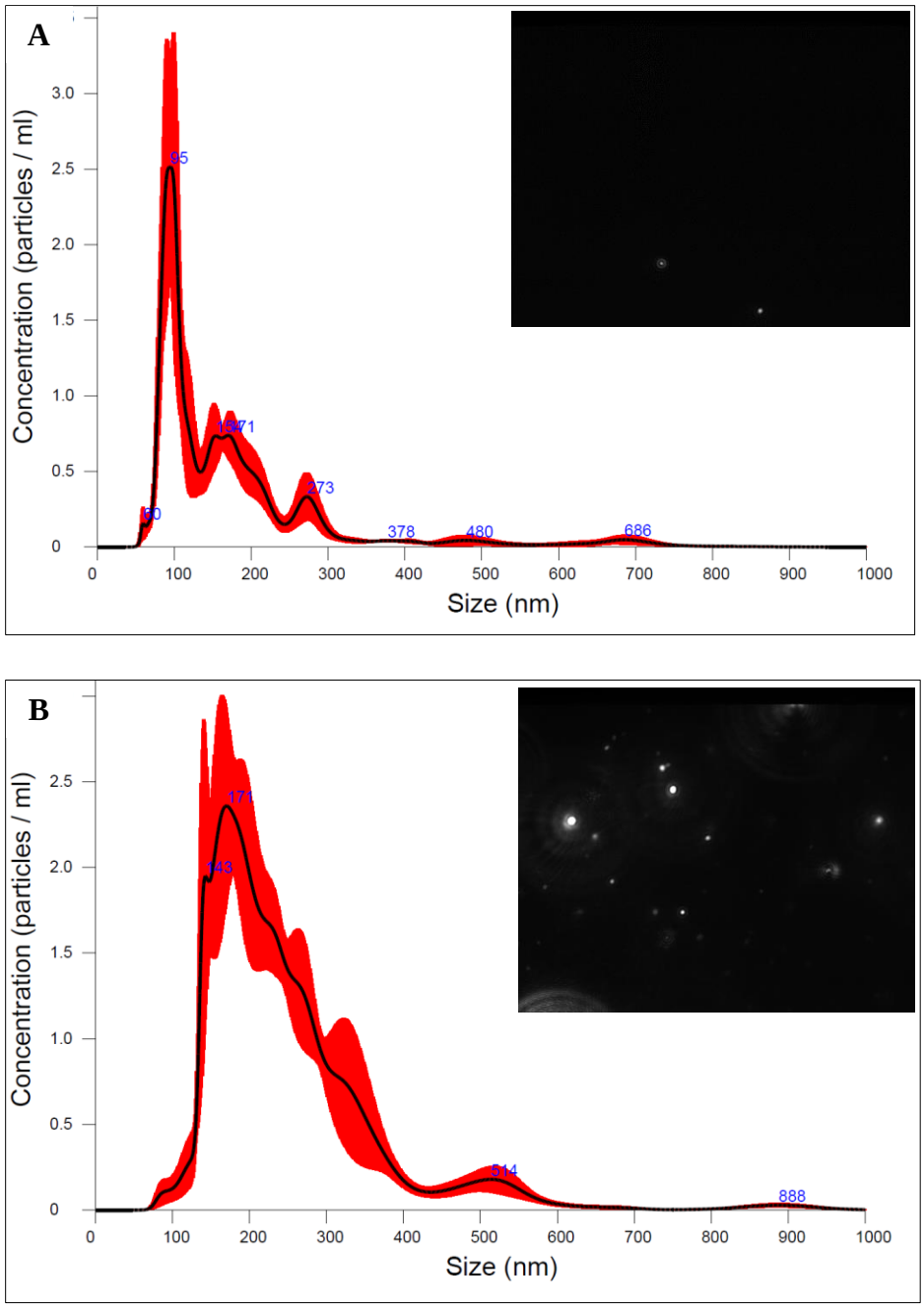

Figure 3.2 Nanoparticle tracking analysis results shown as smoothed histogram presenting average concentration and size of control (A) and micro- and nano-bubbles treated (B) deionized water with the corresponding video frame.

Characterization of MPC dispersions containing MNBs

NTA analysis. Particle size distributions in the C-MPC and MNB-MPC dispersions were also investigated by NTA, and the obtained concentration and size profiles are shown in Figures 3.3A and 3.3B. The MNB treatment resulted in a significant ($P<0.05$) decrease in particle mean diameters (211.7 ± 2.0 nm and 202 ± 2.3 nm for the C-MPC and MNB-MPC dispersions, respectively), suggesting disruption of aggregates. The particle size distribution was D10-154.5; D50-201.3; D90-285.2 nm for C-MPC dispersions. Whereas, MNB-treated MPC dispersions had a D10-148.5; D50-190.2; D90-268.3 nm. This is in line with findings in a study by Gregersen et al. (2019). They used hydrodynamic cavitation treatments to whey protein concentrate (31% dry matter) and observed a significant decrease in D10, D50, D90, and mean diameter. However, the extent of particle size reduction is associated with the initial particle size (Yanjun et al., 2014). Additionally, the particles/frame were also significant ($P<0.05$) higher for the MNB-MPC dispersions. The concentration of MNB-MPC was 3.45×10^9 particles/ml compared to 3.18×10^9 for the C-MPC. NTA provided not only quantitative information but also have provided visual information about the C-MPC and MNB-MPC dispersions. Within the field of point of view, the particles were seen moving under Brownian motion, visualized using the microscope oculars or via the camera.

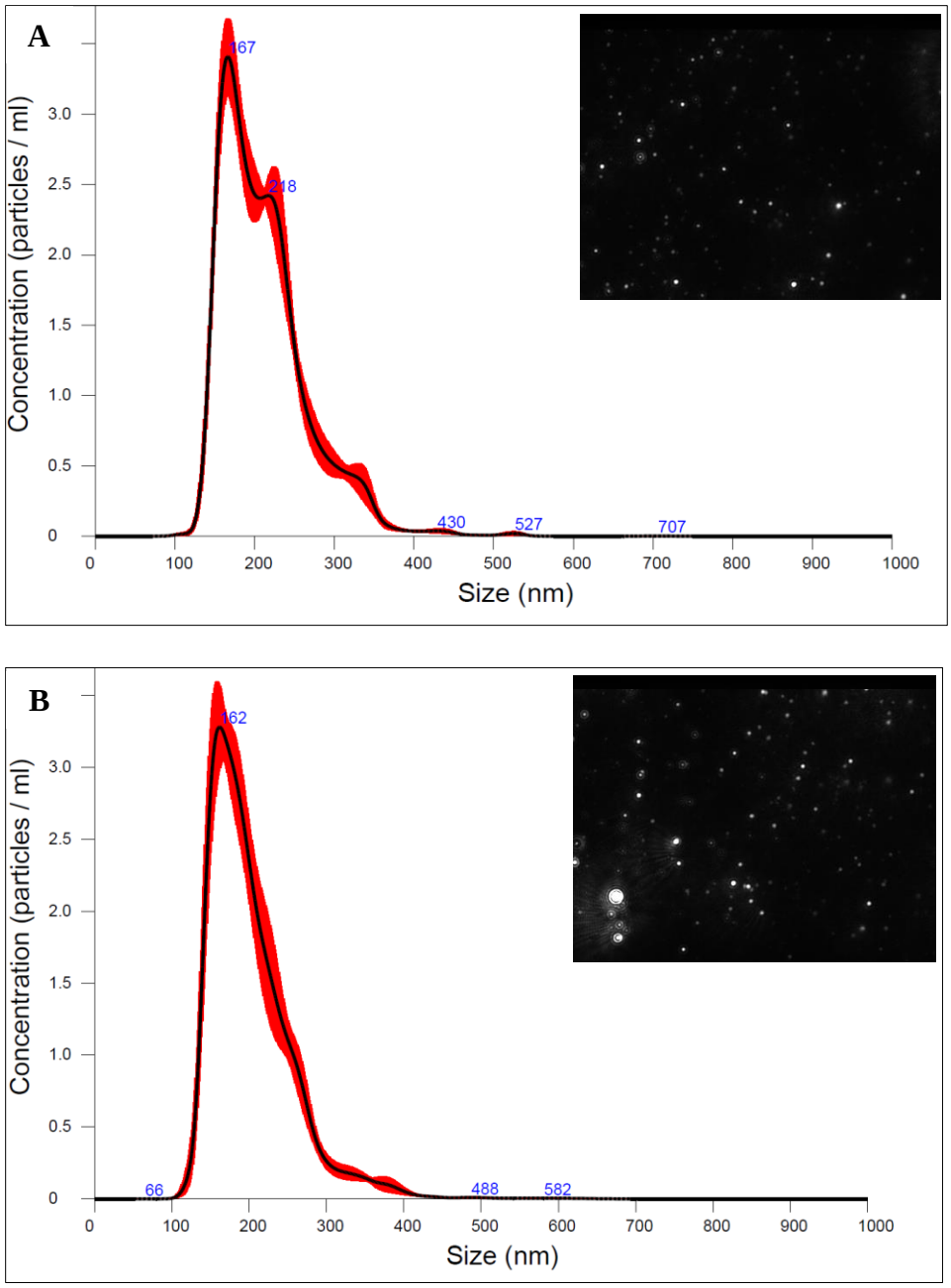

Figure 3.3 Nanoparticle tracking analysis results shown as smoothed histogram presenting average concentration and size of the control (A) and micro- and nano-bubbles treated (B) milk protein concentrate dispersions with their corresponding video frame.

Rheological measurements. Viscosity is a key hindering factor influencing the processability of dairy concentrates, process performance, and product quality (Patil et al., 2021; Bista et al., 2021). As seen in Figure 3.4, there was a significant decrease in viscosity after the MNB treatment. For concentrated protein systems, it is well known that the presence of aggregates can result in a marked increase in viscosity (Nicoud et al., 2015). Based on the results observed, it is suggested that MNB treatment-assisted decrease in viscosity is due to disruption of aggregates, which is also evident from the microstructures (Figures 3.5 and 3.6). The flow curves were measured at a shear rate of 0.1 to 100 s^{-1} for all samples in this study. The viscosity of C-MPC and MNB-MPC dispersions at a shear rate of 100 s^{-1} were 162.40 and 57.58 mPa·s, respectively. This represents a net decrease of ~65% for the MNB-MPC dispersion. Previously, Amamcharla et al. (2017) noted that injecting MNBs with an average diameter in the range of 100 nm to 30 μm helped in viscosity reduction in liquid dairy products. Similarly, Khaira (2020) reported lower apparent viscosity (150 mPa·s; ~30% decrease) of ice cream made with NBs. A net decrease of MPC (23.47% total solids) viscosity of up to ~55% by hydrodynamic cavitation was previously demonstrated by Li et al. (2018); however, the initial viscosity was higher (~200 mPa·s) than in the present study. This is also comparable with the reduction in viscosity reported by Zisu et al. (2013) following the acoustic cavitation of concentrated skim milk with an initial viscosity in the same range as samples analyzed in the current study. Analysis of the viscosity profiles with the power-law model also highlighted the differences in the flow behavior index, n, and the consistency coefficient, κ, for the C-MPC and MNB-MPC dispersions. The n and κ values were 0.44 and 2.30 Pa S^n for C-MPC, whereas it was 0.48 and 0.59 Pa S^n for the MNB-MPC dispersion. A similar trend was observed by mechanical treatment to modify protein structure using acoustic cavitation in studies conducted by Yanjun et al. (2014) and by

Meletharayil et al. (2016) on MPCs and Greek-style yogurts. Marella et al. (2015) used CO_2 injection before/during ultrafiltration on MPCs at 17% total solids and observed a reduction in viscosity of CO_2 injected samples (1.99 mPa s) compared to control (23.6 mPa s).

This decrease in viscosity is attributed to the lesser volume occupied by new aggregates compared with the C-MPC dispersions. The greater voluminosity occurred because of the inclusion of entrapped water in the structure during the aggregation process (Erabit et al., 2013). A high protein to lactose ratio in protein-rich concentrates can result in a higher viscosity and can be attributed to the higher voluminosity of milk proteins. The voluminosity and volume fraction were calculated, and it was found to be 3.47 mL/g and 0.79 for C-MPC, whereas it was 3.27 mL/g and 0.68 for the MNB-MPC dispersions. The higher viscosity can be attributed primarily to the higher voluminosity of the C-MPC dispersions (Sutariya et al., 2017), and the volume fraction, i.e., the place occupied by the particles in solution, is also a function of the viscosity of the dispersion. In fact, the altered microstructure (Figures 3.4 and 3.5) resulted in the decreased volume fraction that can be further linked to decreased product viscosity (Körzendörfer et al., 2019). Very recently, Tian et al. (2021) noted that motion of NBs is limited in high viscosity (~100 mPa·s) samples, keeping the bubble size more stable. The MNB size stability is thus depended to the system viscosity as well, which can directly affect coalescence of NBs (Ritzoulis, 2013). However, the prolonged stability of the bulk MNBs weren't a concern for the present study since the feed was spray dried right after the MNB incorporation. It was previously proven that MNBs can form stable bulk colloidal suspensions of particle/MNB complexes and mitigate aggregation due to their high longevity (Calgaroto et al., 2015; Zhang et al., 2016). Indeed, the bulk MNBs play a significant role as a buffer between milk protein particles which prevents the aggregation of the proteins (Amamcharla et al., 2017). Keeping the viscosity low

also allows the spray drying plant to operate continuously for long hours due to lower occurrences of nozzle blockage and fouling (Westergaard, 2004). Additionally, feed at higher viscosity have a large droplet size resulting from reduced water mobility, leading to improper drying of the final product (Anandharamakrishnan, 2017). Furthermore, viscosity has a direct influence on the size of the milk droplets formed during atomization, reducing viscosity results in improved flowability. Undeniably, viscosity reduction by MNB treatment is consequently beneficial for improving the efficacies and performance of downstream process technologies, including enhanced flux rate during membrane processing (Amamcharla et al., 2017), reduced fouling in evaporators/heat exchangers, and enhanced powder performance with improved powder properties of the dried powder particle. Overall, MNB treatment aids in reducing the viscosity of the feed, allowing higher feed solid content and thus more efficient and economical spray drying.

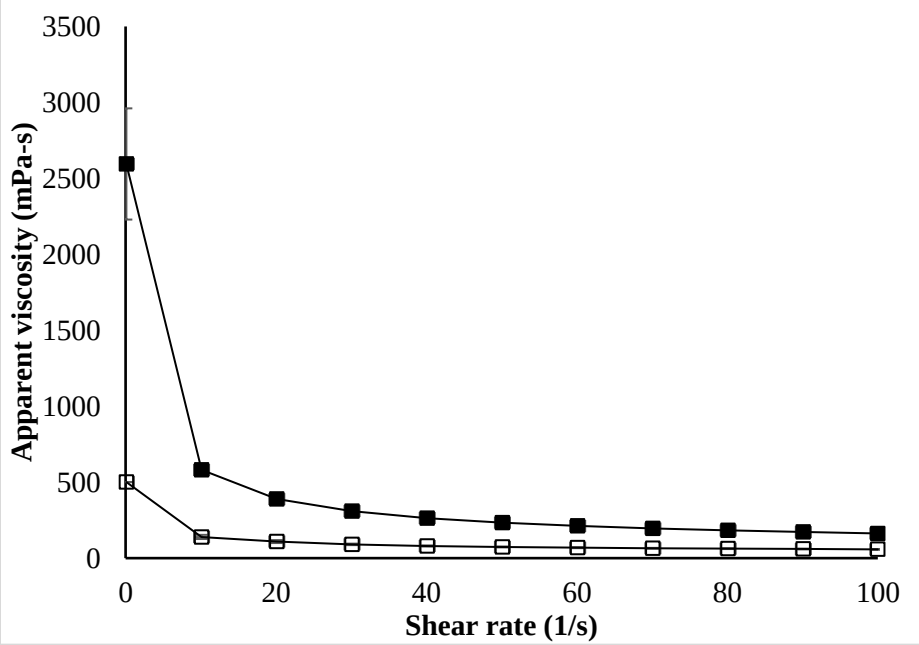

Figure 3.4 Viscosity as a function of shear rate (flow curves) for control (■) and micro- and nano-bubbles treated (□) milk protein concentrate dispersions; n = 4.

Microstructure. CLSM images are shown in Figures 3.4A and 3.4B. The green areas in the images correspond to milk protein and the dark areas correspond to the localized water. From a microscopic point of view, MNB-MPC dispersions exhibited less aggregated structures with minor structural elements compared to C-MPC dispersions. Indeed, it can be visualized from the images that C-MPC was present as larger, discrete, coarse, and non-uniform protein aggregates. Whereas, evenly dispersed and a comparatively more homogeneous protein matrix was observed in MNB-MPC dispersions, visibly indicating the influence of MNB treatment. Overall, the CLSM images exhibited reduced particle size and relatively evenly distributed and smaller particles compared with the C-MPC dispersions. Previously, Körzendörfer et al. (2019) noted that acoustically cavitated Greek yogurt showed a "torn-apart" structure. The microstructure images agreed with the viscosity result that MNB treatment aided viscosity reductions in the MPC systems.

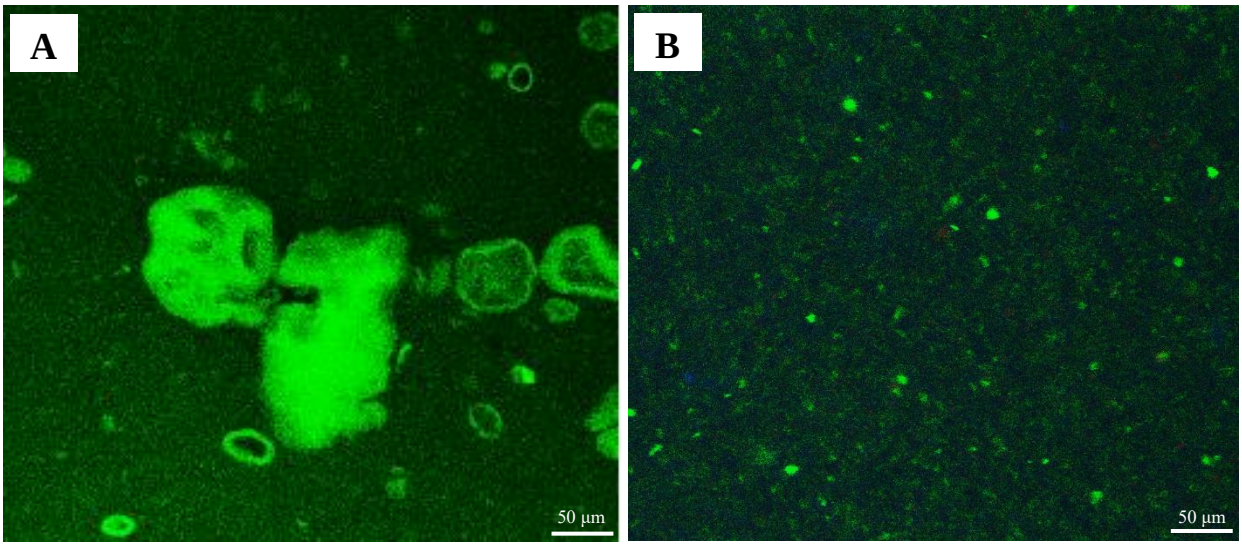

Figure 3.5 Confocal laser scanning microscopy images of control (A) and micro- and nano-bubbles treated (B) milk protein concentrate dispersions before spray drying.

Representative images of TEM are presented in Figure 3.6. The electron-dense areas in the TEM micrographs are casein micelles (Xu et al., 2016). Overall, CLSM and TEM showed the presence of relatively large particle structures in the C-MPC dispersions, which could be attributed to the presence of larger protein aggregates. Figure 3.6A showed a continuous matrix of proteins cluster against the more distributed structures of MNB-MPC dispersions (Figure 3.6B). With the MNB treatment, the distribution of protein molecules is more diffuse, and the gap between the structures of the protein network (the white part of the micrograph) is larger. Large aggregated structures were noticeably reduced in the MNB-MPC. This may be explained by the structural breakdown of the protein aggregates. Although CLSM/TEM showed a more dispersed structure with the MNB treatment of the MPC system., further investigations are needed to confirm if this is a temporary phenomenon or if it causes a permanent viscosity reduction. Overall, based on the analysis of the structure, the influence of MNBs on the rheological properties of C-MPC and MNB-MPC dispersions were clearly interpreted.

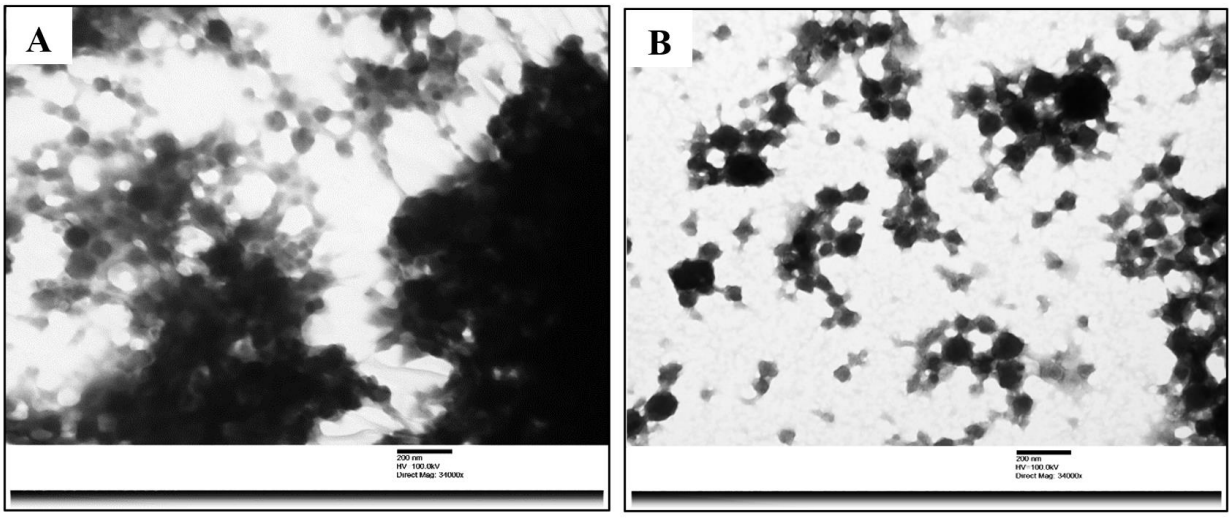

Figure 3.6 Representative transmission electron microscopy images of control (A) and micro- and nano-bubbles treated (B) milk protein concentrate dispersions before spray drying.

Characterization of MPC powders

Rehydration behavior. The rehydration of MPC powders is a multi-stage process, and MPC powders with higher protein contents typically show poor wettability and solubility (Crowley et al., 2015). Kher et al. (2007) reported that the conformational modifications of the protein during processing could be responsible for the loss of solubility. The solubility index of the C-MPC and MNB-MPC powders were 83 ± 1% and 94 ± 2%, respectively. Several pre-treatments (N_2/CO_2 air injection, microfluidization, acoustic cavitation, etc.) before spray drying were previously studied to improve the solubility of MPC powders. McSweeney et al. (2021) have previously reported an improved dissolution of N_2 injected MPC powders (control: 83.6% and N_2 treated: 96.2%). The more porous structure of MNB-MPC powder particles and the presence of large air voids between these powder particles possibly assisted enhanced water transfer while also improving the physical space between casein micelles and reducing protein-protein interactions (McSweeney et., 2021). Udabage et al. (2012) studied the application of the static high-pressure treatment on MPCs and have reported an increase in solubility for the treated samples compared to the control MPC powders. Previously, Yanjun et al. (2014) have noted an increased solubility (35.78% to 88.30%) of power ultrasound pre-treated MPC powders after 5 min of ultrasound treatment.

Focused beam reflectance measurement has proved to be a suitable technique for studying the rehydration of MPC powders (Hauser and Amamcharla, 2016). Figures 3.7A and 3.7B shows the changes in the counts for fine (<10 μm) and large (150-300 μm) particles for the C-MPC and MNB-MPC powders. It was observed that fine particle counts (Figure 3.7A) increased at a higher rate for MNB-MPC powders compared with the C-MPC powders. As can be observed, the large particle counts for MNB-MPC decreased rapidly, whereas the large

particle counts for C-MPC had a gradual reduction. The time required for the primary particles to disintegrate was lower in the MNB-MPC, further confirming the positive effect of the MNB treatment on rehydration. The fine particle counts for both C-MPC and MNB-MPC powders were similar for the first 300 s, but then the rate of increase in fine counts were higher for MNB-MPC as compared to C-MPC. At 0 s, C-MPC and MNB-MPC had a fine particle count of 17,000 and 25,000, respectively. MNB-MPC was able to reach a fine count of 86,000 by 500 s and maintained this count for the remainder of the experiment; however, C-MPC could only attain a count of 76,000 by 500 s. Hauser and Amamcharla (2016) noted a particle count of 62,000 by 900 s for fresh MPC powders and reported this count was maintained for the remainder of the experiment. Similar results were also obtained in a study by Gandhi et al. (2017), and it was noted that the rate of increase in fine counts were higher for well-soluble MPC powders. The large particle counts (Figure 3.7B) increased for the first 300 s for C-MPC and MNB-MPC powders, although it was significantly higher for the C-MPC. The increase in the large particle counts can be attributed to the initial aggregation of the powder particles. Larger particle counts decrease more rapidly for MNB-MPC, which indicated the faster disintegration of larger particles into smaller ones for MNB-MPC. The MNB-MPC attained the lowest large particle count around 500 s and C-MPC reached the lowest large particle count around 1,500 s. The counts for large particles at 500 s were found to be 125 and 20 for C-MPC and MNB-MPC powders, respectively. Interpretation of focused beam reflectance measurement data matches the overall trend reported by Crowley et al. (2015) and Hauser and Amamcharla (2016). Bouvier et al. (2013) reported that extrusion-porosified MPC powder particles had higher porosity and improved rehydration as compared to conventionally spray-dried MPC powder. The presence of void structures might have promoted the structural collapse of powder particles while

rehydration and interactions between poorly dispersible micellar casein at the particle surface are considered to hinder the rehydration of MPC (Anema et al., 2006; Mimouni et al., 2009, 2010). Previously, researchers at Kansas State University have injected MNBs prior to spray drying and reported that non-fat dry milk and MPC powders exhibited a highly porous structure (Amamcharla, et al., 2017), and indeed these pores act as water-communicating channels during MPC powder rehydration (Bouvier et al., 2013). Furthermore, as the protein powder particles rapidly disperse and solubilize by disintegrating into smaller particles, fouling of process equipment can be minimized (Gandhi et al., 2017).

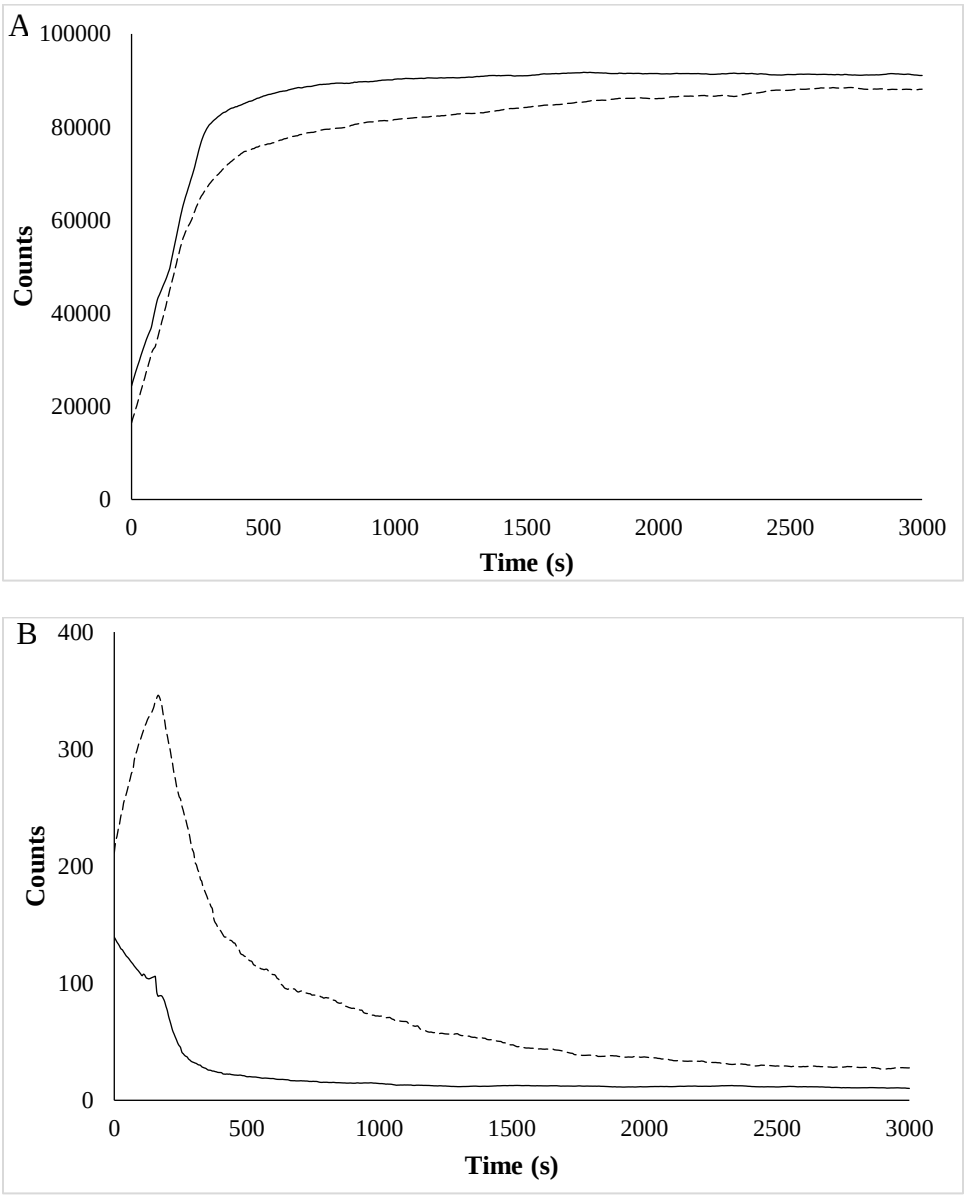

Figure 3.7 Changes in fine (<10 μm) (A) and large (150-300 μm) (B) counts obtained from data collected using the focused beam reflectance measurement for the spray-dried control (--) and micro- and nano-bubbles treated (-) milk protein concentrate powders at a dissolution temperature of 40ºC.

Particle size distribution. The particle size distribution results indicated the differences in the particle size distribution of reconstituted C-MPC and MNB-MPC dispersions (data not shown). MNB treatment resulted in a significant ($P<0.05$) decrease in the average particle size diameter (from 237.2 nm to 221.7 nm). The particle size and zeta potential measurements in this study were measured only after a 24 h rehydration time, and the observed effects may be more noticeable after shorter rehydration times. After MNB treatment, size distributions were observed to be monomodal, with a complete absence of secondary peaks associated with dispersed powder particles, suggesting complete dissolution were achieved. McSweeney et al. (2021) reported that N_2 injected MPC powders exhibited bimodal volume-based distributions on stirring for 1 h in water at 23°C, suggesting that casein micelles weren't released from primary powder particles. However, $D_{[4,3]}$ values of 13.6 μm for N_2 injected MPC were reported as compared to 83.7 μm for regular MPC powders, suggesting air injection techniques can help in improving rehydration rate of MPC powders. Previously, Mimouni et al. (2009) reported that 8 h of stirring at 24°C was required to fully solubilize a MPC powder (85%, w/w, protein). The net charge of the sample is a good indicator of the stability of the system as it is evidence of electrostatic interaction. The zeta potential of the MPC dispersions were found to be 22.02 and 27.94 mV for C-MPC and MNB-MPC samples, respectively. High zeta-potential absolute values indicate improved stability against aggregation. These results are similar to those reported in the literature (Crowley et al., 2018).

Microstructure. Representative SEM images of the C-MPC and MNB-MPC powders are presented in Figure 3.8. The powder particles of C-MPC and MNB-MPC powders were relatively smooth, although particles are less round-shaped in C-MPC, which agrees with the circularity results from morphology studies (Babu et al., 2021). Differences in morphology were

observed between C-MPC and MNB-MPC powders; only minor dents are distinguishable at the surface of the MNB-MPC particles. In comparison, the C-MPC displayed more deeper dents at the particle surface. Compared with the C-MPC (Figure 3.8A), MNB-MPC had fewer small particles trapped in dents of large particles. A similar surface appearance (MPC85) was demonstrated in a previous study (Fang et al., 2012) and for acoustically cavitated MPC powders (Yanjun et al., 2014), and such surfaces indicated shrinkage of the protein material (Mimouni et al., 2010).

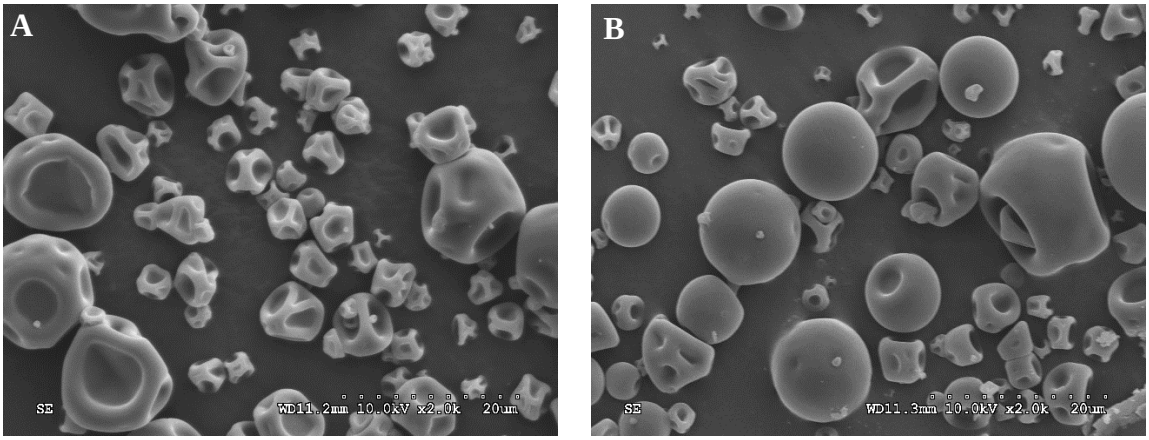

Figure 3.8 Scanning electron micrographs (× 5000) of spray dried milk protein concentrate powders: control (A) and micro- and nano-bubbles treated (B).

Representative TEM images of the reconstituted C-MPC and MNB-MPC powders are shown in Figure 3.9. The MNB-MPC powder particles were observed as smaller aggregates; however, C-MPC showed a distribution with relatively large aggregates. The observed microstructure was similar to that previously reported using TEM by Lie-Piang et al. (2021). They noted casein micelle clusters within the diameter size range of 600-800 nm initially on reconstituted studied skim milk powder, but size decreased considerably with the reconstitution time. The MNB treatment aided in weakening the aggregate structures, leading to fragmentation and complete hydration of the powder, which is relatable to the particle size distribution results.

TEM images (Figure 3.9b) revealed that the size of MNB-MPC particles decreased with the MNB treatment.

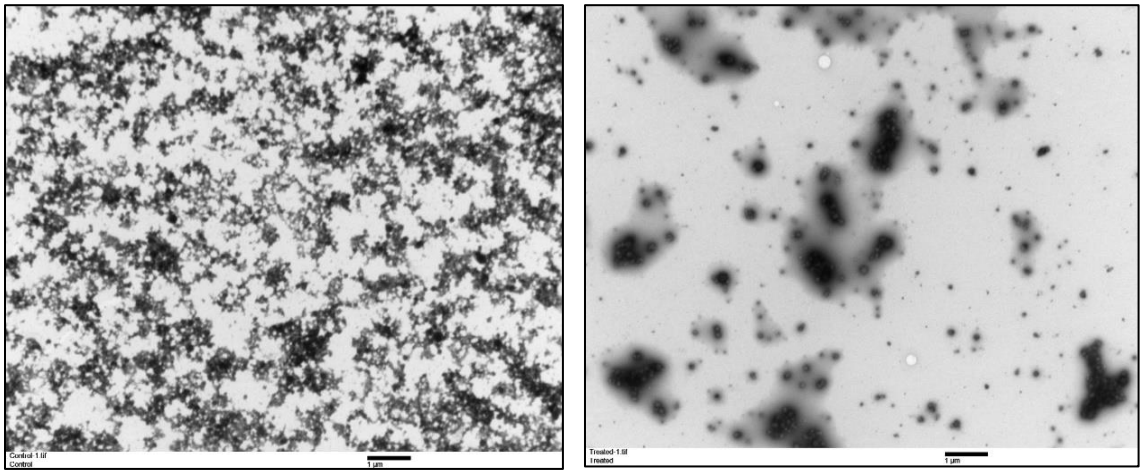

Figure 3.9 Representative transmission electron microscopy images of the reconstituted spray dried control (A) and micro- and nano-bubbles treated (B) milk protein concentrate powders (Magnification and scale: 5800x and 1 μm).

Conclusions

MNB treatment is a scalable and robust process technology. Controlling the viscosity of the feed concentrates promote high-solids drying, and therefore MNB treatment would play an important role in the overall performance of the spray-drying plant. A net decrease in viscosity by 65% with MNB treatment compared to the control solution could help reducing fouling of heat exchangers, improved heat transfer during evaporation, and reduce blocking of spray drying nozzles while ensuring consistent manufacture of high-quality MPC powders. This decrease in viscosity also translated to reduction in particle size. Moreover, with CLSM and TEM characterization, more information was provided from the microstructure aspect to explain the rheological phenomenon that was observed. Furthermore, with the MNB treatment, enhanced rehydration performance was achieved. From the findings of this study, MNB treatment can be

used as a physical pre-treatment before spray drying, and it also represents a potential for a more energy-saving drying process while providing enhanced powder performance.

Acknowledgements

The authors acknowledge the financial support from National Dairy Council (Rosemont, IL) and Midwest Dairy Foods Research Center (St. Paul, MN). Authors also thank Mr. Ravi Thakkar for SEM support, Dr. Tej Shrestha for NTA support, and Dr. Dan Boyle for help with CLSM and TEM analysis. This project is Kansas State Research and Extension contribution number 22-054-J.

References

Adhikari, B. M., Truong, T., Prakash, S., Bansal, N., and Bhandari, B. 2020. Impact of incorporation of CO_2 on the melting, texture and sensory attributes of soft-serve ice cream. Int. Dairy J. 109:104789.

Agarwal, A., Ng, W. J., and Liu, Y. 2011. Principle and applications of microbubble and nanobubble technology for water treatment. Chemosphere. 84:1175-1180.

Agarwal, S., R. L. W. Beausire, S. Patel, and H. Patel. 2015. Innovative uses of milk protein concentrates in product development. J. Food Sci. 80:23-29.

Ahmadi, R., and Khodadadi Darban, A. 2013. Modeling and optimization of nano-bubble generation process using response surface methodology. Int. J. Nanosci. Nanotechnol. 9:151-162.

Ahmadi, R., Khodadadi, D. A., Abdollahy, M., and Fan, M. 2014. Nano-microbubble flotation of fine and ultrafine chalcopyrite particles. Int. J. Min. Sci. Technol. 24:559-566.

Alheshibri, M., Al Baroot, A., Shui, L., and Zhang, M. 2021. Nanobubbles and Nanoparticles. Curr. Opin. Colloid Interface Sci. 55:101470.

Amamcharla, J., Li, B., and Liu, Z. 2017. Use of micro-and nano-bubbles in liquid processing. United States. Patent number: WO2017127636A1.

Anandharamakrishnan, C., 2017. Handbook of Drying for Dairy Products. John wiley & sons inc.

Anema, S. G., D. N. Pinder, R. J. Hunter., and Y. Hemar. 2006. Effects of storage temperature on the solubility of milk protein concentrate (MPC85). Food Hydrocoll. 20:386-393.

Augustin, M. A., Sanguansri, P., Williams, R., and Andrews, H. 2012. High shear treatment of concentrates and drying conditions influence the solubility of milk protein concentrate powders. J. Dairy Res. 79:459-468.

Azevedo, A., Etchepare, R., Calgaroto, S., and Rubio, J. 2016. Aqueous dispersions of nanobubbles: Generation, properties and features. Miner. Eng. 94:29-37.

Babu, K. S., and Amamcharla, J. 2018. Application of front-face fluorescence spectroscopy as a tool for monitoring changes in milk protein concentrate powders during storage. J. Dairy Sci. 101:10844-10859.

Babu, K. S., and Amamcharla, J. K. 2021b. Application of micro- and nano-bubbles to improve the processability of milk protein concentrates and its influence on the rehydration properties of spray dried milk protein concentrate powders. J. Dairy Sci. (not published).

Babu, K. S., Siliveru, K., Amamcharla, J. K., Vadlani, P. V., and Ambrose, R. K. 2018. Influence of protein content and storage temperature on the particle morphology and flowability characteristics of milk protein concentrate powders. J. Dairy Sci. 101:7013-7026.

Babu, K.S., and J.K. Amamcharla. 2021. Rehydration characteristics of milk protein concentrate powders monitored by electrical resistance tomography. JDS Communications. doi:10.3168/jdsc.2021-0125.

Babu, K.S., Siliveru, K., and J.K. Amamcharla. 2021. Influence of micro- and nano-bubbles on morphological characteristics and flow properties of milk protein concentrate powders. JDS Communications.

Bansal, N., Truong, T., and Bhandari, B. 2017. Feasibility study of lecithin nanovesicles as spacers to improve the solubility of milk protein concentrate powder during storage. Dairy Sci. Technol. 96:861-872.

Bian, Q., S. Sittipod, A. Garg and R. P. K. Ambrose. 2015. Bulk flow properties of hard and soft wheat flours. J. Cereal Sci. 63:88-94.

Bista, A., McCarthy, N., O'Donnell, C. P., and O'Shea, N. 2021. Key parameters and strategies to control milk concentrate viscosity in milk powder manufacture. Int. Dairy J. 121:105120.

Bouvier, J.M., Collado, M., Gardiner, D., Scott, M., and Schuck, P., 2013. Physical and rehydration properties of milk protein concentrates: comparison of spray-dried and extrusion-porosified powders. Dairy Sci. Technol. 93, 387–399.

Calgaroto, S., Azevedo, A., and Rubio, J. 2015. Flotation of quartz particles assisted by nanobubbles. Int J Miner Process. 137:64-70.

Caric, M., and Kalab, M. 1987. Effects of drying techniques on milk powders quality and microstructure: A review. Food Structure, 6:171-180.

Chamberland, J., Benoit, S., Doyen, A., and Pouliot, Y. 2020. Integrating reverse osmosis to reduce water and energy consumption in dairy processing: a predictive analysis for Cheddar cheese manufacturing plants. J. Water Process. Eng. 38:101606.

Crowley, S. V., B. Desautel, I. Gazi, A. L. Kelly, T. Huppertz., and O'Mahony J. A. 2015. Rehydration characteristics of milk protein concentrate powders. J. Food Eng. 149:105-113.

Crowley, S. V., E. Burlot, J. V. Silva, N. A. McCarthy, H. B. Wijayanti, M. A. Fenelon, A. L. Kelly., and O'Mahony J. A. 2018. Rehydration behaviour of spray-dried micellar casein concentrates produced using microfiltration of skim milk at cold or warm temperatures. Int. Dairy J. 81:72-79.

Crowley, S. V., Gazi, I., Kelly, A. L., Huppertz, T., and O'Mahony, J. A. 2014. Influence of protein concentration on the physical characteristics and flow properties of milk protein concentrate powders. J. Food Eng. 135:31-38.

Ebina, K., Shi, K., Hirao, M., Hashimoto, J., Kawato, Y., Kaneshiro, S., Morimoto, T., Koizumi, K., and Yoshikawa, H. 2013. Oxygen and air nanobubble water solution promote the growth of plants, fishes, and mice. PloS one. 8:e65339.

Erabit, N., Flick, D., and Alvarez, G. 2013. Effect of calcium chloride and moderate shear on β-lactoglobulin aggregation in processing-like conditions. J. food Eng. 115:63-72.

Fang, Y., S. Rogers, C. Selomulya., and X. D. Chen. 2012. Functionality of milk protein concentrate: Effect of spray drying temperature. Biochem. Eng. J. 62:101-105.

Fitzpatrick, J. J. 2007. Particle properties and the design of solid food particle processing operations. Food Bioprod. Process. 85:308-314.

Fox, M., Akkerman, C., Straatsma, H., and De Jong, P. 2010. Energy reduction by high dry matter concentration and drying. New Food. 60-63.

Fu, X., Huck, D., Makein, L., Armstrong, B., Willen, U., and Freeman, T. 2012. Effect of particle shape and size on flow properties of lactose powders. Particuology. 10:203-208.

Gaiani, C., Schuck, P., Scher, J., Desobry, S., and Banon, S. 2007. Dairy powder rehydration: influence of protein state, incorporation mode, and agglomeration. J. Dairy Sci. 90:570-581.

Gandhi, G., J. K. Amamcharla, and D. Boyle. 2017. Effect of milk protein concentrate (MPC80) quality on susceptibility to fouling during thermal processing. Lebensm. Wiss. Technol. 81:170–179.

Gregersen, S. B., Wiking, L., Bertelsen, K. B., Tangsanthatkun, J., Pedersen, B., Poulsen, K. R., Andersen Ulf., and Hammershøj, M. 2019. Viscosity reduction in concentrated protein solutions by hydrodynamic cavitation. Int. Dairy J. 97:1-4.

Hanrahan, F. P., Tamsma, A., Fox, K. K., and Pallansch, M. J. 1962. Production and properties of spray-dried whole milk foam. J. Dairy Sci. 45:27-31.

Hauser, M., and Amamcharla, J. 2016. Novel methods to study the effect of protein content and dissolution temperature on the solubility of milk protein concentrate: Focused beam reflectance and ultrasonic flaw detector-based methods. J. Dairy Sci. 99:3334-3344.

Havea, P. 2006. Protein interactions in milk protein concentrate powders. Int. Dairy J. 16:415-422.

Ilari, J. L. 2002. Flow properties of industrial dairy powders. Le Lait. 82:383-399.

Jadhav, A. J., and Barigou, M. 2020. Bulk nanobubbles or not nanobubbles: That is the question. Langmuir. 36:1699-1708.

Jan, S., Ghoroi, C., and Saxena, D. C. 2017. A comparative study of flow properties of basmati and non-basmati rice flour from two different mills. J. Cereal Sci. 76:165-172.

Jannesari, M., Akhavan, O., Madaah Hosseini, H. R., and Bakhshi, B. 2020. Graphene/CuO_2 Nanoshuttles with Controllable Release of Oxygen Nanobubbles Promoting Interruption of Bacterial Respiration. ACS Appl. Mater Interfaces. 12:35813-35825.

Jeevanandam, J., Barhoum, A., Chan, Y. S., Dufresne, A., and Danquah, M. K. 2018. Review on nanoparticles and nanostructured materials: history, sources, toxicity and regulations. Beilstein J. Nanotechnol. 9:1050-1074.

Jenike, A. W. 1976. Storage and Flow of Solids, Bulletin No. 123 (Utah Engineering Station, Salt Lake City, Utah).

Keogh, K., Murray, C., Kelly, J., and O'Kennedy, B. 2004. Effect of the particle size of spray-dried milk powder on some properties of chocolate. Le Lait. 84:375-384.

Keogh, M. K., Murray, C. A., and T O'Kennedy, B. 2003. Effects of ultrafiltration of whole milk on some properties of spray-dried milk powders. Int. Dairy J. 13:995-1002.

Kim, E. H. J., Chen, X. D., and Pearce, D. 2005. Effect of surface composition on the flowability of industrial spray-dried dairy powders. Colloids Surf. B Biointerfaces. 46:182-187.

Körzendörfer, A., Schäfer, J., Hinrichs, J., and Nöbel, S. 2019. Power ultrasound as a tool to improve the processability of protein-enriched fermented milk gels for Greek yogurt manufacture. J. Dairy Sci. 102:7826-7837.

Kosasih, L., Bhandari, B., Prakash, S., Bansal, N., and Gaiani, C. 2016. Physical and functional properties of whole milk powders prepared from concentrate partially acidified with CO2 at two temperatures. Int. Dairy J. 56:4-12.

Kudo, Y., Yasuda, M., and Matsusaka, S. 2020. Effect of particle size distribution on flowability of granulated lactose. Adv. Powder Technol. 31:121-127.

Lapčík, L., Lapčíková, B., Otyepková, E., Otyepka, M., Vlček, J., Buňka, F., and Salek, R. N. 2015. Surface energy analysis (SEA) and rheology of powder milk dairy products. Food Chem. 174:25-30.

Leturia, M., M. Benali, S. Lagarde, I. Ronga., and K. Saleh. 2014. Characterization of flow properties of cohesive powders: A comparative study of traditional and new testing methods. Powder Technol. 253:406-423.

Li, K., Woo, M. W., Patel, H., Metzger, L., and Selomulya, C. 2018. Improvement of rheological and functional properties of milk protein concentrate by hydrodynamic cavitation. J. Food Eng. 221:106-113.

Lie-Piang, A., Leeman, M., Castro, A., Börjesson, E., and Nilsson, L. 2021. Investigating the effect of powder manufacturing and reconstitution on casein micelles using asymmetric flow field-flow fractionation (AF4) and transmission electron microscopy. Food Res. Int. 139:109939.

Liu, G., Wu, Z., and Craig, V. S. 2008. Cleaning of protein-coated surfaces using nanobubbles: an investigation using a quartz crystal microbalance. J. Phys. Chem. C. 112:16748-16753.

Marella, C., Salunke, P., Biswas, A. C., Kommineni, A., and Metzger, L. E. 2015. Manufacture of modified milk protein concentrate utilizing injection of carbon dioxide. J. Dairy Sci. 98: 3577-3589.

McCarthy, N. A., Kelly, P. M., Maher, P. G., and Fenelon, M. A. 2014. Dissolution of milk protein concentrate (MPC) powders by ultrasonication. J. Food Eng. 126:142-148.

McSweeney, D. J., Maidannyk, V., O'Mahony, J. A., and McCarthy, N. A. 2021. Influence of nitrogen gas injection and agglomeration during spray drying on the physical and bulk handling properties of milk protein concentrate powders. J. Food Eng. 293:110399.

Meletharayil, G.H., Metzger, L.E., Patel, H.A., 2016. Influence of hydrodynamic cavitation on the rheological properties and microstructure of formulated Greek-style yogurts. J. Dairy Sci. 99:8537-8548.

Mimouni, A., Deeth, H. C., Whittaker, A. K., Gidley, M. J., and Bhandari, B. R. 2009. Rehydration process of milk protein concentrate powder monitored by static light scattering. Food Hydrocoll. 23:1958-1965.

Mimouni, A., H. C. Deeth, A. K. Whittaker, M. J. Gidley., and B. R. Bhandari. 2010. Investigation of the microstructure of milk protein concentrate powders during rehydration: Alterations during storage. J. Dairy Sci. 93:463-472.

Mitra, H., H. A. Pushpadass, M. E. E. Franklin, R. P. K. Ambrose, C. Ghoroi., and S. N. Battula. 2017. Influence of moisture content on the flow properties of basundi mix. Powder Technol. 312:133-143.

Nicoud, L., Lattuada, M., Yates, A., and Morbidelli, M. 2015. Impact of aggregate formation on the viscosity of protein solutions. Soft matter. 11:5513-5522.

Patil, M. H., Tanguy, G., Floch-Fouéré, C. L., Jeantet, R., and Murphy, E. G. 2021. Energy usage in the manufacture of dairy powders: Advances in conventional processing and disruptive technologies. Drying Technol. 1595-1613.

Phan, K. K. T., Truong, T., Wang, Y., and Bhandari, B. 2020. Nanobubbles: Fundamental characteristics and applications in food processing. Trends Food Sci Technol. 95:118-130.

Power, O. M., Maidannyk, V., McSweeney, D. J., Fenelon, M. A., O'Mahony, J. A., and McCarthy, N. A. 2020. Water sorption and hydration properties of high protein milk powders are influenced by enzymatic crosslinking and calcium chelation. Powder Technol. 364:680-688.

Rennie, P. R., Chen, X. D., Hargreaves, C., and Mackereth, A. R. 1999. A study of the cohesion of dairy powders. J. Food Eng. 39:277-284.

Ritzoulis, C. 2013. Introduction to the physical chemistry of foods. CRC Press.

Schuck, P. 2011. Milk powder: physical and functional properties of milk powders. 2nd ed. J.W. Fuquay, P.F. Fox (Eds.), McSweeney PLH encyclopedia of dairy science. 3:117-124

Sutariya, S. G., Huppertz, T., and Patel, H. A. 2017. Influence of milk pre-heating conditions on casein–whey protein interactions and skim milk concentrate viscosity. Int. Dairy J. 69:19-22.

Temesgen, T., Bui, T. T., Han, M., Kim, T. I., and Park, H. 2017. Micro and nanobubble technologies as a new horizon for water-treatment techniques: Review Adv. Colloid Interfac. Sci. 246:40-51.

Tian, Y., Zhang, Z., Zhu, Z., and Sun, D. W. 2021. Effects of nano-bubbles and constant/variable-frequency ultrasound-assisted freezing on freezing behaviour of viscous food model systems. J. Food Eng. 292:110284.

Udabage, P., Puvanenthiran, A., Yoo, J. A., Versteeg, C., and Augustin, M. A. 2012. Modified water solubility of milk protein concentrate powders through the application of static high pressure treatment. J. Dairy Res. 79:76-83.

Weijs, J. H., Seddon, J. R., and Lohse, D. 2011. Diffusive shielding stabilizes bulk nanobubble clusters. Chemphyschem. 13:2197-2204.

Westergaard, V., 2004. Milk Powder Technology: Evaporation and Spray Drying.

Xu, Y., Liu, D., Yang, H., Zhang, J., Liu, X., Regenstein, J. M., Hemar, Y., and Zhou, P. 2016. Effect of calcium sequestration by ion-exchange treatment on the dissociation of casein micelles in model milk protein concentrates. Food Hydrocoll. 60:59-66.

Yanjun, S., Jianhang, C., Shuwen, Z., Hongjuan, L., Jing, L., Lu, L., ... and Jiaping, L. 2014. Effect of power ultrasound pre-treatment on the physical and functional properties of reconstituted milk protein concentrate. J. Food Eng. 124:11-18.

Zhang, M., and Seddon, J. R. 2016. Nanobubble–nanoparticle interactions in bulk solutions. Langmuir. 32:11280-11286.

Zisu, B., Schleyer, M., and Chandrapala, J. 2013. Application of ultrasound to reduce viscosity and control the rate of age thickening of concentrated skim milk. Int. Dairy J. 31:41-43.

Chapter 4 - Influence of micro- and nano-bubble treatment on morphological characteristics and flow properties of spray-dried milk protein concentrate powders[1]

Abstract

This study investigated the morphological and bulk handling properties of milk protein concentrate (MPC) powders manufactured from incorporating MNBs prior to spray drying. Control MPC powders (C-MPC; no MNB treatment) and MNB treated MPC powders (MNB-MPC; MPC dispersions passed through the MNB system and subsequently spray dried) were characterized in terms of particle size, shape factors, stability, variable flow rate, shear cell tests, compressibility, and wall friction. MPC powders produced after the MNB injection process had significantly lower bulk density, better flowability, and lower basic flow energy. Shear tests showed that C-MPC powders were more cohesive than MNB-MPC powders. MNB-MPC powders had lower flow rate index values, lower wall friction angles, more rounded shape, and significant difference in powder compressibility compared to C-MPC powders. Overall, the results demonstrated that MNB treatment of liquid MPC dispersions prior to spray drying, can produce ingredients with comparable morphological characteristics while improving the bulk powder properties.

---

[1]Submitted for publication: JDS Communications

Introduction

The high-protein/low-lactose content with attractive functional and nutritional qualities make milk protein concentrate (MPC) powders an ideal ingredient in various dairy and food product formulations. However, impaired rehydration and bulk flow characteristics during storage challenges the end-users to incorporate the MPC powders in a formulation. Protein content and storage time/temperature are some of the critical factors that influence the functionality of MPC powders (Babu and Amamcharla, 2018; Babu and Amamcharla, 2021). The flow properties of skim milk powder, whole milk powder, whey protein concentrates, and MPC powders have been well characterized (Fitzpatrick, 2007; Kim et al., 2005; Crowley et al., 2014). Modifying powder particle structure may influence the physical attributes of the powder (density, particle size, porosity, and particle morphology), and these influence the bulk handling of powders industrially. Bouvier et al. (2013) used extrusion-porosification to produce MPC powders with improved dispersibility and increased particle porosity. After spray drying, the powder is transferred to storage bins or silos and can go through numerous handling steps (Ilari, 2002). Additionally, as a dairy ingredient, MPC powders are likely to be stored in silos prior to usage. Therefore, understanding the overall flow behavior and how they may behave during storage and handling is critical. MPC35 are considered to be free-flowing, whereas MPCs with 60 and 70% were easy flowing (Crowley et al., 2014) and MPC80, MPC85, and MPC90 were noted to be cohesive and claimed to have relatively poor flowability (Crowley et al., 2014; Babu et al., 2018). Therefore, alternative techniques to improve flow characteristics of MPCs are of significant interest.

Microbubbles (MBs; size range:10-50 μm) and nanobubbles (NB; Size: <200 nm) are gas-filled entities within a bulk liquid (Agarwal et al., 2011; Temesgen et al., 2017). The

techniques to incorporate MNBs in bulk liquid include hydrodynamic/acoustic cavitation, electrochemical cavitation, membranes, and mechanical agitation (Phan et al., 2020). MNBs offer substantial improvements in applications such as wastewater treatment, mining, agriculture, food processing, and medicine (Liu et al., 2008; Jannesari et al., 2020; Temesgen et al., 2017; Amamcharla et al., 2017). Recently, the potential applications of NBs in food and dairy processing industries have been thoroughly reviewed (Phan et al., 2020; Zhang et al., 2022; Babu and Amamcharla, 2022b). Ebina et al. (2013) noted a significant increase in O_2 content in water (7.7 to 31.7 mg/ L) when incorporated as O_2 MNBs. In the food processing sector, the use of CO_2 and N_2 are getting more attention. This could be due to their high solubility and relatively low reactivity. Application of CO_2-MNBs significantly decreased the scooping hardness and melting rate of soft-serve ice cream, and also enhanced the overall acceptability of soft-serve ice cream (Adhikari et al., 2020). Very recently, Babu et al. (2022) envisaged MNB treatment as a new process method to improve the rheological and functional characteristics of Greek-style yogurt. Previously, McSweeney et al. (2021) observed better rehydration behavior of N_2 injected MPC powders. The influence of CO_2 injection on the physical and functional properties of whole milk powder has been described by Kosasih et al. (2016). They noted that CO_2 injection prior to spray drying increased powder dispersibility, porosity, and occluded air content. Hanrahan et al. (1962) examined the impact of N_2 injection into whole milk concentrate before spray drying and described an increase in dispersibility and powder particle size. However, limited research has been implemented regarding the use of gas injection to modify powder particle structure and improve the subsequent flow properties of high-protein dairy ingredients. The effect of MNBs on the physical properties of high-protein powders has not been previously investigated but may assist the manufacture of MPC powders with improved flow behavior. Therefore, the objective

of this research was to characterize the physical and bulk handling properties of MNB-MPC powders compared to control MPC.

Materials and Methods

Experimental approach

A benchtop MNB generation system based on hydrodynamic cavitation was designed and assembled at Kansas State University. More details about the MNB treatment procedure can be found elsewhere (Babu and Amamcharla, 2022a). The MPC dispersions were prepared using two independent lots of MPC powder with 85% protein content obtained from a commercial dairy ingredient provider within the USA. The average protein, moisture, fat, lactose, and ash content as per the certifacte of anlysis provided by the supplier for the MPC85 were 86.85% (w/w), 5.25% (w/w), 0.93% (w/w), 4.79% (w/w) and 6.68% (w/w), respectively. Control MPC (C-MPC; MPC dispersions pumped through the diaphragm pump without air injection) and MNB incorporated MPC (MNB-MPC; MNB treated using a venturi gas injector) were prepared and subsequently spray-dried dried in a lab-scale spray dryer (YC-015, Shanghai Pilotech Instrument & Equipment Co., Ltd., China). The inlet temperature was set at 180ºC, and the outlet temperature ranged between 60-65ºC. The spray pressure was maintained at 30 psi, and the average relative humidity was 52%. The spray-dried MPC powders were collected and sealed in Whirl-Pak bags (Nasco, Fort Atkinson, WI) for morphological and flow characterization. The morphological and flow characteristics of the resultant MPC powders were analyzed using PROC GLMMIX procedure of SAS (Version 9.4, SAS Institute Inc., Cary, NC).

Morphological characteristics

Morphological characteristics of C- and MNB-MPC powders were analyzed by Malvern Morphologi G3ID (Malvern Instruments, Worcestershire, UK) following method by Babu et al.

(2018). The circle equivalent diameter (CED), high sensitivity circularity (HSC), elongation, solidity mean, and convexity were calculated from the 2-dimensional images. Circularity (range 0 to 1) describes how close the shape of the particle is to a perfect circle, whereas convexity (range 0 to 1) is a measure of the surface roughness of a particle. A smooth particle has a convexity of 1, whereas an irregularly shaped particle or a very spiky one has a convexity closer to 0. Circle or square has an elongation value of 0, whereas shapes with large aspect ratios have an elongation closer to 1. Solidity describes the amount to which a shape is convex or concave. The solidity of a completely convex shape is 1. Whereas, the farther the solidity deviates from 1, the greater the extent of concavity in the structure.

Flow properties

The FT4 powder rheometer (Freemans Technology, Tewkesbury, UK) was used to evaluate the powder rheology of the C- and MNB-MPC powders following the method described by Babu et al. (2018). The samples were conditioned using the conditioning cycle to ensure the repeatability of the results and to remove any packing stress. Measuring the flow properties for characterizing powder flow using FT4 powder rheometer include various flow, compressibility, and shear cell tests. Basic flowability energy (BFE), stability index (SI), specific energy (SE), flow rate index (FRI), and bulk density were obtained from the flow tests. Measurements were performed using the cylindrical cell in which powders were pre-consolidated under a 9 kPa normal stress. Cohesion, unconfined yield strength (UYS), major principle stress (MPS), and flow function (FF) were obtained from the shear tests.

Statistical analysis

Statistical analysis of the C-MPC and MNB-MPC dispersions and resultant C-MPC and MNB-MPC powders were analyzed using PROC GLMMIX procedure of SAS (Version 9.4, SAS Institute Inc., Cary, NC).

Results and Discussion

Morphological characteristics

The morphological properties of C- and MNB-MPC powders are summarized in Table 1. The CED of MPC powder particles decreased with the MNB treatment. Particle size of the final powder is dependent on the viscosity of the feed. (Caric and Kalab, 1987). Keogh et al. (2003) also found that the particle size of spray-dried milk powders increased linearly with an increase in the apparent viscosity. The HSC results confirmed that the morphology of MNB-MPC powder exhibited more round-shaped particles compared to C-MPC powders (Table 1). Interestingly, the aspect ratio, elongation, solidity, and convexity were comparable for both the C- and MNB-MPC powders. Similarly, Kudo et al. (2020) studied the effect of particle size distribution on flowability of granulated lactose and noted dependency of flow properties on particle shape was minimal. Figure 4.1 shows the 2-dimensional shape of the largest C- and MNB-MPC powder particle. The measured CED was 7.24 μm for the C-MNC. In contrast, CED was significantly ($P>0.05$) lower with the MNB treatment and was found to be 6.91 μm for the MNB-MPC powder particles. The particle size changes were identical to those previously noted for hydrodynamic-cavitated MPC powders (Li et al., 2018). In contrast, the incorporation of N_2 into the MPC concentrate significantly increased the size of the regular MPC powder particles from 73 μm to 78 μm. However, the CO_2 injection of whole milk concentrates showed a particles size ~15 μm (D50) for both the control and treated powder samples. Milk concentrates with a higher

viscosity form larger droplets when atomized, resulting in powder with a larger particle size (Anandharamakrishnan, 2017; Power et al., 2020). The observed differences in particle size, structure, and shape appeared to have a large impact on its physical characteristics and have also positively influenced the rehydration behavior (Babu and Amamcharla, 2021b). Several powder properties such as solubility, morphology, and flow characteristics are determined by its particle size distribution, which is primarily governed by feed characteristics and conditions maintained during further processing of the retentates (Schuck, 2011). Overall, morphological results suggested that MNB treatment prior to spray drying wouldn't drastically alter the final powder morphology while delivering desired viscosity reductions, helping in potential energy savings in the spray drying process.

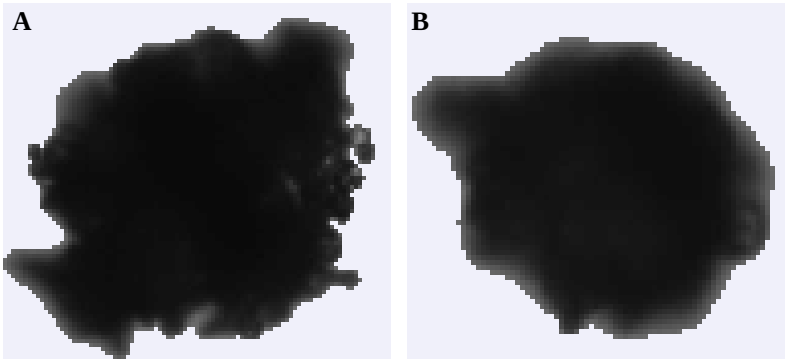

Figure 4.1 Two-dimensional images showing the shape: obtained from the Morphologi G3ID for the largest particle observed for the (A) control and (B) micro- and nano-bubbles treated milk protein concentrate powders.

Flow properties

The dynamic flow and shear flow properties of C- and MNB-MPC powders are summarized in Table 1. The BFE value of C-MPC was significantly different ($P < 0.05$) from that of MNB-MPC powder, indicating that the flow behavior of MNB-MPC powder would be better than the C-MPC powder (Table 1). It can be noted that BFE of MNB-MPC powders were

relatively lower compared to C-MPC powder samples composed of smaller and/or irregular particles with greater interparticle friction. Previously, Lapčík et al. (2015) reported lower BFE values (127 to 157 mJ) for skim milk powder, demineralized whey powder, and whey powders. Whereas, the BFE of MPC powders generally range from 510-930 mJ (Babu et al., 2014). C- and MNB-MPC powder are relatively stable and do not agglomerate during handling after being subjected to flow under high stress. The SI of C- and MNB-MPC powders were 1.03 and 0.96, respectively, and can be considered acceptable for a stable powder (0.9 to 1.1), and more than 1.1 would be considered unstable (Bian et al., 2015). Both C- and MNB-MPC powder had average flow rate sensitivities because the FRI value was less than 1.5. This shows that the C- and MNB-MPC powders were not remarkably cohesive (Leturia et al., 2014). Indeed, the FRI of C-MPC was not significantly ($P>0.05$) different from the MNB-MPC powders. The SE decreased significantly ($p < 0.05$) with the MNB treatment. The SE values depend on the cohesive and mechanical interlocking forces between the powder particles and are only slightly influenced by compressibility. The SE value for MNB-MPC was lower than C-MPC, indicating that it was the least cohesive sample in an unconfined flow regime and was consistent with a relatively low BFE value. Overall, a higher BFE value (lower flowability) and higher SE value (higher cohesivity) of C-MPC as compared to MNB-MPC showed that it was a less stable sample. The general trend observed was an improvement of the dispersion, flow, and packing properties after the MNB treatment. The difference in flow energies between the C- and MNB-MPC powders can be explained by the differences in size distribution, shapes, and bulk density (0.15 ± 0.01 and 0.08 ± 0.01 g/mL for C- and MNB-MPC powders, respectively). The C-MPC exhibited higher flow energy than the MNB-MPC, which is attributed to particle mechanical interlocking resulting from the higher surface roughness and dents, revealed from the SEM

images (Babu and Amamcharla, 2021b). It was previously found by Fu et al. (2012) that powders with the highest sphericity had better flowability. Similarly, in this study, MNB-MPC had the most spherical powder particles (Table 1).

Table 4.1 Morphological characteristics, dynamic flow and shear flow properties the control (C-MPC) and micro- and nano-bubbles treated milk protein concentrate (MNB-MPC) powders.

Properties	C-MPC	MNB-MPC
Circle equivalent diameter (µm)	7.27 ± 0.05 [a]	6.91± 0.01 [b]
High sensitivity circularity	0.883 ± 0.001 [a]	0.893 ± 0.001 [b]
Aspect ratio	0.824 ± 0.000 [a]	0.823 ± 0.000 [b]
Elongation	0.175 ± 0.000 [a]	0.177 ± 0.000 [b]
Solidity	0.981 ± 0.000 [a]	0.979 ± 0.000 [b]
Convexity	0.989 ± 0.000 [a]	0.986 ± 0.000 [b]
Basic flow energy (mJ)	507.59 ± 6.39 [a]	434.05 ± 6.85 [b]
Stability index	1.03 ± 0.00 [a]	0.96 ± 0.02 [b]
Flow rate index	1.58 ± 0.03 [a]	1.42 ± 0.04 [a]
Specific energy (mJ/g)	40.66 ± 1.97 [a]	17.43 ± 0.49 [b]
Unconfined yield stress (kPa)	6.13 ± 0.02 [a]	3.37 ± 0.06 [b]
Cohesion (kPa)	1.60 ± 0.01 [a]	1.02 ± 0.01 [b]
Major principle stress (kPa)	15.82 ± 0.22 [a]	12.29 ± 0.07 [b]
Angle of internal friction (º)	35.89 ± 0.80 [a]	27.26 ± 0.97 [b]
Flow function coefficient	2.58 ± 0.03 [a]	3.50 ± 0.11 [b]

[a-b]Mean values for different shape factors and flow/shear properties within a row with different superscript differ ($P < 0.05$); n=4.

Shear properties provide insights as to whether the C- and MNB-MPC powders will move from a static condition to dynamic flow or whether bridging, blockages, and stoppages are likely. UYS, Cohesion, MPS, and AIF of C-MPC powders were higher than MNB-MPC powders, indicating under consolidation, the flow behavior of MNB-MPC would be better than that of C-MPC powders. The higher cohesion and AIF values of C-MPC powders suggest that there could be potential interlocking. The UYS decreased from 6.13 to 3.37 kPa with the MNB treatment. The shear parameters, AIF and MPS significantly ($P<0.05$) decreased from 35.89 to 27.26° and 15.82 to 12.29 kPa, respectively, with the MNB treatment. Likewise, Crowley et al. (2014) reported a wall friction angle of 21.7° for a regular MPC80 powder, which differs from the value for C-MPC powders in the current study, possibly due to differences in powder particle size reported in the current study. Based on the FF classification by Jenike (1976), a powder is cohesive if its FF ranges between 2 and 4 and very cohesive between 1 and 2. Therefore, the flow behavior of C- and MNB-MPC powders could be classified as "cohesive," although the MNB-MPC had a significantly ($p < 0.05$) higher FF value. The higher the flow function value, the easier the bulk solid can flow (Bian et al., 2015). The results obtained agreed with those of Fitzpatrick et al. (2004) and differences in the flow properties of powder particles can be due to inter-particle interactions during flow (Mitra et al., 2017). Rennie et al. (1999) noted that powder cohesiveness decreases as particle size increases. However, both C- and MNB-MPC powders was classified as cohesive despite having a higher CED for C-MPC powders. Correlating SEM micrographs (Babu and Amamcharla, 2021b) and shear data, it was evident that C-MPC powders encouraged particle-to-particle interaction than MNB-MPC powders.

Furthermore, the results from compressibility testing revealed that the percent change in volume increased with normal stress applied for both C- and MNB-MPC powders (Figure 4.2).

The rearrangement of finer particles in the MNB-MPC could have resulted in higher compressibility. This could be due to the compact particle packing and increases in interparticle surface contact. Previously, McSweeney et al. (2021) noted that N_2 injected MPC powders were more compressible (50.4%) compared to regular MPC powders (41.5%). Likewise, fine particles exhibit higher compressibility than the coarser ones because of the greater surface area (Jan et al., 2017). Overall, the morphological and flow results suggested that MNB-MPC powders had a higher proportion of regular-shaped particles and a comparatively smoother surface (Table 1), confirming that it was more easy flowing or less cohesive than C-MPC powders. These observed difference in particle structure and shape also play a critical role in the physical characteristics and rehydration properties of MPC powders (McSweeney et al., 2021; Babu and Amamcharla, 2021b).

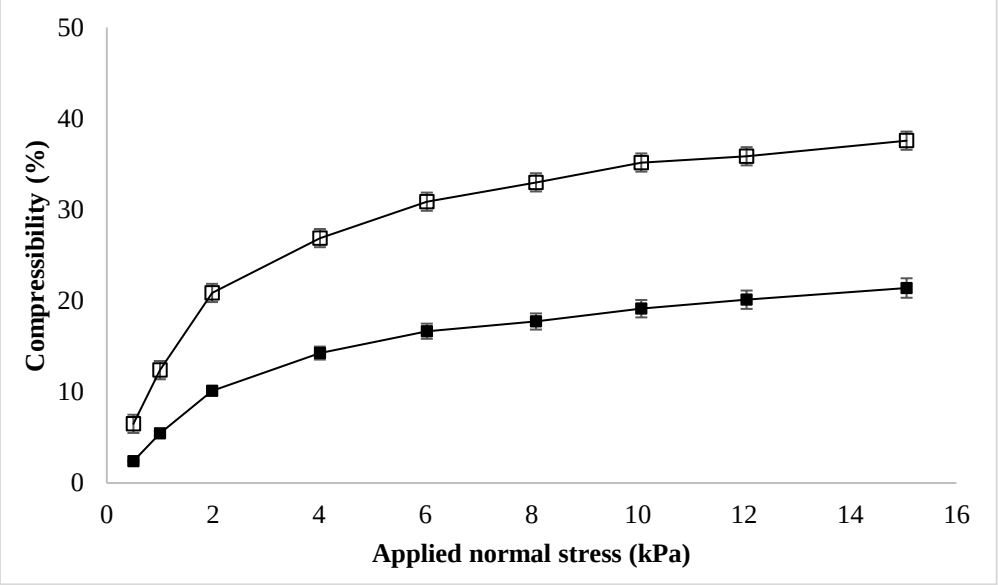

Figure 4.2 Compressibility of the control (■) and micro- and nano-bubbles treated (□) milk protein concentrate powders; n=4.

Conclusions

MNB technologies have received substantial attention for industrial applications due to the low cost, eco-friendliness, and scale-up ease. MNB treatment is a robust process technology and MNB treatment resulted in improving the flow performance of MPC powders. From the findings of this study, MNB treatment can be used as a physical pre-treatment before spray drying, and it represents a potential for a more energy-saving drying process while providing better powder flow properties without having an impact on the morphological characteristics.

References

Adhikari, B. M., Truong, T., Prakash, S., Bansal, N., and Bhandari, B. 2020. Impact of incorporation of CO_2 on the melting, texture and sensory attributes of soft-serve ice cream. Int. Dairy J. 109:104789.

Agarwal, A., Ng, W. J., and Liu, Y. 2011. Principle and applications of microbubble and nanobubble technology for water treatment. Chemosphere. 84:1175-1180.

Amamcharla, J., Li, B., and Liu, Z. 2017. Use of micro-and nano-bubbles in liquid processing. United States. Patent number: WO2017127636A1.

Anandharamakrishnan, C., 2017. Handbook of Drying for Dairy Products. John wiley & sons inc.

Babu, K. S., Siliveru, K., Amamcharla, J. K., Vadlani, P. V., and Ambrose, R. K. 2018. Influence of protein content and storage temperature on the particle morphology and flowability characteristics of milk protein concentrate powders. J. Dairy Sci. 101:7013-7026.

Babu, K. S., and Amamcharla, J. K. 2018. Application of front-face fluorescence spectroscopy as a tool for monitoring changes in milk protein concentrate powders during storage. J. Dairy Sci. 101:10844-10859.

Babu, K.S., and J.K. Amamcharla. 2021. Rehydration characteristics of milk protein concentrate powders monitored by electrical resistance tomography. J. Dairy Sci. Comm. 2:313-318.

Babu, K. S., and Amamcharla, J. K. 2022a. Application of micro- and nano-bubbles in spray drying of milk protein concentrates. J. Dairy Sci. (Accepted).

Babu, K. S., and Amamcharla, J. K. 2022b. Generation methods, stability, detection techniques, and applications of bulk nanobubbles in agro-food industries: a review and future perspective. Crit. Rev. Food Sci. Nutr. (Submitted).

Babu, K. S., Liu, D. Z., and Amamcharla, J. K. 2022. Application of Micro-and Nano-Bubbles as a Tool to Improve the Rheological and Microstructural Properties of Formulated Greek-Style Yogurts. Foods 11:619.

Bian, Q., S. Sittipod, A. Garg and R. P. K. Ambrose. 2015. Bulk flow properties of hard and soft wheat flours. J. Cereal Sci. 63:88-94.

Bouvier, J.M., Collado, M., Gardiner, D., Scott, M., and Schuck, P., 2013. Physical and rehydration properties of milk protein concentrates: comparison of spray-dried and extrusion-porosified powders. Dairy Sci. Technol. 93, 387–399.

Caric, M., and Kalab, M. 1987. Effects of drying techniques on milk powders quality and microstructure: A review. Food Structure, 6:171-180.

Crowley, S. V., Gazi, I., Kelly, A. L., Huppertz, T., and O'Mahony, J. A. 2014. Influence of protein concentration on the physical characteristics and flow properties of milk protein concentrate powders. J. Food Eng. 135:31-38.

Ebina, K., Shi, K., Hirao, M., Hashimoto, J., Kawato, Y., Kaneshiro, S., Morimoto, T., Koizumi, K., and Yoshikawa, H. 2013. Oxygen and air nanobubble water solution promote the growth of plants, fishes, and mice. PloS one. 8:e65339.

Fitzpatrick, J. J. 2007. Particle properties and the design of solid food particle processing operations. Food Bioprod. Process. 85:308-314.

Fu, X., Huck, D., Makein, L., Armstrong, B., Willen, U., and Freeman, T. 2012. Effect of particle shape and size on flow properties of lactose powders. Particuology. 10:203-208.

Hanrahan, F. P., Tamsma, A., Fox, K. K., and Pallansch, M. J. 1962. Production and properties of spray-dried whole milk foam. J. Dairy Sci. 45:27-31.

Ilari, J. L. 2002. Flow properties of industrial dairy powders. Le Lait. 82:383-399.

Jan, S., Ghoroi, C., and Saxena, D. C. 2017. A comparative study of flow properties of basmati and non-basmati rice flour from two different mills. J. Cereal Sci. 76:165-172.

Jannesari, M., Akhavan, O., Madaah Hosseini, H. R., and Bakhshi, B. 2020. Graphene/CuO_2 Nanoshuttles with Controllable Release of Oxygen Nanobubbles Promoting Interruption of Bacterial Respiration. ACS Appl. Mater Interfaces. 12:35813-35825.

Jenike, A. W. 1976. Storage and Flow of Solids, Bulletin No. 123 (Utah Engineering Station, Salt Lake City, Utah).

Keogh, M. K., Murray, C. A., and T O'Kennedy, B. 2003. Effects of ultrafiltration of whole milk on some properties of spray-dried milk powders. Int. Dairy J. 13:995-1002.

Kim, E. H. J., Chen, X. D., and Pearce, D. 2005. Effect of surface composition on the flowability of industrial spray-dried dairy powders. Colloids Surf. B Biointerfaces. 46:182-187.

Kosasih, L., Bhandari, B., Prakash, S., Bansal, N., and Gaiani, C. 2016. Physical and functional properties of whole milk powders prepared from concentrate partially acidified with CO2 at two temperatures. Int. Dairy J. 56:4-12.

Kudo, Y., Yasuda, M., and Matsusaka, S. 2020. Effect of particle size distribution on flowability of granulated lactose. Adv. Powder Technol. 31:121-127.

Leturia, M., M. Benali, S. Lagarde, I. Ronga., and K. Saleh. 2014. Characterization of flow properties of cohesive powders: A comparative study of traditional and new testing methods. Powder Technol. 253:406-423.

Li, K., Woo, M. W., Patel, H., Metzger, L., and Selomulya, C. 2018. Improvement of rheological and functional properties of milk protein concentrate by hydrodynamic cavitation. J. Food Eng. 221:106-113.

Lapčík, L., Lapčíková, B., Otyepková, E., Otyepka, M., Vlček, J., Buňka, F., and Salek, R. N. 2015. Surface energy analysis (SEA) and rheology of powder milk dairy products. Food Chem. 174:25-30.

Liu, G., Wu, Z., and Craig, V. S. 2008. Cleaning of protein-coated surfaces using nanobubbles: an investigation using a quartz crystal microbalance. J. Phys. Chem. C. 112:16748-16753.

Mitra, H., H. A. Pushpadass, M. E. E. Franklin, R. P. K. Ambrose, C. Ghoroi., and S. N. Battula. 2017. Influence of moisture content on the flow properties of basundi mix. Powder Technol. 312:133-143.

Phan, K. K. T., Truong, T., Wang, Y., and Bhandari, B. 2020. Nanobubbles: Fundamental characteristics and applications in food processing. Trends Food Sci Technol. 95:118-130.

Power, O. M., Maidannyk, V., McSweeney, D. J., Fenelon, M. A., O'Mahony, J. A., and McCarthy, N. A. 2020. Water sorption and hydration properties of high protein milk powders are influenced by enzymatic crosslinking and calcium chelation. Powder Technol. 364:680-688.

Rennie, P. R., Chen, X. D., Hargreaves, C., and Mackereth, A. R. 1999. A study of the cohesion of dairy powders. J. Food Eng. 39:277-284.

Schuck, P. 2011. Milk powder: physical and functional properties of milk powders. 2nd ed. J.W. Fuquay, P.F. Fox (Eds.), McSweeney PLH encyclopedia of dairy science. 3:117-124

Temesgen, T., Bui, T. T., Han, M., Kim, T. I., and Park, H. 2017. Micro and nanobubble technologies as a new horizon for water-treatment techniques: Review Adv. Colloid Interfac. Sci. 246:40-51.

Zhang, Z. H., Wang, S., Cheng, L., Ma, H., Gao, X., Brennan, C. S., and Yan, J. K. 2022. Micro-nano-bubble technology and its applications in food industry: A critical review. Food Rev. Int. 1-23.

Chapter 5 - Influence of bulk nanobubbles generated by acoustic cavitation to improve the processability of milk protein concentrate

Abstract

Bulk nanobubbles (BNBs) are nano-scaled bubbles (50-700 nm) with unique properties and offer potential applications in the dairy and food industry. The overall objective of the present study was to use a continuous acoustic cavitation technique at 20 kHz capable of delivering up to 1.5 kW of power with a continuous flow cell design was employed to incorporate BNBs in milk protein concentrates (MPCs) to improve the processability. The first objective of this study was to characterize the BNBs in deionized (DI) water in terms of concentration and mean diameter using a nanoparticle tracking system. The mean diameter of BNB was 231.5±5.3 nm, respectively. BNB concentration significantly increased ($P < 0.05$) with the increase in amplitude. The second objective of this study was to evaluate the presence of BNB on the processability of MPC dispersions. Three lots of MPC powders were obtained from a commercial manufacturer. Randomized complete block design with total solids (TS; 15 and 19%) and amplitude (0, 50, 75, and 90%) as independent factors were studied. MPC powders were reconstituted to desired total solids and exposed to acoustic cavitation to generate BNBs as per the experimental design. The treated MPC dispersions were analyzed for rheology, functional properties, and microstructure. Additionally, the selected combinations were spray-dried using the spray dryer to characterize and compare the resultant BNB-MPC powder with the C-MPC powder. The apparent viscosity of the untreated MPC was 68.90 and 201.57 mPa·s at 100 s^{-1} for 15 and 19% TS, respectively. The viscosity decreased to 5.55 and 15.43 mPa·s at 100 s^{-1} for 15 and 19% TS, respectively, after the acoustic cavitation. The viscosity significantly decreased ($P < 0.05$) at all the amplitudes studied. The improvement in powder rehydration with the BNB treatment was attributed to the powder microstructure. BNB-MPC powders had significantly lower bulk density and unique bulk powder properties. In conclusion, the BNB treatment helps to reduce the viscosity and therefore this study suggests the potential of using BNB treatment for a more energy-

efficient drying process, while maintaining and/or improving the physicochemical properties of the resultant powders.

Introduction

Nano-scaled materials are constantly evolving, and they have an outstanding possibility to bring a lot of significant advantages for practical applications in various manufacturing sectors. The last two decades have seen substantial academic and industrial interest in investigations on the unique properties of extremely ultrafine bubbles or nanobubbles (NBs). Ordinary bubbles have larger diameters causing them to rise quickly to the surface of an aqueous solution, collapse or burst out of solution, and disappear. However, NBs have shown to remain in liquid for an extended period of time (Favvas et al., 2021). NBs are gas-filled cavities within liquids having diameters < 1μm. In recent years, two types of nanobubbles have been studied: (i) surface nanobubbles, which form at solid-liquid interfaces, and (ii) bulk nanobubbles (BNBs), which exist in the bulk liquid. Unlike ordinary bubbles, nanobubbles exhibit high stability, negative surface charge, and a large surface-to-volume ratio. In the present study, we have explored the possibility of generating BNBs using a continuous acoustic cavitation technique. Very recently, the proof of the existence of BNBs generated using acoustic cavitation was given by Jadhav and Barigou (2020). Acoustic cavitation involves the generation, expansion, growth, and adiabatic collapse of microbubbles. The collapse and disappearance of such microbubbles give rise to the formation of BNBs. The effects of ultrasonic frequency and power on the formation of nanobubbles were previously investigated (Yasuda, Matsushima, & Asakura, 2019). The BNBs were created in their study by sonicating ultrapure water, and the concentration of NBs rose under low-frequency and high-power ultrasound settings. BNBs are gaining popularity because they can enhance surface area, promote mass transfer, and change the physicochemical

properties of a medium (Ahmed et al., 2018). The existence and stability of NBs have been verified and applied in a variety of science fields. Although theoretical research on BNBs are currently lacking, multiple applications of BNBs in diverse sectors, such as water treatment, surface cleaning, and in food and agriculture applications were previously reviewed (Phan, Truong, Wang, & Bhandari, 2020; Zhang et al., 2022).

Milk protein concentrate (MPC) powders are dairy ingredients with protein content ranging from 35 to 90% (w/w) and are widely used in various food product formulations such as beverages, yogurts, and protein bars to improve their nutritional, functional, and sensory properties. The MPCs are manufactured from skim milk using ultrafiltration and diafiltration to selectively remove lactose and minerals. Subsequently, unit operations like reverse-osmosis/evaporation and spray drying are employed to manufacture MPC in powder form. Simple and innovative strategies before spray drying are of critical consideration for the dairy industry producing MPCs. One of the key challenges encountered by the MPC manufacturers during the processing is the high viscosity after ultrafiltration and evaporation. Reducing viscosity and aiding an increase in the solid levels before spray drying can offer significant savings on the overall energy cost of powder production. On the other side, it is also a challenge for the end-user to incorporate the MPC powders in a formulation due to their poor rehydration properties, which are influenced by intrinsic powder properties, such as surface and bulk composition, rehydration conditions, storage, etc. Numerous studies have investigated ways to improve their rehydration behavior via tailoring the behavior of its components, through alteration of the ionic environment of the retentate. Mechanical pre-treatments before spray drying have also been shown to improve the solubility and other functional properties of MPC powders: nitrogen gas injection (McSweeney et al., 2021), extrusion porosification (Bouvier et

al., 2013), and hydrodynamic cavitation (Li et al., 2018). In the present work, we are exploring the possibility of utilizing BNBs for improving the processability, rehydration, and bulk handling properties of MPCs. This study aims to i) characterize the BNBs generated by continuous acoustic cavitation in deionized water in terms of concentration and mean diameter; ii) evaluate the effect of BNB on rheology, physicochemical, and microstructure of MPC dispersions; and iii) investigate the rehydration and bulk properties of BNB treated MPC powders.

Materials and methods

Generation of bulk nanobubble

BNBs were generated by continuous acoustic cavitation using a 20 kHz probe-type processor (VCX 1500, Sonics & Materials, USA) capable of delivering up to 1.5 kW of power with a flow cell design, as shown in Figure 5.1. A new clean titanium probe of 1-inch diameter and 9-inch length was used to acoustically cavitate the bulk liquid flowing at a rate of 10 mL/min using a peristaltic pump (Watson Marlow, USA). The temperature of the sample throughout the BNB incorporation was controlled at 20°C by using a recirculating cooler.

Characterization of bulk nanobubble

Lately, the experimental works on the existence of BNBs have been debated by various research groups. One research group claims to have presented unquestionable evidence for the existence of BNBs in pure water (Jadhav and Barigou, 2020). In contrast, another research group clearly disagrees and rule out the possibility of the existence of BNBs in pure water (Rak et al., 2019; Rak and Sedlák, 2020). Nanoparticle tracking analysis (NTA) using the Malvern NanoSight LM10 is a firmly established method that gives real-time visualization, size, and concentration of nanoparticles or nanobubbles in the bulk liquid. The control and the BNB incorporated DI water was characterized in terms of concentration and mean diameter using the

nanoparticle tracking system. Rak et al. (2019) demonstrated that acoustic cavitation generates fine metal (titanium) nanoparticles from the disintegration of the surface of the ultrasonic probe leading to the generation of nanoparticles which are, however, not BNBs. Indeed, NTA cannot differentiate between the nanoparticles and the BNBs. Therefore, the non-existence/traces of titanium nanoparticles were also determined using inductively coupled plasma mass spectrometry. The sample was then transferred to the Perkin Elmer NexIon 350 inductive coupled plasma-mass spectrometry for analyzing titanium concentration in bulk NB suspensions. These measurement techniques and their protocols are discussed in more detail elsewhere (Jadhav and Barigou, 2020; Nirmalkar et al., 2019).

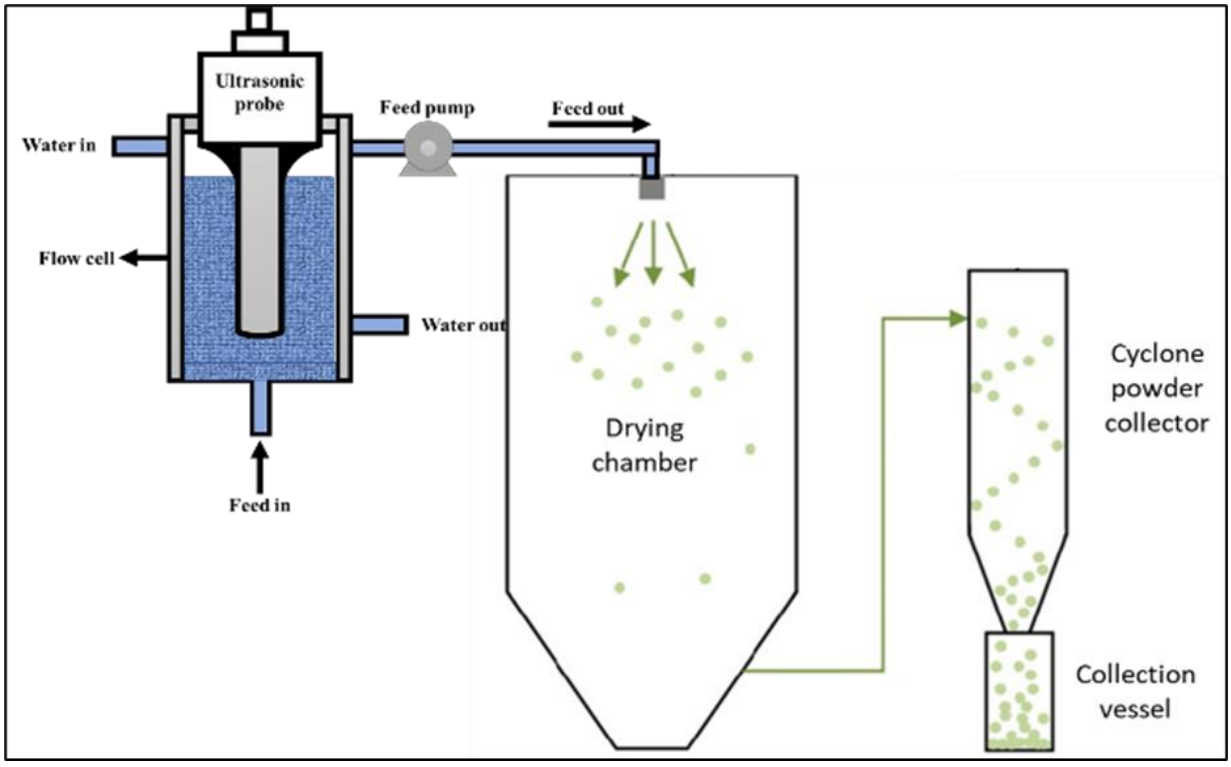

Figure 5.1 Schematic for the experimental setup for continuous acoustic cavitation processing with direct spray drying.

Experimental approach

Three lots of MPC85 powders were obtained from a commercial manufacturer and a randomized complete block design with total solids (15 and 19%, w/w) and ultrasonic amplitude (0, 50, 75, and 90%) as independent factors were studied. The average protein, moisture, fat, lactose, and ash content of the MPC85 used for this study was 86.05% (w/w), 5.11% (w/w), 0.93% (w/w), 4.81% (w/w) and 6.65% (w/w), respectively. Briefly, MPC85 powders were reconstituted to 15 and 19% TS in DI water and left overnight in a refrigerator. Samples were equilibrated to 20°C in a water bath following overnight storage and treated using the continuous acoustic cavitation system as per the experimental design. Control MPC (C-MPC; without BNBs) and BNB-treated MPC (BNB-MPC; BNB incorporated) were compared and evaluated for physical, rheological, morphological, and functional properties. Additionally, selected combinations (19% TS; amplitude 50 and 90%) were spray-dried using the spray dryer to characterize and compare the resultant BNB-MPC powder with the C-MPC powder.

Rheological measurements of C- and BNB-MPC dispersions

The C- and BNB-MPC liquid dispersions were characterized in terms of its rheological properties. Additionally, the voluminosity and volume fraction of casein micelles were determined by rheometry following a method by Nöbel et al. (2016). Additionally, frozen samples of the C- and BNB-MPC liquid dispersions were thawed in a refrigerator at 4 °C for 1 day, followed by further thawing in a water bath at 45 °C for either 30 min and were tested for rheological, properties. The continuous rotational flow measurement was done using a stress-strain-controlled rheometer (MCR-92 Anton Paar) at a varied shear rate from 0.01 s^{-1} to 100 s^{-1} at 20°C, and the data obtained were also fitted to the power-law model using Equation 1.

$$\eta = \kappa \times \gamma^{(n-1)} \qquad (1)$$

where η is the viscosity (Pa·s), n is the flow behavior index, and κ is the consistency coefficient ($Pa \cdot s^n$).

Particle size distribution of C- and BNB-MPC dispersions

The average particle size of C- and BNB-MPC dispersions were measured by dynamic laser light scattering using a particle size analyzer at 20ºC (DelsaMax PRO; Beckman Coulter, USA). The C- and BNB-MPC dispersions were prepared for particle size analysis by diluting 1:100 (v/v) using deionized water before measurements.

Microstructure of C- and BNB-MPC dispersions

The microstructure of C-MPC and BNB-MPC dispersions were studied using confocal laser scanning microscopy (CLSM), following the method described in Gandhi et al. (2017). Samples were prepared for CLSM by diluting 1:100 (v/v) using deionized water before measurements. Proteins were stained using the Fast green FCF (Sigma-Aldrich, St. Louis, MO, USA) stain. Stock solution of Fast green (5 mg dye in 5 mL water) was applied to the sample for 5-10 min. The stained samples were analyzed in LSM 5 Pa (Zeiss, Thornwood, NY, USA). Three-dimensional images were obtained by scanning the sample across a defined section along the z-axis. Transmission electron microscopy was also used to image C- and BNB-MPC dispersions in order to characterize the microstructure. Samples were analyzed for morphology using negative-staining technique. One drop of the diluted sample was mounted on Formvar/carbon-coated 200-mesh copper grids (Electron Microscopy Sciences, Fort Washington, PA) for 2 min. Subsequently, combined with a drop of 2% uranyl acetate and left for 30 s before the excess liquid was drawn off with a filter paper and was examined using a CM 100 TEM (FEI Company, Hillsboro, OR) operating at 100 kV and images captured with a digital

camera (model C8484, Hamamatsu, Bridgewater, NJ) using the AMT software (Advanced Microscopy Techniques, Chazy, NY).

Calcium ion activity and heat coagulation time of C- and BNB-MPC dispersions

The Calcium ion activity of the all the C- and BNB-MPC dispersions were measured using Accumet combination ion-selective electrode (Fisher Scientific, Pittsburgh, PA, USA). A fisher scientific accumet AP63 portable pH meter was used to record the pH on the C-and BNB-SMC dispersions. For determining the heat coagulation time C- and BNB-MPC dispersions, 3 mL of the sample was filled in a heat-resistant screw cap test tubes (8 mL, 17 mm dia. x 63 mm height) (DWK Life Science, Milville, NJ). The test tubes were inserted on the stainless-steel rack. The rack along with tubes was immersed in an oil bath (Narang Scientific Works Pvt. Ltd, New Delhi, India) maintained at 140°C and placed on the rocker. Heat coagulation time was noted as the time elapsed between dipping the samples in the hot oil bath and the onset of first visible clots/flakes. (Crowley et al., 2014; Meena et al., 2016).

Gel electrophoresis of C- and BNB-MPC dispersions

The C-and BNB-SMC dispersions for gel electrophoresis were diluted to 0.5% protein content and vortexed. The diluted samples were analyzed with gel electrophoresis techniques reducing sodium dodecyl sulfate polyacrylamide gel electrophoresis (SDS-PAGE) (Richa and Amamcharla, 2020).

Fluorescence spectroscopy of C- and BNB-MPC dispersions

Front-face fluorescence spectra of the C-and BNB-MPC dispersions were collected using a LS50B Luminescence spectrometer (PerkinElmer) following a method by (Richa and Amamcharla, 2020). The spectral data generated were also used to determine fluorescence of

advanced Maillard products and soluble tryptophan (FAST) index (Damjanovic Desic and Birlouez-Aragon, 2011). Tryptophan fluorescence of the soluble fraction at 290/340 nm and fluorescence of advanced Maillard products measured at 360/420 nm were used to calculate FAST index. Additionally for the control and BNB treated spray dried and reconstituted MPC dispersions, the soluble phase was prepared and analyzed for using right-angle fluorescence analysis following a method by (Richa and Amamcharla, 2020).

Spray drying of the bulk nanobubble incorporated MPC dispersions

Additionally, selected combinations (19% TS; amplitude 50 and 90%) were spray-dried using the spray dryer (YC-015; Shanghai Pilotech Instrument & Equipment Co. Ltd.) to characterize and compare the resultant BNB-MPC powder with the C-MPC powder. The inlet temperature was set at 180°C, and the outlet temperature ranged between 60 and 65°C. The spray pressure was maintained at 206.84 kPa, and the relative humidity of the room was periodically recorded using a digital humidity meter (Traceable Humidity Meter, Fisher Scientific). The spray-dried C- and BNB-MPC powders were collected and sealed in Whirl-Pak bags (Nasco) for further analysis.

Rehydration characteristics of spray dried C- and BNB-MPC powders

The rehydration behavior of the C- and BNB-MPC powder were studies using three techniques: first the solubility of the powders was estimated based on the total solids in the supernatant obtained by centrifugation at 700 × g for 10 min at 25°C as described by Anema et al. (2006). Then the amount of soluble material in the MPC was calculated. Also, the dissolution characteristics of the C- and BNB-MPC powders were evaluated using the focused beam reflectance measurement method (Babu and Amamcharla, 2018). The ITS p2+ system (Industrial Tomography Systems, Manchester, UK) in circular vessel configuration was also used for

monitoring the dissolution of the C- and BNB-MPC powders. Real-time tomographic data was gathered by the sensors during the dissolution process as they evolve through contrasts in the electrical properties of during powder dissolution (Babu and Amamcharla, 2021).

Microstructure of spray dried C- and BNB-MPC powder

The microstructure of C- and BNB-MPC powders were examined using a scanning electron micrography (SEM) according to the method described by Mimouni et al. (2010). The C- and BNB-MPC powders were chopped at room temperature using an injector blade (71990, Electron Microscopy Sciences, Hatfield, PA, USA). After chopping, the C- and BNB-MPC powders were directly mounted onto a carbon double-sided adhesive tape on microscopy stubs and sputter-coated with palladium using a Denton Vacuum Desk II sputter coater (Denton Vacuum, Moorestown, NJ) for 15 min to avoid the charge buildup under the electron beam. The imaging was performed using a S-3500N (Hitachi Science Systems Ltd., Tokyo, Japan) and was examined by a secondary electron detector operating at 10 kV and the cross-section of C- and BNB-MPC powders samples were observed.

Physical properties and flow characterization of spray dried C- and BNB-MPC powders

The circle equivalent diameter (CED) of C- and BNB-MPC powders were analyzed by Malvern Morphologi G3ID (Malvern Instruments, Worcestershire, UK) following method by Babu et al. (2018). The CED was calculated from the 2-D images. The FT4 powder rheometer (Freemans Technology, Tewkesbury, UK) was used to evaluate the powder rheology of the C- and BNB-MPC powders following the method described by Babu et al. (2018). Cohesion, unconfined yield strength (UYS), major principle stress (MPS), and flow function (FF) were obtained from the shear tests.

Statistical Analysis

Measurements of C- and BNB-MPC dispersion and powder characteristics were performed in triplicate, with results presented as mean ± standard deviation. Data were analyzed as a completely randomized design with total solids (15 and 19% TS, w/w) and amplitude (0, 50, 75, and 90%) as independent factors for C- and BNB-MPC dispersions and 19% TS with amplitude of 50 and 90% for C- and BNB-MPC powders. Analysis of variance was carried out using the statistical software SAS (PROC GLIMMIX, Version 9.4; SAS® Institute, Inc., Cary, NC, USA) statistical analysis package. The level of significance was set at $P < 0.05$.

Results and discussion

Characterization of bulk nanobubble

One of the common methods that are reported to produce bulk nanobubbles are based on acoustic cavitation (Jadhav and Barigou, 2020; Nirmalkar et al., 2019). NTA and inductively coupled plasma mass spectrometry to provide this distinctive evidence on the existence of BNBs generated by acoustic and to demonstrate that the nano-entities observed in DI water are indeed gas-filled domains (BNBs), and to test the efficiency of the continuous acoustic cavitation system to efficiently generate BNBs. Figure 5.2 shows the NTA results obtained from control and BNB-treated DI water. The Nanosight showed a significant increase in particle concentration upon the BNB treatment, suggesting that the acoustic cavitation was efficient in generating BNBs. BNB treated DI water (90% amplitude) had a mean particle size of 235.5 ± 102.3 nm. The particle size distribution of the BNBs was D10, 134.3; D50, 209.2; D90, 369.6 nm. The concentration was found to be 2.41×10^8 and 1.19×10^9 particles/mL for DI water and BNB treated (90% amplitude) DI water, respectively. In other words, the concentration of BNB treated DI water was significantly higher compared to the DI water (~1 billion nanobubbles/mL).

Previously, Yasuda et al (2019) generated BNBs from ultrasonic irradiation (frequency of 22 kHz) and noted a BNB size of 50-220 nm. Likewise, Jadhav and Barigou (2020) and Nirmalkar et al. (2019) also have used acoustic cavitation and generated BNBs that were stable in pure water. Furthermore, BNB treated DI water samples had the presence of titanium in only trace amount (0.00017 μg/mL), implying the presence of titanium contamination could not be blamed for the detected nano-entities using NTA, which agrees with that reported by other researchers (Jadhav and Barigou, 2020a, 2020b). This observation further confirms the presence of BNBs generated via acoustic cavitation. In contrast, some researchers have reported presence of nanoparticles are misinterpreted as BNBs (Rak and Sedlák, 2020). Nevertheless, there is no definite consensus in the literature yet as to why the BNBs have an incredible longevity, an the BNB stability remains a mystery to date.

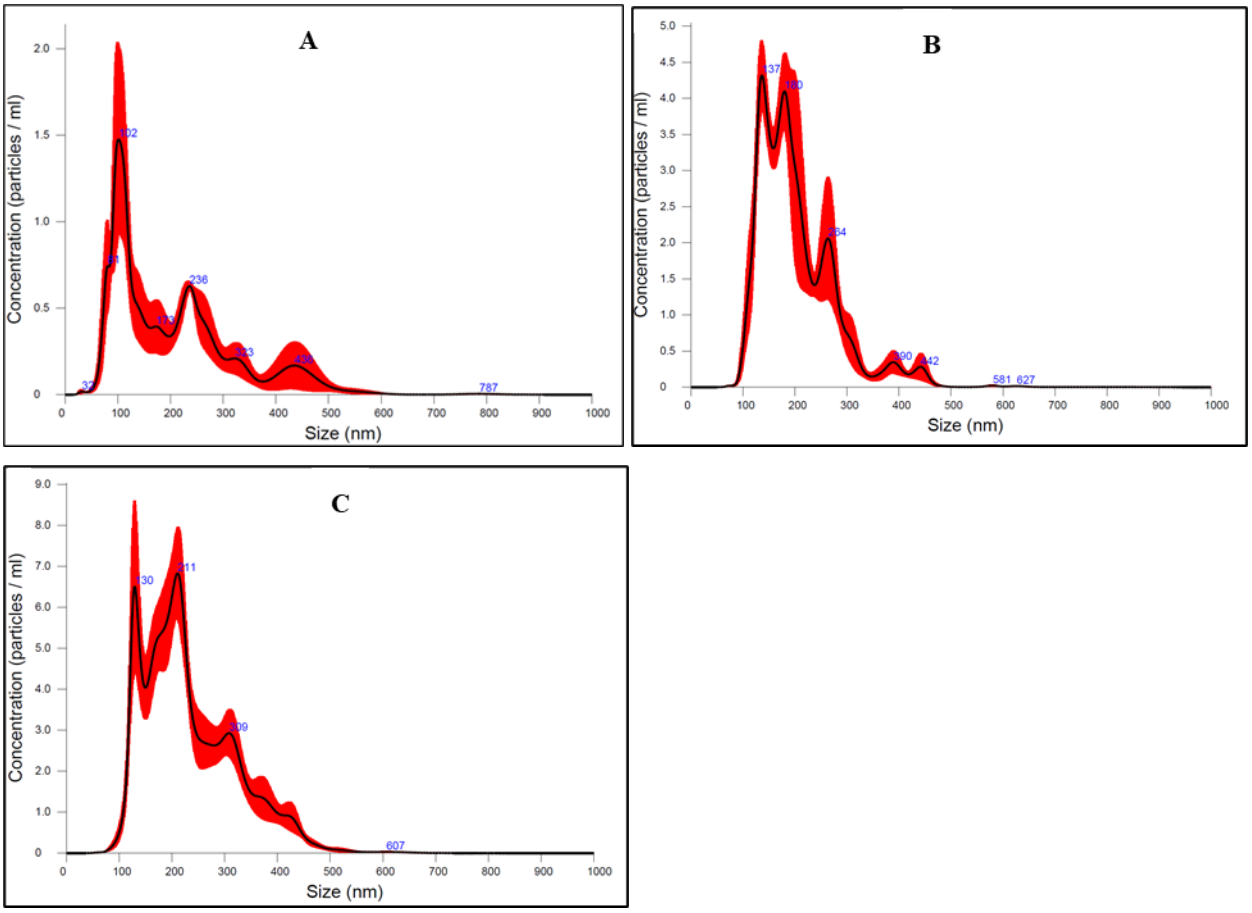

Figure 5.2 Nanoparticle tracking analysis (NTA) results shown as smoothed histogram presenting averaged concentration and size of deionized water: (A) control, (B) bulk nanobubble treatment at 50% amplitude, and (C) bulk nanobubble treatment at 90% amplitude.

Viscosity measurements of C- and BNB-MPC dispersions

The general flow characterization of the C- and BNB-MPC dispersions are shown in Figure 2. All samples exhibited a non-Newtonian shear thinning behavior. Compared to the C-MPC, the viscosity significantly decreased ($P < 0.05$) at all the amplitudes (50, 75, and 90%) studied. However, it was observed that with the increase in amplitude, the viscosity of MPC dispersions were not significantly ($P > 0.05$) different from each other. The apparent viscosity of the C-MPC was 68.90 and 201.57 mPa·s at 100 s^{-1} for 15 and 19% TS, respectively. The viscosity significantly ($P < 0.05$) decreased to 5.55 and 15.43 mPa·s at 100 s^{-1} for 15 and 19%

TS, respectively, after the treatment at 90% amplitude. Similar reduction in apparent viscosity values were observed after the treatment at 50 and 75% amplitude. This represents a net decrease of ~90% viscosity in the for BNB-MPC, when compared to the C-MPC. This was also supported by visual observations in the microstructure. A similar trend was reported in a study conducted by Li et al. (2018) using hydrodynamic cavitation, with the decrease in viscosity in MPC retentates at cavitation frequency of 25 and 50 Hz. Analysis of the viscosity profiles with the power-law model also highlighted the differences in the flow behavior index, n, and the consistency coefficient, κ, for the C- and BNB-MPC dispersions. At 19% total solids, the n and κ values were 0.44 and 2.90 Pa S^n for C-MPC, whereas it was 0.74 and 0.06 Pa S^n for the BNB-MPC (90% amplitude) dispersion. The higher viscosity can be attributed primarily to the higher voluminosity of the C-MPC dispersions (Sutariya et al., 2017). The voluminosity and volume fraction were also calculated, and it was found to be 3.87 mL/g and 0.74 for C-MPC, whereas it was 2.88 mL/g and 0.55 for the BNB-MPC (90% amplitude) dispersion. The present study is also supported by Zisu et al. (2013), who found a significant change in the rheological properties by acoustic cavitation of concentrated skim milk. They noted a reduction in viscosity of ~10%. Remarkably, the effect of acoustic cavitation was more pronounced for age thickened samples for which a reduction (~17%). Chen et al. (2011) hypothesized that during the acoustic cavitation process, bubble implosion produced shock waves, which led to viscous dissipative eddies that develop shear stresses in the medium, therefore lowering the viscosity. Additionally, when BNBs are introduced into the MPC systems, they function as a buffer between milk protein particles, thereby preventing the aggregation of the proteins. Previously, Yanjun et al. (2014) have studied influence of ultrasound on MPC systems and noted that sonication breaks apart large aggregates leading to a decrease in particle size and a lower viscosity. Amamcharla et al. (2017) have

reported that introducing bulk MNBs with an average diameter of 100 nm to 30 µm reduced viscosity in liquid dairy products. Similarly, Khaira et al. (2020) found that ice cream prepared with NBs had a decreased apparent viscosity (30% reduction). The viscosity dropping effect of NB treatment for a 7-day test period (at 23 and 4ºC) in apple juice concentrate and canola oil was demonstrated by Phan et al. (2021). Additionally, the freeze-thawed C- and BNB-MPC dispersions exhibited similar behavior to that of the samples tested immediately after the BNB incorporation, a decreased viscosity was demonstrated (Table 5.1 and 5.2). The observed differences in viscosity could be directly related to particle size and microstructure. Researchers have previously reported that when BNBs made in pure water were frozen and then thawed, they appeared to vanish, and the various causes of this disappearance is discussed elsewhere (Jadhav and Barigou, 2020a; Nirmalkar et al., 2018). Interestingly, Jadhav and Barigou (2021) observed that nano-entities floating in water disintegrate into fine bubbles after being frozen and thawed, which tend to re-cluster and restore their initial stable size fast when shaken vigorously, or gradually if held undisturbed for many days. For concentrated milk protein systems, it is well established that the presence of aggregates can result in a marked increase in viscosity (Nicoud et al., 2015). Thus, based on the current findings it is implied that the acoustic cavitation assisted decrease in viscosity is due to disruption of aggregates. Overall, BNB treatment can be a more efficient processing approach than other convectional ones, also can be envisaged as a novel "green" approach.

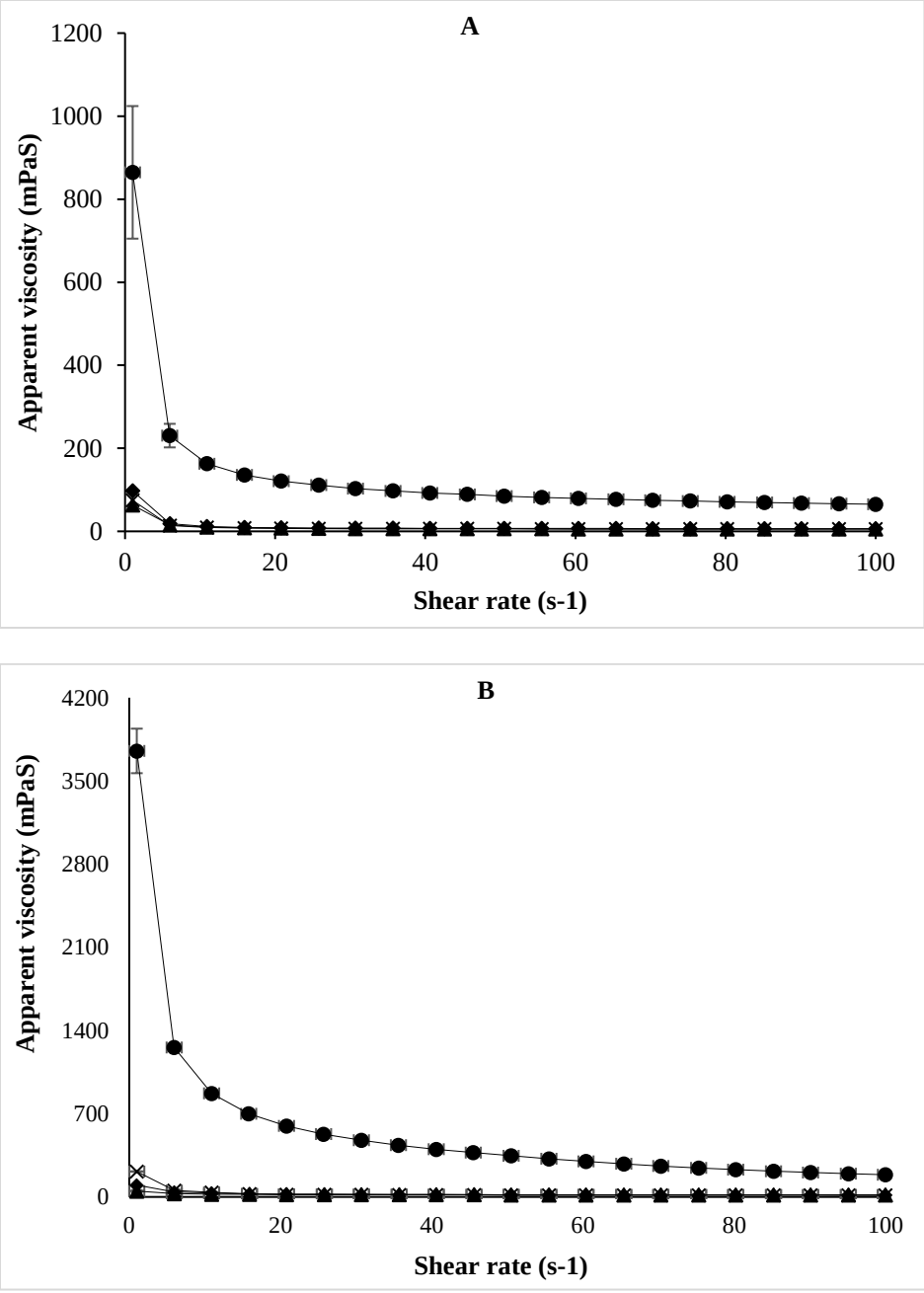

Figure 5.3 Apparent viscosity versus shear rate plot of control (●) and bulk nanobubble treated 15% (A) and 19% (B) total solids milk protein concentrate dispersions at amplitude of 50 (×), 75 (♦), and 90 % (▲), respectively.

Values are the means of data from duplicate analysis from three lots of MPC powders, with the standard deviation indicated by error bars.

Table 5.1 Rheological characterization of control and bulk nanobubble treated milk protein concentrate dispersions (Total solids:15%).

Amplitude (%)	Apparent viscosity at 100 s^{-1} (mPaS)	Consistency Coefficient (K) (PaS^n)	Flow behavior index (η)	Volume fraction	Voluminosity (mL/g)	Apparent viscosity at 100 s^{-1} after thawing (mPaS)
0	68.90 ±	0.84 ±	0.42 ±	0.70 ±	4.64 ±	91.71 ±
	2.67 [a]	0.04 [a]	0.06 [a]	0.01 [a]	0.01 [a]	3.02 [a]
50	6.72±	0.05 ±	0.54 ±	0.53 ±	3.50 ±	14.20 ±
	1.21[b]	0.03 [b]	0.07 [b]	0.03 [b]	0.02 [b]	1.25 [b]
75	6.09±	0.05 ±	0.51 ±	0.48 ±	3.19 ±	13.48 ±
	0.21 [b]	0.02 [b]	0.08 [b]	0.02 [b]	0.01 [b]	0.02 [b]
90	5.55±	0.03 ±	0.62 ±	0.46 ±	3.04 ±	13.13 ±
	0.78 [b]	0.01 [b]	0.06 [b]	0.01 [b]	0.02 [b]	1.11 [b]

[a-b] Mean within a column with different superscript differ ($P<0.05$) n=3

Table 5.2 Rheological characterization of control and bulk nanobubble treated milk protein concentrate dispersions (Total solids:19%).

Amplitude (%)	Apparent viscosity at 100 s^{-1} (mPaS)	Consistency Coefficient (K) (PaS^n)	Flow behavior index (η)	Volume fraction	Voluminosity (ml/g)	Apparent viscosity at 100 s^{-1} after thawing (mPaS)
0	201.57 ±	2.90 ±	0.44 ±	0.74 ±	3.87 ±	222.47 ±
	12.98 [a]	1.23 [a]	0.08 [a]	0.01 [a]	0.02 [a]	10.05 [a]
50	17.56 ±	0.10 ±	0.57 ±	0.60 ±	3.17 ±	35.52 ±
	0.48 [b]	0.03 [b]	0.03 [a]	0.01 [b]	0.01 [b]	1.55 [b]
75	16.86 ±	0.09 ±	0.58 ±	0.60 ±	3.16 ±	33.51 ±
	0.83 [b]	0.03 [b]	0.03 [a]	0.02 [b]	0.01 [b]	2.01 [b]
90	15.43 ±	0.06 ±	0.74 ±	0.55 ±	2.88 ±	31.19 ±
	0.52 [b]	0.01 [b]	0.05 [a]	0.09 [b]	0.05 [b]	0.59 [b]

[a-b] Mean within a column with different superscript differ ($P<0.05$) n=3

Particle size analysis of C- and BNB-MPC dispersions

The results of particle size analysis of C- and BNB-MPC dispersions are given in Table 5.3. Analysis of the particle size distribution showed the presence of relatively large particles in the C-MPC, which could be attributed to the presence of large protein aggregates. The cavitation treatments at all amplitudes introduced a significant decrease in mean particle size for both 15 and 19% TS. BNB treatment indicated an absence of insoluble particles in the size range >10 μm, and this was further supported by the voluminosity data, playing a key role in controlling viscosity. Based on the analysis of particle size distribution, the viscosity reduction was suggested to be linked to a reduction in the presence of large particles, possibly due to disruption of aggregates. These findings were also supported by CLSM and TEM images (Figure 5.4 and 5.5). Similarly, Zisu et al. (2010) used continuous acoustic cavitation (20 kHz; flowrate, 0.3 L/min; amplitude at 30 and 60%) in whey protein and milk protein retentate and have noted that force generated through acoustic cavitation resulted in a decrease in particle size of aggregates. Yanjun et al. (2014) showed that the particle size of MPC dispersions is reduced by acoustic cavitation because of the disruption of aggregated protein network (20 kHz; amplitude, 50%).

Calcium ion activity and heat coagulation time of C- and BNB-MPC dispersions

Table 5.3 shows the calcium ion activity and heat coagulation time of C- and BNB-MPC dispersions. The results given in Table 5.3 showed that presence of BNBs have an insignificant ($P>0.05$) effect on pH, calcium ion activity, and heat coagulation time. To summarize, in C- and BNB-MPC dispersions, any of the colloid reactions induced by the BNBs did not lead to remarkable differences in casein aggregation behavior. The increase in calcium ion activity with decreasing pH described in this study was also consistent with those shown in rehydrated MPC powders as reported by Crowley et al. (2014).

Table 5.3 Particle size, turbidity, and FAST Index values of control and bulk nanobubble treated milk protein concentrate dispersions.

Total solids (%)	Amplitude (%)	Mean diameter (nm)	FAST Index	Heat coagulation time (min)	pH	Calcium ion activity (mM)
15	0	214.25 ± 5.78 [a]	17.14 ± 1.89 [a]	9.33 ± 0.05 [a]	6.72 ± 0.01[a]	1.18 ± 0.04 [a]
	50	165.13 ± 2.12 [b]	17.95 ± 1.74 [a]	9.13 ± 0.49 [a]	6.71 ± 0.01 [a]	1.20 ± 0.11 [a]
	75	161.81 ± 7.08 [b]	17.87 ± 1.11 [a]	8.98 ± 0.51 [a]	6.71 ± 0.01 [a]	1.22 ± 0.01 [a]
	90	156.76 ± 7.29 [b]	17.45 ± 0.97 [a]	8.29 ± 0.46 [a]	6.67 ± 0.01 [b]	1.27 ± 0.01 [a]
19	0	304.74 ± 6.08 [a]	18.15 ± 1.27 [a]	4.53 ± 0.76 [a]	6.73 ± 0.01 [a]	1.26 ± 0.02 [a]
	50	170.61± 4.57 [b]	18.64 ± 2.23 [a]	4.76 ± 0.02 [a]	6.72 ± 0.02 [a]	1.27 ± 0.01 [a]
	75	163.69 ± 8.55 [b]	18.49 ± 1.05 [a]	4.95 ± 0.01 [a]	6.73 ± 0.02 [a]	1.33 ± 0.03 [a]
	90	159.65 ± 8.39 [b]	18.80 ± 1.58 [a]	4.33 ± 0.02 [a]	6.66 ± 0.01 [b]	1.38 ± 0.02 [a]

[a-b] Mean within a column with different superscript differ ($P<0.05$) n=3

Microstructure of C- and BNB-MPC dispersions

The microstructure of C-and BNB-MPC dispersions (treated at 90% amplitude) are shown in Figure 5.4. The rheological characteristics of dispersions treated with BNBs clearly suggested that structural configurations had changed. CLSM and TEM was used to analyze the microstructures of C-and BNB- MPC dispersions. The CLSM revealed any noticeable microstructural changes upon the BNB treatment. However, the TEM micrographs of C-MPC dispersions (Figure 6.5A) revealed dense cross-linked network structural design. In contrast, less dense structure was seen in the BNB-MPC dispersion, along with thinner protein network. This can be attributed to the physical shear caused by ultrasound, which resulted in the protein aggregates being effectively broken, thus decreasing the particle size. However, the network structure appeared more homogenous and with a higher degree of branching for the C-MPC, when the dispersions were not exposed to BNBs, which could explain the higher viscosity observed in the C-SMCs. Wang et al. (2021) showed that the shear force and turbulence generated by acoustic cavitation could cause protein dispersion, and the particle size of the complexes significantly reduced. The BNB-MPC dispersions showed a significant reduction in large aggregate formations. The structural disintegration of protein aggregates caused by bubble implosion during the hydrodynamic cavitation process might explain this. Indeed, by acting as a spatial buffer between particles in the milk system and resulting in decreased viscosity, BNB may have assisted in the prevention of protein aggregation. Previously, Babu et al. (2022) have noted noticeable microstructural changes in Greek-style yogurts upon NB treatment. Although TEM revealed a more scattered structure when the MPC system was treated with BNB, additional research is needed to determine if this is a transitory phenomenon or whether it results

in a permanent viscosity decrease. Overall, the impact of BNB on the rheological characteristics of C-and BNB-MPC dispersions was clearly characterized based on structural analysis.

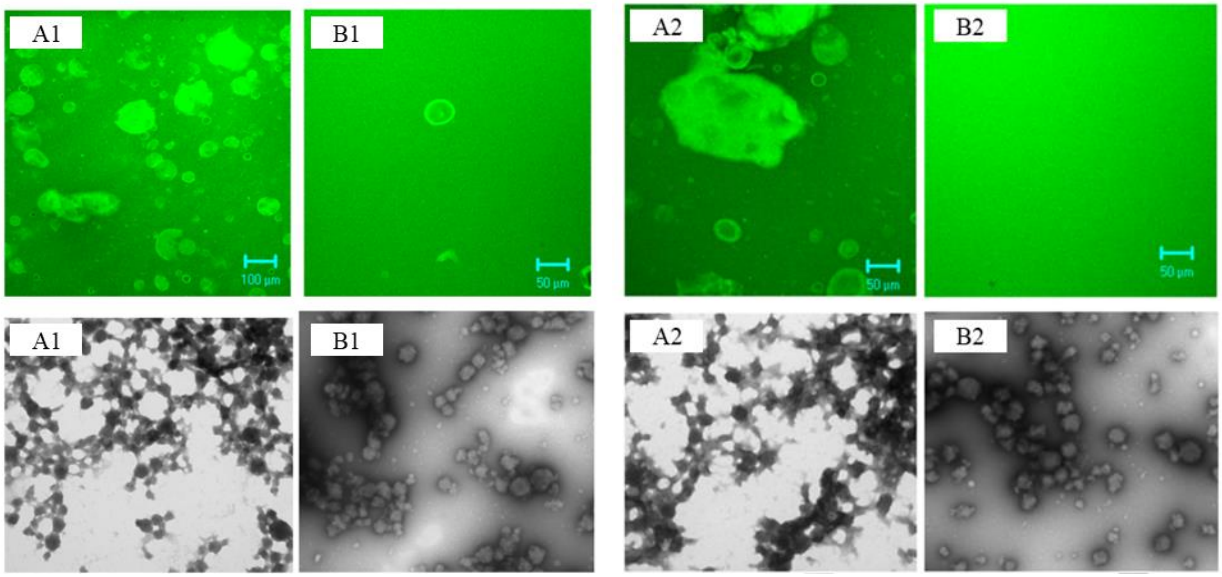

Figure 5.4 Representative confocal laser scanning microscopy and transmission electron microscopy images of control (A) and bulk nanobubble treated (B) milk protein concentrate dispersions at (1) 15% and (2) 19% total solids. (Magnification and scale: 34000× and 200 nm).

Fluorescence spectroscopy of C- and BNB-MPC dispersions

The tryptophan emission spectra of C-and BNB-MPC dispersions sample derived from TS of 15 and 19% exhibited a peak at ~340 nm. In BNB BNB-MPC dispersions, no wavelength shift was observed in the maxima of tryptophan on changing the amplitude (Figure 5.5). It should be noted that emission of tryptophan is highly sensitive to its local environment, and the lack of remarkable spectral peak shifts in both C-and BNB-MPC dispersions demonstrated the absence of any protein conformational changes during the BNB incorporation. The decrease in tryptophan fluorescence intensity is credited to protein-protein interactions between denatured whey proteins with casein micelles (Kulmyrzaev et al., 2005). Likewise, no wavelength shift or

remarkable change in intensity was observed in the Maillard emission spectra of the C-and BNB-MPC dispersions samples. The FAST index is referred as a sensitive indicator of the advanced Maillard reaction (Birlouez-Aragon et al., 2002). As the amplitude increased, there was a slight increase in FAST index; however, was insignificant (Table 5.3).

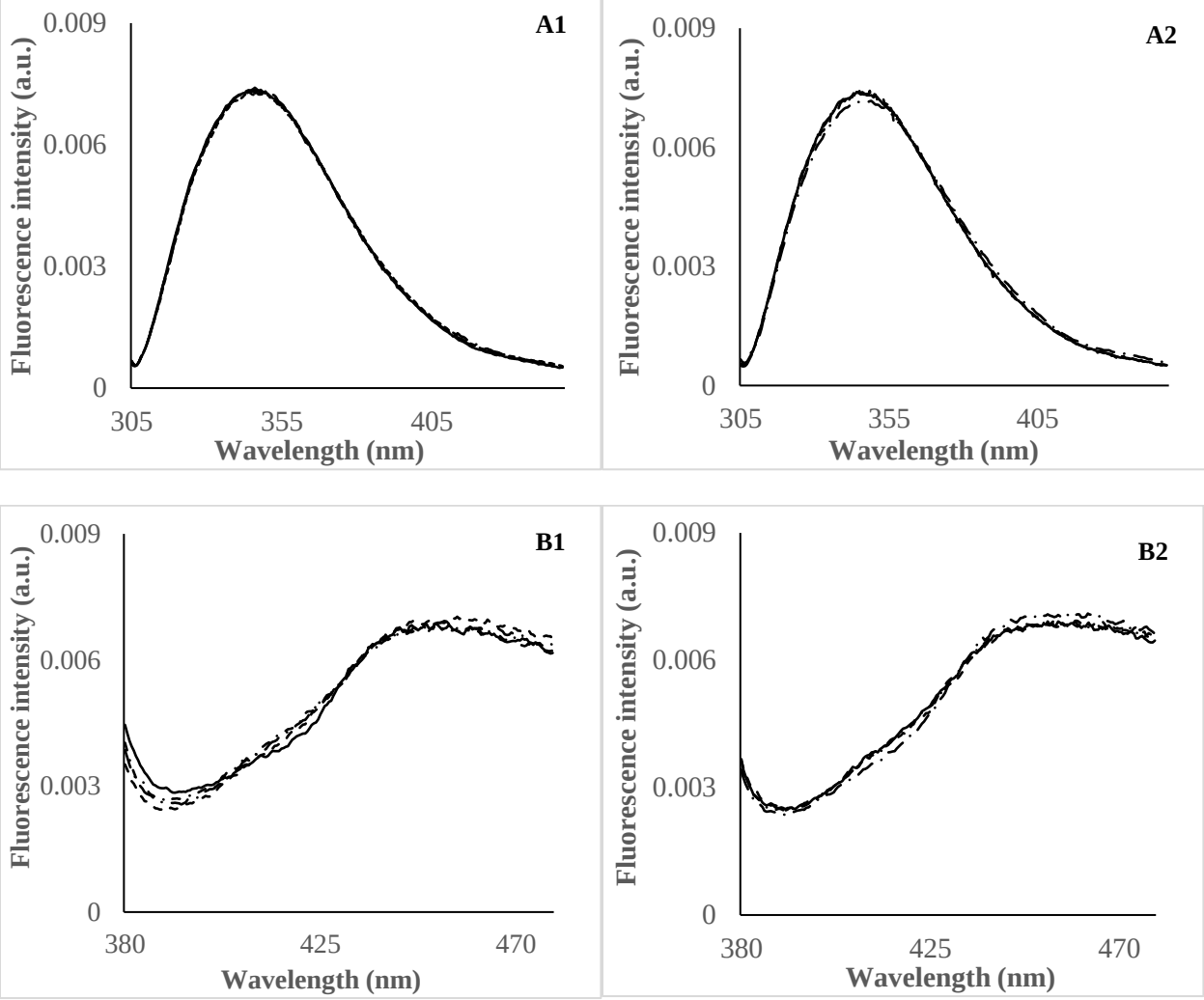

Figure 5.5 Front-face spectrofluorometric spectra for (A) tryptophan and (B) Maillard emission for, (1) 15% total solids MPC dispersion and (2) 19% total solids MPC dispersion of control (solid) and bulk nanobubble treated milk protein concentrate dispersions at amplitude of 50 (dash), 75 (dash dot), and 90 % (long dash dot), respectively.

Gel electrophoresis of C- and BNB-MPC dispersions

Protein profiles (SDS-PAGE) for C-and BNB-MPC dispersions analyzed under reducing before and after BNB treatment are shown in Figure 5.6. Under reducing conditions, the protein patterns of the BNB samples tested for both the TS (Figure 5.6; lanes 3–5) were similar to that of the C-MPC dispersions. This observation confirmed that the molecular weight of the proteins was not changed by the acoustic treatment. Yanjun et al. (2014) and Zisu et al. (2010) used native SDS-PAGE to determine effects of ultrasonicated MPC and whey protein concentrate and noted SDS-PAGE did not show significant changes compared to the control samples. Likewise, McCarthy at al. (2014) noted protein profiles of ultrasonicated MPC dispersions is temperature dependent and increasing exposure time without temperature control led to a significant increase in the level of denatured whey proteins.

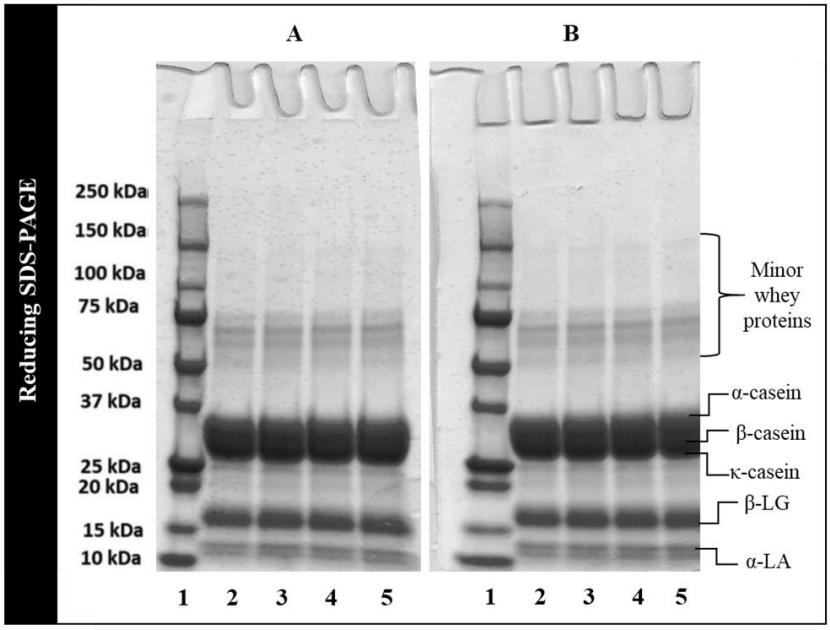

Figure 5.6 The reducing SDS-PAGE pattern of control and bulk nanobubble treated milk protein concentrate dispersions at 15% (A) and 19% total solids. Lane 1 = molecular weight ladder; lane 2 = control (0% amplitude); lane 3 = 50% amplitude; lane 4 = 75% amplitude; lane 5 = 90% amplitude.

Microstructure of spray dried C- and BNB-MPC powders

SEM analysis provides an overview on the shape and size of the C-and BNB-MPC powder particles. Noticeable changes in the microstructure of C-and BNB-MPC powders (19% TS treated at 90% amplitude) were revealed from the SEM analysis (Figure 5.7). The C-MPC powder particle displayed a hollow interior surrounded by a highly compacted shell. Whereas the BNB incorporation resulted in particles with numerous holes of different sizes throughout the powder particle matrix. McSweeney et al. (2021) and Bouvier et al. (2013) used N_2 and CO_2 before spray drying to produce MPC powders with similar particle structure. Indeed, the particles associated with the BNB treated powders with these porous structures and are proposed to improve the rehydration behavior of the BNB-MPC powders. When comparing the rehydration behavior of the two powders, the BNB-MPC powders showed a much higher solubility index than C-MPC powders.

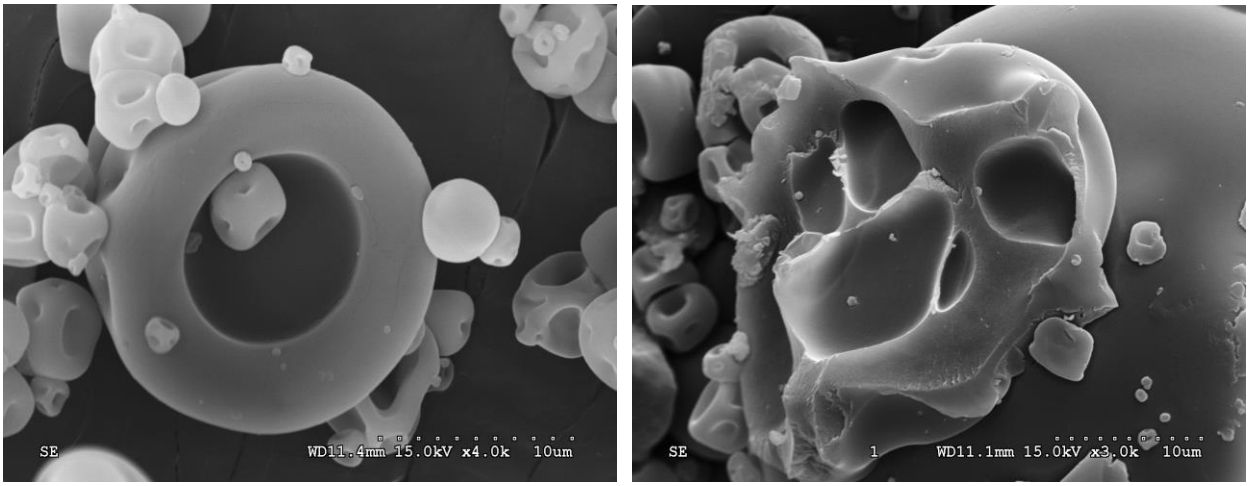

Figure 5.7 Typical scanning electron microscopy pictures of chopped spray-dried milk protein concentrate powder particle: control and NB-treated milk protein concentrate powders treated at 90% amplitude.

Rehydration characterization of spray dried C- and BNB-MPC powders

The solubility index of the C-and BNB-MPC powders were 83 ± 0.69, 91.99 ± 0.68 (50% amplitude), and 94.57 ± 0.33 % (90% amplitude), respectively. Very recently, McSweeney et al. (2021) have noted an improved dissolution of N_2 injected MPC powders (control: 83.6% and N_2 treated: 96.2%). The more porous structure of BNB-MPC powder particles and the presence of large air voids between these powder particles have aided in the enhanced water transfer while also improving the physical space between casein micelles and reducing protein-protein interactions (McSweeney et., 2021). Similarly, Marella et al. (2015) have noted an improved dissolution of CO_2 injected and stored (0-180 day) MPC powders. They have noted that the change in solubility between the control and CO_2 treated samples suggests that calcium and other minerals are involved in MPC solubility behavior. In contrast, Li et al. (2018) used hydrodynamic cavitation and noted that the solubility values did not vary much for the MPC powders (dissolution at room temperature control: 88.63% and treated-rotor speed at 50 Hz: 89.22%). Udabage et al. (2012) investigated the application of the static high-pressure treatment on MPCs and have reported an increase in solubility for the treated samples compared to the control MPC powders. Previously, Yanjun et al. (2014) have observed an increased solubility (35.78% to 88.30%) of acoustically pre-treated MPC powders after 5 min of ultrasound treatment. The rehydration properties of the BNB treated MPC powders were examined and compared with those of C-MPC powders using the FBRM technique. The FBRM tracked the number of fine particles (<10 μm) as a function of dissolution time (Figure 5.8). The results showed that for the BNB-MPC powders the large particles disintegrated into fine particles at a faster rate compared to C-MPC powders, suggesting water was able to penetrate the particles faster to quickly dissolve. The rate of water transfer during rehydration was supported by the

presence of these large air voids and pores throughout the particle-matrix, Bouvier et al. (2013) reported similar solubility improvements using extrusion-porosification. Similar findings were also found by Gagan et al. (2017), it was noted that the rate of increase in fine counts were higher for well-soluble MPC powders. Interpretation of FBRM data matches the overall trend reported by Crowley et al. (2015) and Hauser and Amamcharla (2016b).

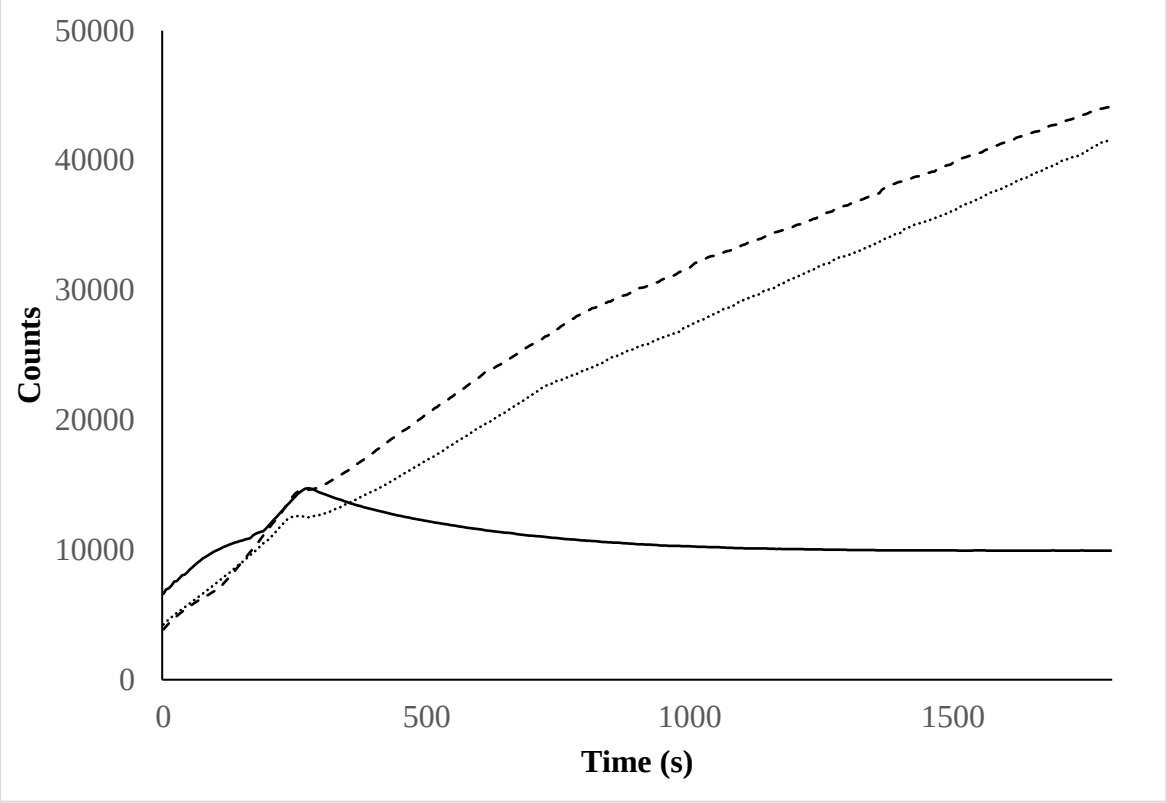

Figure 5.8 Changes in fine (<10 μm) counts obtained from data collected using the focused beam reflectance measurement for the spray-dried control (-), (..)bulk nanobubble treated (50% amplitude), and (--) bulk nanobubble treated (90% amplitude)milk protein concentrate powders at a dissolution temperature of 20ºC.

Additionally, ERT was used to determine the rehydration characteristics. Figure 5.9 show the overall mean conductivity of the C-and BNB-MPC powders using the circular configuration. At the end of the 15-min dissolution time, the overall mean conductivity from the circular

configuration was found to be 0.108 ± 0.004 mS/cm for C-MPC powders, which is significantly ($P < 0.05$) different. The BNB treated MPC powders at amplitude 50 and 90% had overall mean conductivity of 0.110 ± 0.025 mS/cm and 0.111 ± 0.004 mS/cm (90%), respectively. Additionally, tomograms were stacked to form a 3D image. At the end of the 15-min dissolution time, dissolution characteristics for MPC powders it is evident from Figure 5.10. As the dissolution time increased, more minerals were being released, and a noted increase in conductivity was visible. The sensing plane P1 had an overall mean conductivity of 0.109 mS/cm for C-MPC powders; however, for BNB-MPC powders, sensing planes P1 had an overall mean conductivity of 0.119 mS/cm.

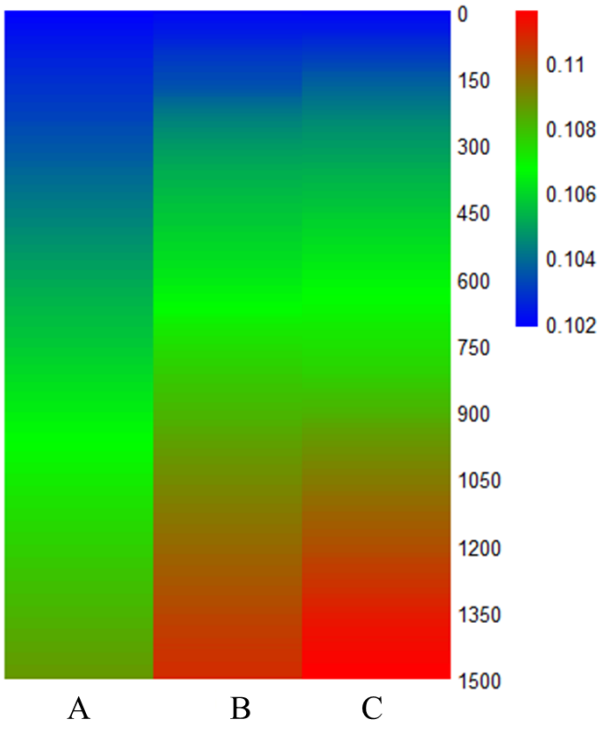

Figure 5.9 Overall mean conductivity results obtained from the electrical resistance tomography system (A) control, (B) bulk nanobubble treated (50% amplitude), and (C) bulk nanobubble treated (90% amplitude) milk protein concentrate powders using circular probe configurations during the dissolution at room temperature.

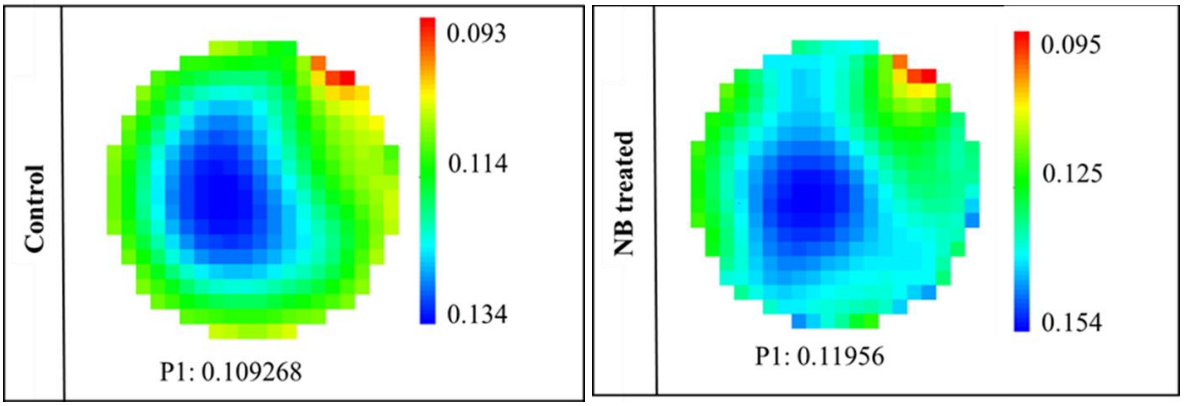

Figure 5.10 Representative tomogram images obtained from the electrical resistance tomography system at the end of 15 Min dissolution.

Physical properties and flow characterization of spray dried C- and BNB-MPC powders

The CED was calculated through converting the 2-D image of particle to a circle of equivalent area to the 2-D image. At least 10,000 particles were examined for each C- and BNB-MPC powders with results averaged. The effect of BNB treatment on CED of powder particle is displayed in Table 5.5, whereby the CED values were 6.08 and 6.53 μm for 50 and 90% amplitude, respectively compared to 5.88 μm for the C-MPC powders. The incorporation of BNBs have slightly increased the CED of the MPC powder particles this can be attributed to the expansion of gas bubbles within the liquid droplets directly after atomizing (McSweeney et al., 2021). Similarly, upon the N_2 injection to MPC concentrates before spray drying, McSweeney et al. (2021) noted an increase in the size of the regular MPC powders. The MPC powders produced with the BNB incorporation had lower bulk density values. Likewise, McSweeney et al. (2021) noted similar decrease in bulk density values of MPC powders upon N2 incorporation. The UYS values of the MPC powders decreased with the BNB treatment. Additionally, the UYS decreased from 1.94 to 1.56 kPa with an increase in the amplitude. A significant decrease ($P <$

0.05) in cohesion values were observed with the BNB treatment. This could be due to the differences in particle arrangement and particle interlocking in the treated MPC powders (Babu et al., 2018). According to the Jenike flow classification, powders with a flow index value between 4-10 are easy flowing and flow index < 4 are considered as cohesive powders (Jenike, 1964). Therefore, C- and BNB-MPC powders were categorized as not cohesive over the stress applied. Previously, Rennie et al. (1999) noted that the powder cohesiveness decreases as particle size increases. The BNB incorporation did alter the angle of internal friction; it was significantly different for the control (~42°) in comparison to the BNB-MPC powders (~36° at 90% amplitude; Table 5.5). Increased wall friction can put a lot of stress on the wall of silos, making it difficult to remove and unload powders (Fitzpatrick et al., 2004). Additionally, improved physical and shear related properties were observed in the BNB-MPC powders. Therefore, BNB treatment will assist both the processing operations (storage/handling) and aids in developing milk protein ingredients with enhanced functionality for various R&D formulations.

Table 5.4 Morphological characteristics and shear flow properties the control (C-MPC) and bulk nanobubble treated milk protein concentrate (BNB-MPC) powders.

Properties	C-MPC	BNB-MPC powders	
		Amplitude-50%	Amplitude-90%
Circular equivalent diameter (µm)	5.88 ± 0.12 [a]	6.08 ± 0.01 [a]	6.53 ± 0.01 [a]
Bulk density (g/ml)	0.55 ± 0.04 [a]	0.38 ± 0.01 [b]	0.37 ± 0.01 [b]
Unconfined yield stress (kPa)	2.51 ± 0.13 [b]	1.94 ± 0.71 [b]	1.56 ± 0.37 [b]
Cohesion (kPa)	0.61 ± 0.02 [a]	0.37 ± 0.01 [a]	0.34 ± 0.01 [a]
Major principle stress (kPa)	15.62 ± 0.31 [a]	15.63 ± 0.17 [a]	15.11 ± 0.66 [a]
Angle of internal friction (º)	42.85 ± 0.19 [a]	38.98 ± 1.11 [b]	36.45 ± 1.89 [b]
Flow function coefficient	7.02 ± 0.56 [a]	8.35 ± 0.01 [b]	10.48 ± 0.02 [b]

[a-b]Mean values for different morphology and shear properties within a row with different superscript differ ($P < 0.05$); n=3.

Conclusions

During spray drying processes, concentrations of retentate are limited by the maximum viscosity that the atomizer can effectively atomize or by fouling of the evaporator prior to drying. Lowering the viscosity of the feed offers possibility of drying MPC retentates at significantly higher solid concentrations and thus more efficient spray drying. Moreover, viscosity has a direct influence on the size of the droplets formed during atomization, reduced viscosity results in powder with improved flowability. Therefore, being able to reduce viscosity of the MPC retentates results in a reduction in both capital and operational costs. Overall, viscosity is one of the limiting factors in many process operations and BNB treatment can provide a convenient and low-cost alternative to control the viscosity without the use of any chemical additives. In the present study, BNB incorporation using a continuous acoustic cavitation processing method was developed and successfully utilized for improving the processability of milk protein concentrates for the first time. Overall, our findings support that acoustic cavitation can provide a new processing tool to control the viscosity of high protein concentrates, and it represents a potential for a more energy efficient drying process while providing enhanced functional properties of the final powder. For instance, solubility is a critical property of MPC powders. Any improvement in the solubility of commercial milk protein powders results in a potential improvement in their industrial application. Furthermore, BNB incorporation results in enhanced powder functionality while avoiding the use of any chemical additives. Besides, BNB treatment is an eco-friendly, scalable, and robust process technology. Further academic-industrial collaborations can stimulate the research in this area of science by considering the immediate potential commercial applications of BNB technologies in various dairy products.

References

Agarwal, S., Beausire, R. L., Patel, S., & Patel, H. (2015). Innovative uses of milk protein concentrates in product development. *Journal of food science*, *80*(S1), A23-A29.

Amamcharla, J., Li, B., & Liu, Z. (2017). Use of micro-and nano-bubbles in liquid processing. *United States*.

Ahmed, A. K. A., Shi, X., Hua, L., Manzueta, L., Qing, W., Marhaba, T., & Zhang, W. (2018). Influences of air, oxygen, nitrogen, and carbon dioxide nanobubbles on seed germination and plant growth. *Journal of agricultural and food chemistry*, *66*(20), 5117-5124.

Anandharamakrishnan, C. (Ed.). (2017). *Handbook of drying for dairy products*. John Wiley & Sons.

Anema, S. G., Pinder, D. N., Hunter, R. J., & Hemar, Y. (2006). Effects of storage temperature on the solubility of milk protein concentrate (MPC85). *Food Hydrocolloids*, *20*(2-3), 386-393.

Azevedo, A., Etchepare, R., Calgaroto, S., & Rubio, J. (2016). Aqueous dispersions of nanobubbles: Generation, properties and features. *Minerals Engineering*, *94*, 29-37.

Birlouez-Aragon, I., Sabat, P., & Gouti, N. (2002). A new method for discriminating milk heat treatment. *International Dairy Journal*, *12*(1), 59-67.

Crowley, S. V., Burlot, E., Silva, J. V., McCarthy, N. A., Wijayanti, H. B., Fenelon, M. A., ... & O'Mahony, J. A. (2018). Rehydration behaviour of spray-dried micellar casein concentrates produced using microfiltration of skim milk at cold or warm temperatures. *International Dairy Journal*, *81*, 72-79.

Crowley, S. V., Desautel, B., Gazi, I., Kelly, A. L., Huppertz, T., & O'Mahony, J. A. (2015). Rehydration characteristics of milk protein concentrate powders. *Journal of Food Engineering*, *149*, 105-113.

De Kort, E., Minor, M., Snoeren, T., van Hooijdonk, T., & van der Linden, E. (2012). Effect of calcium chelators on heat coagulation and heat-induced changes of concentrated micellar casein solutions: The role of calcium-ion activity and micellar integrity. *International Dairy Journal*, *26*(2), 112-119.

Favvas, E. P., Kyzas, G. Z., Efthimiadou, E. K., & Mitropoulos, A. C. (2021). Bulk nanobubbles, generation methods and potential applications. *Current Opinion in Colloid & Interface Science*, *54*, 101455.

Flysjö, A. M. (2012). Greenhouse gas emissions in milk and dairy product chains: Improving the carbon footprint of dairy products.

Hemar, Y., Augustin, M. A., Cheng, L. J., Sanguansri, P., Swiergon, P., & Wan, J. (2011). The effect of pulsed electric field processing on particle size and viscosity of milk and milk concentrates. *Milchwissenschaft-Milk Science International*, *66*(2), 126.

Jadhav, A. J., & Barigou, M. (2021). On the clustering of bulk nanobubbles and their colloidal stability. *Journal of Colloid and Interface Science*, *601*, 816-824.

Jadhav, A. J., & Barigou, M. (2020a). Bulk nanobubbles or not nanobubbles: that is the question. *Langmuir*, *36*(7), 1699-1708.

Jadhav, A. J., & Barigou, M. (2020b). Response to "Comment on Bulk Nanobubbles or Not Nanobubbles: That is the Question". *Langmuir*, *37*(1), 596-601.

Khaira, N. M., Abd Rahmana, N. A., Baharuddina, A. S., Hafidb, H. S., & Wakisakab, M. (2020). Capturing the impact of nanobubble liquid in enhancing the physical quality of ice cream. *Journal of Agricultural and Food Engineering*, *2*, 0012.

Kulmyrzaev, A. A., Levieux, D., & Dufour, É. (2005). Front-face fluorescence spectroscopy allows the characterization of mild heat treatments applied to milk. Relations with the denaturation of milk proteins. *Journal of Agricultural and Food Chemistry*, *53*(3), 502-507.

Li, K., Woo, M. W., Patel, H., Metzger, L., & Selomulya, C. (2018). Improvement of rheological and functional properties of milk protein concentrate by hydrodynamic cavitation. *Journal of Food Engineering*, *221*, 106-113.

Phan, K., Truong, T., Wang, Y., & Bhandari, B. (2021). Effect of CO2 nanobubbles incorporation on the viscosity reduction of fruit juice concentrate and vegetable oil. *International Journal of Food Science & Technology*, *56*(9), 4278-4286.

Marella, C., Salunke, P., Biswas, A. C., Kommineni, A., & Metzger, L. E. (2015). Manufacture of modified milk protein concentrate utilizing injection of carbon dioxide. *Journal of Dairy Science*, *98*(6), 3577-3589.

McCarthy, N. A., Kelly, P. M., Maher, P. G., & Fenelon, M. A. (2014). Dissolution of milk protein concentrate (MPC) powders by ultrasonication. *Journal of Food Engineering*, *126*, 142-148.

McSweeney, D. J., Maidannyk, V., O'Mahony, J. A., & McCarthy, N. A. (2021a). Rehydration properties of regular and agglomerated milk protein concentrate powders produced using nitrogen gas injection prior to spray drying. *Journal of Food Engineering*, *305*, 110597.

McSweeney, D. J., Maidannyk, V., O'Mahony, J. A., & McCarthy, N. A. (2021b). Influence of nitrogen gas injection and agglomeration during spray drying on the physical and bulk handling properties of milk protein concentrate powders. *Journal of Food Engineering*, *293*, 110399.

Moejes, S. N., Visser, Q., Bitter, J. H., & Van Boxtel, A. J. B. (2018). Closed-loop spray drying solutions for energy efficient powder production. *Innovative Food Science & Emerging Technologies*, *47*, 24-37.

Nöbel, S., Kern, C., Sonne, A., Bähler, B., & Hinrichs, J. (2016). Apparent voluminosity of casein micelles in the temperature range 35–70° C. *International Dairy Journal*, *59*, 80-84.

Nicoud, L., Lattuada, M., Yates, A., & Morbidelli, M. (2015). Impact of aggregate formation on the viscosity of protein solutions. *Soft Matter*, *11*(27), 5513-5522.

Nirmalkar, N., Pacek, A. W., & Barigou, M. (2019). Bulk nanobubbles from acoustically cavitated aqueous organic solvent mixtures. *Langmuir*, *35*(6), 2188-2195.

Nirmalkar, N., Pacek, A. W., & Barigou, M. (2018). Interpreting the interfacial and colloidal stability of bulk nanobubbles. *Soft matter*, *14*(47), 9643-9656.

Phan, K. K. T., Truong, T., Wang, Y., & Bhandari, B. (2020). Nanobubbles: Fundamental characteristics and applications in food processing. *Trends in Food Science & Technology*, *95*, 118-130.

Rak, D., & Sedlák, M. (2020). Comment on “bulk nanobubbles or not nanobubbles: that is the question”. *Langmuir*, *36*(51), 15618-15621.

Rak, D., Ovadová, M., & Sedlák, M. (2019). (Non) existence of bulk nanobubbles: the role of ultrasonic cavitation and organic solutes in water. *The journal of physical chemistry letters*, *10*(15), 4215-4221.

Sutariya, S. G., Huppertz, T., & Patel, H. A. (2017). Influence of milk pre-heating conditions on casein–whey protein interactions and skim milk concentrate viscosity. *International Dairy Journal*, *69*, 19-22.

Udabage, P., Puvanenthiran, A., Yoo, J. A., Versteeg, C., & Augustin, M. A. (2012). Modified water solubility of milk protein concentrate powders through the application of static high pressure treatment. *Journal of dairy research*, *79*(1), 76-83.

Yanjun, S., Jianhang, C., Shuwen, Z., Hongjuan, L., Jing, L., Lu, L., ... & Jiaping, L. (2014). Effect of power ultrasound pre-treatment on the physical and functional properties of reconstituted milk protein concentrate. *Journal of Food Engineering*, *124*, 11-18.

Yasuda, K., Matsushima, H., & Asakura, Y. (2019). Generation and reduction of bulk nanobubbles by ultrasonic irradiation. *Chemical Engineering Science*, *195*, 455-461.

Yasuda, K., Matsushima, H., & Asakura, Y. (2019). Generation and reduction of bulk nanobubbles by ultrasonic irradiation. *Chemical Engineering Science*, *195*, 455-461.

Zhang, Z. H., Wang, S., Cheng, L., Ma, H., Gao, X., Brennan, C. S., & Yan, J. K. (2022). Micro-nano-bubble technology and its applications in food industry: A critical review. *Food Reviews International*, 1-23.

Zisu, B., Bhaskaracharya, R., Kentish, S., & Ashokkumar, M. (2010). Ultrasonic processing of dairy systems in large scale reactors. *Ultrasonics Sonochemistry*, *17*(6), 1075-1081.

Chapter 6 - Effect of bulk nanobubbles during ultrafiltration on membrane performance

Abstract

Continuous acoustic/hydrodynamic cavitation technique was used to generate bulk nanobubbles (BNBs). The objective of this study was to evaluate the influence of BNB incorporation during the ultrafiltration (UF) process of skim milk. Three lots of non-fat dry milk powders were obtained from a commercial manufacturer. Powders were reconstituted to total solids of 25% and were incorporated with BNBs during the UF processing. Both lab and pilot-scale UF experiments were conducted to evaluate the effect of BNB incorporation on UF process by evaluating permeate flux, membrane microstructure, fouling resistance, energy consumption, and skim milk concentrate (SMC) characteristics. For both the lab/pilot-scale runs, after the initial water flux measurements, the membrane was fouled with the skim milk concentrate dispersions operated at 20°C under a constant transmembrane pressure 30 psi in constant concentration mode (the permeate was returned to the feed tank at regular 10-min intervals) and the total run time was fixed for 1 hour. UF experiments on the control SMC dispersions (C-SMC; no BNB treatment) and BNB-treated SMC dispersions (BNB-SMC; BNB-treated) were performed in duplicates. The results showed that BNB treatment had a significant effect on permeate flux in both the lab and pilot-scale runs. The permeate flux of the C-SMC was 9.27 and 6.89 $kg/h \cdot m^2$ for the lab and pilot-scale UF runs, respectively. The permeate flux significantly increased ($P < 0.05$) to 14.57 and 9.59 $kg/h \cdot m^2$ for the lab and pilot-scale UF runs, respectively after the BNB treatment. The confocal laser scanning microscopy was used to measure the thickness of fouled layer. It was observed that the measured thickness of C-SMC (45.17 um) was notably different from the BNB-SMC (19.01 um) fouled membrane. BNB incorporation also

resulted in a significant decrease ($P < 0.05$) in apparent viscosity (C-SMC and BNB-SMC: 8.99 and 4.94 mPa·s at 100 s^{-1}, respectively). In conclusion, the BNB treatment helped to improve UF membrane performance and therefore this study suggests the potential of using BNB treatment for a more efficient UF processing.

Introduction

Membrane technology is one of the key unit operations in the dairy industry for fractionation of milk into different protein- or lactose-rich ingredients. The range of membrane separation techniques has been broadened to span the full milk composition spectrum due to technological advancements in the creation of novel membranes, process engineering advances, and a better knowledge of the functioning of milk components. Milk components may be recovered and purified using advanced membrane techniques. It also extends the shelf life of milk without exposing it to heat, standardizes milk components for designing various milk products. Among them, the pressure-driven membrane processes, such as microfiltration, ultrafiltration (UF) and nanofiltration and reverse osmosis, have been applied in dairy food industries to treat the raw material streams and co-products. The driving force of these membrane processes is the transmembrane pressure (TMP). For that, pressure-driven membrane processes can be characterized according to these two parameters (TMP and molecular weight cut-off or pore size of membranes). In this sense, microfiltration requires > 100,000 Da and 0.1-2 bar; UF utilizes 1000-100,000 Da and 2-10 bar; nanofiltration uses 100-1000 Da and 5-40 bar; and reverse osmosis needs 1-100 Da and 30-100 bar. Notably, the dairy industry has been one of the pioneers in the development of UF equipment and procedures. In recent years, there has been enhanced interest in evaluating the performance and efficiency of UF membranes for the production of protein-rich ingredients. Many researchers have studied the UF systems under

different processing conditions (Marella et al., 2015; Puri, Singn, and O'Mahony, 2020). Furthermore, the pH and temperature at which the UF process is carried out has a significant impact on the structure and functioning of protein components generated from it (Luo, Ramchandran, and Vasiljevic, 2015; Luo, Vasiljevic, and Ramchandran, 2016). However, membrane performance is one topic of concern during the application of membrane processing in dairy processing. Unfortunately, membrane fouling caused by the deposition of biological macromolecules/particles on the membrane surface or into the membrane pores limits the application of membrane processing. Therefore, innovative and profitable solutions to prevent membrane fouling and to increase permeate flux must be sought in order to lower the operating and maintenance expenses involved with membrane processing.

Nanobubbles (NBs) are gaseous entities, with size of 100nm -10 μm (Liu et al., 2008), whereas micro or macro bubbles have diameters of >50 μm (Agarwal and Liu, 2011). Although there is no universally accepted classification for bubbles based on size, previous researchers have classified bubbles as NBs and micro-nano bubbles (diameter 200 nm to 10 μm) in terms of the diameter of bubbles. Very recently, the proof of the existence of BNBs generated using acoustic cavitation was given by Jadhav and Barigou (2020). Acoustic cavitation involves the generation, expansion, growth, and adiabatic collapse of microbubbles. The collapse and disappearance of such microbubbles give rise to the formation of bulk NBs. Membrane filtration combined with NBs was previously used in water treatment methods that efficiently avoids or decreases membrane fouling (Wu et al., 2008). On both hydrophobic and hydrophilic surfaces, electrochemically produced NBs were found to efficiently remove adsorbed proteins (e.g., bovine serum albumin) (Chen et al., 2006, Liu et al., 2008). Air flow rate and NB size have an impact on membranes, according to Tian et al. (2010). Continuous air bubbling has been

demonstrated to be effective in reducing fouling and the size of NBs impacted membrane fouling (Tian et al., 2010). according to According to Chen et al. (2006), acoustic stream and ultrasonically induced turbulence were responsible for fouling removal and prevention. Despite these advancements in study, the impact of NBs on the defouling process of membrane filtration has yet to be fully understood. Another critical property of MNBs is the generation of hydroxyl radicals during the collapse of NBs, which has been studied for degradation of organic pollution and water disinfection (Agarwal, Ng, and Liu, 2011). The addition of MBs to chemical cleaning solutions improves performance by agitating the fouling layer on membrane surfaces (Wilson, 2013). Turbulences in the liquid medium are caused by the repulsive forces between the NBs and NBs have been utilized to agitate and remove particles from membrane surfaces as a result. Cui and Taha (2003) found that applying the gas-liquid two-phase flow to the feed stream boosted the permeate flux of the downward crossflow ultrafiltration operation by 220%. The disruption of the concentration polarization layer by air bubbles is the cause of the fast increase in permeate flow. Furthermore, Ghadimkhani, Zhang, and Marhaba (2016) proved that introducing air NBs to ceramic membranes may de-foul them. Additionally, acoustic cavitation-based techniques have gained increasing attention as a technique of fouling control in recent years. Several different mechanisms may lead to particle release from a particle-fouled surface as a result of ultrasound. In the present study, therefore, we investigated the application of bulk NBs (BNBs) generated by acoustic and hydrodynamic cavitation on the improvement of membrane performance and the resultant skim milk concentrates (SMC) were also characterized in terms of functional properties.

Materials and methods

Experimental approach

To better understand the membrane performance with BNB incorporated feed, some UF operation factors (average flux, overall and irreversible/reversible resistance) were comprehensively investigated. It is expected that our findings can provide support for a better understanding of the roles of BNBs in improving UF membrane performance. Laboratory and pilot scale UF experiments were conducted to evaluate the effect of BNBs on overall membrane performance. The study aimed to develop an alternative more efficient BNB-assisted UF processing with SMC dispersions at 25% total solids as a model system. As described below, laboratory-scale UF experiments (Phase-I) were conducted to investigate the BNB-assisted (BNBs produced using acoustic cavitation) UF processing. Additionally, pilot-scale experiments (Phase-II) were conducted where SMC dispersions were introduced with BNBs generated using both acoustic and hydrodynamic cavitation.

BNB generation systems used

Acoustic cavitation

The schematic diagram of the lab and pilot scale set-ups used in phases I and II of this research is shown in Figures 6.1 and 6.2, respectively. In this research, the BNBs were generated by both acoustic and hydrodynamic cavitation techniques. BNBs were generated by continuous acoustic cavitation using a 20 kHz probe-type processor (VCX 1500, Sonics & Materials, USA) capable of delivering up to 1.5 kW of power with a flow cell design. In phase-I of the study, a probe of 1-inch diameter and 9-inch length was used to acoustically cavitate the bulk SMC dispersions flowing at a rate of ~2.64 L/min using a diaphragm liquid pump (KNF, Model: NF1.300KT.18S, Trenton, NJ). In phase-II of the study, the same acoustic cavitation system with

a Flowjet duplex diaphragm pump (Xylem, Model: D3835H5011A, Irvine, CA) with a flow rate of ~7.57 L/min was used with a flow cell design.

Hydrodynamic cavitation

A venturi-type air injector (Hydra-Flex, Savage, MN) was also used for the generation of BNBs with a flow cell design. The custom-built BNB system was connected to the Flowjet diaphragm pump (Xylem, Model: D3835H5011A, Irvine, CA). The size of the BNBs were controlled by adjusting the airflow through the injector using the air flow meter 4140 (TSI, Shoreview, MN).

Characterization of BNBs in water

The existence of BNBs remains as a mystifying and trending area of research due to their exceptional longevity and other extraordinary properties that are investigated by many research groups worldwide (Phan et al., 2020). In this study, a nanoparticle tracking analyzer (NTA) was used to measure BNB concentration and mean diameter. NTA measurements were carried out using the Malvern NanoSight LM10 (NanoSight, Amesbury, United Kingdom). The control- and BNB treated DI water was characterized in terms of concentration and mean diameter using the NTA. All measurements were done at room temperature.

Phase I: Lab-scale experiments

The schematic diagram of the lab-scale set-up used in phases-I of this research is shown in Figure 6.1. One lot each of nonfat dry milk (NDM) powder was procured from three different commercial manufacturers. In phase-I of the study, the NDM powders were rehydrated to 25% (w/w) total solids with deionized water and stored overnight at 4°C to ensure complete hydration. For each lot, the UF of the reconstituted SMC dispersions were carried out at 20ºC using a bench-top plate and frame system (SmartFlow Technologies, Apex, NC) equipped with a

10-KDa cut-off polyethersulfone (PES) membrane (Hannifin Corp, Oxnard, CA) in a flat sheet configuration at a constant TMP of 30 Psi. Approximately, 1 L of SMC dispersion was tempered to 20°C and was maintained at that temperature using a custom-made chiller during the UF run. At the start of each UF run, deionized water was circulated through the system at 3L/min at TMP of 30 Psi and the initial water flux was recorded for the first 15 minutes. After the initial water flux measurements, the membrane was fouled with the SMC dispersions for 1 hour at TMP 30 Psi in constant concentration mode. UF experiments on the control SMC dispersions (C-SMC; pumped through the system without BNB treatment) and BNB-treated SMC dispersions (BNB-SMC; BNB-treated using the acoustic cavitation system) were then performed in duplicates. The retentate was returned to the feed tank. At the same time, permeate was collected in a glass beaker (Pyrex glass beaker, Fisher Scientific, Pittsburgh, PA) which was placed on an electronic balance for recording the weight measurements. In constant concentration mode, the permeate was returned to the feed tank at regular 10-minute intervals, and the total run time was 1 hour resulting in 6 measurements. The viscosity profile of the retentate was immediately taken at every 10-minute interval. The retentate and permeate samples were collected and stored for further analysis. To determine the extent of fouling, 4 L of deionized water was circulated through the system, and subsequently, the water flux was recorded for the next 15 minutes.

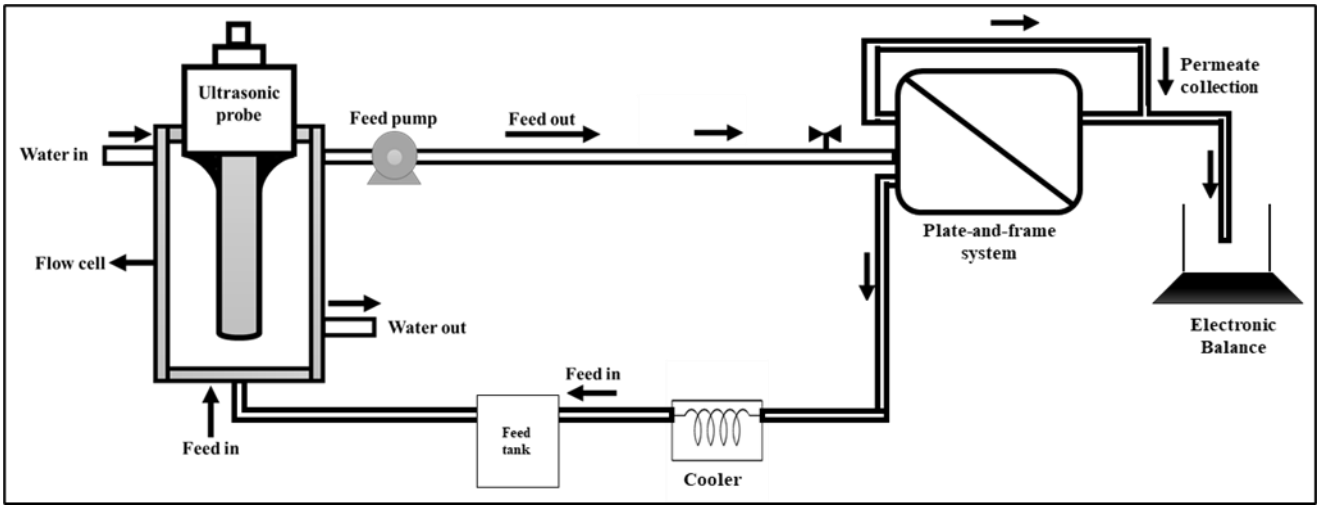

Figure 6.1 Lab scale ultrafiltration set up with the plate-and-frame system.

Characterization of the SMC dispersions

Physicochemical analysis: A fisher scientific Accumet AP63 portable pH meter was used to record the pH on the C-and BNB-SMC dispersions. The conductivity of the SMC dispersion was measured using a conductivity meter (Accument, Fisher Scientific, Waltham, MA). The density of the C-and BNB-SMC dispersions was measured using a gravimetric method using Grease pycnometers (Fisher Scientific, Pittsburgh, PA, USA). The surface tension of C-and BNB-SMC dispersions were measured using an automatic surface tensiometer (Model BZY-102, Anhui, China) (Olusanya et al., 2021). Distilled water was used for calibration with a surface tension of 71.66 mN/m. Using a spirit lamp, the platinum ring was soaked in acetone was flamed at a 45° angle for about 1 min. The ring was then rinsed with deionized water and put in the flame for 20 seconds. This step was done to eliminate any impurities from past use that might have influenced the reading.

Rheological measurements: The viscosity of C-and BNB-SMC dispersions during the UF run and the viscosity of the retentate and permeate samples at the end of the UF run was measured at 20ºC using a stress-strain-controlled rheometer (MCR-92 Anton Paar, Vernon Hills,

IL) equipped with a 50 mm diameter stainless steel cone with an angle 1° and 101 μm gap. Flow curves were analyzed at shear rates between 1 and 100 s^{-1}. The data obtained was fitted to the power-law model to get the consistency coefficient and flow behavior index.

Microstructure: The microstructure of C-and BNB-SMC dispersions after the UF runs were studied using confocal laser scanning microscopy (CLSM), following the method described by Gandhi et al. (2017). Samples were prepared for CLSM by diluting 1:100 using DI water before measurements. Proteins were stained using the Fast green FCF (Sigma-Aldrich, St. Louis, MO) stain. The stock solution of Fast green (5 mg dye in 5 mL water) was applied to the sample for 5-10 min. The stained samples were analyzed in LSM 5 Pa (Zeiss, Thornwood, NY). Three-dimensional images were obtained by scanning the sample across a defined section along the z-axis.

Transmission electron microscopy (TEM) was also used to image C-and BNB-SMC dispersions after the UF run in order to illustrate the differences in microstructure. Samples were analyzed using the negative-staining technique. The dispersions were diluted at 1:100 with DI water. One drop of the diluted sample was mounted on Formvar/carbon-coated 200-mesh copper grids (Electron Microscopy Sciences, Fort Washington, PA) for 2 min. Subsequently, it was combined with a drop of 2% uranyl acetate, left for 30 s; the excess liquid was wiped off with a filter paper and was examined using a CM 100 TEM (FEI Company, Hillsboro, OR) operating at 100 kV and images captured with a digital camera (model C8484, Hamamatsu, Bridgewater, NJ) using the AMT software (Advanced Microscopy Techniques, Chazy, NY).

Membrane performance: Phase I

Permeation flux*:* Average flux is the permeate flow rate through the membrane and is expressed in kilograms per m^2 and hour ($kg/h \cdot m^2$) as given in equation 1:

$$\text{Permeation flux} = \frac{Permeation\ flow\ rate\ (kg/h),}{Surface\ area\ of\ membrane\ (m^2)} \quad (1)$$

Resistance*:* Membrane resistance was characterized using the method according to Méthot-Hains et al. (2016). Membrane fouling was characterized using the resistance-in-series model according to Equation 2.

$$R_t = Rm + R_{irr} + R_{rev} \quad (2)$$

where R_t is the total resistance (m^{-1}), R_m is the membrane resistance (m^{-1}), R_{irr} is the irreversible resistance (m^{-1}), and R_{rev} is the reversible resistance (m^{-1}). The R_m, R_{irr}, and R_{rev}, can be determined using Equations (3), (4), and (5).

$$R_m = \frac{TMP}{\mu \times Jw} \quad (3)$$

$$R_{irr} = \frac{TMP}{\mu \times JR} \quad (4)$$

$$R_m = \frac{TMP}{\mu \times JE} \quad (5)$$

where TMP is the transmembrane pressure (Pa), μ is the permeate viscosity ($Pa \cdot s^{-1}$), Jw is the water flux ($m^3/m^2 \cdot s$), J_R is the water flux ($m^3/m^2 \cdot s$) after membrane rinsing, and J_E is the permeation flux ($m^3/m^2 \cdot s$) at the end of UF (at 1 h run period).

Membrane microstructure

CLSM was used to obtain high resolution optical images of fouled C-and BNB-SMC PES membranes. Samples were stained following a method by Gandhi et al. (2018) and each sample were analyzed in CLSM 5 Pascal (Zeiss, Arlington, VA). The CLSM images were analyzed using the CLSM software to calculate quantitative parameters such as thickness of the fouled layer.

Energy consumption

The energy consumption during the lab scale UF runs was measured using the power consumption meter (6769N11, McMaster-Carr). It measures the amount of power the pump uses and can also calculate energy costs associated with it. The power consumption meter was plugged directly into an outlet, and the pump was plugged into the front of the meter.

Phase II: Pilot-scale experiments

The schematic diagram of the pilot scale set-up used in phase-II of this research is shown in Figure 6.1. NDM powder was procured from a commercial supplier, and the UF experiments were done in duplicates. In phase-II of the study, the NDM powders were rehydrated to 25% (w/w) total solids with deionized water and stored overnight at 4°C to ensure complete hydration. Approximately 10 gallons of SMC dispersions were tempered to 20°C and were maintained at that temperature using a using the plate-heat exchanger (AGC Heat Transfer, Portland, OR) system during the UF process. The UF was performed using a PES spiral wound membrane module 4333 K131-VSV (Koch membrane systems, USA). The membrane element was 109 mm in diameter and 940 mm in length and had a surface area of 7.1 m^2 with a 1.1 mm feed spacer and a 10-KDa cut-off. UF was performed at 20°C using a 35 Psi TMP and the same module and UF membrane were used for all UF runs. A centrifugal pump (Reliance Electric Company, Cleveland, OH) with a flow rate of 35 GMP was used to circulate the SMC dispersions to the membrane cell, and the feed returned to the tank through the heat exchanger, which was maintained at 20°C using the chilled water recirculation set-up using the plate-heat exchanger (AGC Heat Transfer, Portland, OR). The retentate was returned to the feed tank while permeate was collected in a bucket and weighed in an electronic balance (Cardinal, Webb City, MO). In constant concentration mode, the permeate was also returned to the feed tank at regular

10-minute intervals, and the total run time was 1 hour. Before and after each UF run, the membrane was rinsed, and the water flux was measured. Immediately after rinsing with 45°C water for 15 minutes in recirculation mode, the second cleaning step was performed using the alkaline membrane cleaner at 45°C (Ecolab Inc., USA) in 15 minutes recirculation mode followed by cleaning with 45°C water. UF on the control SMC dispersions (C-SMC; pumped through the system without BNB treatment) and BNB-treated SMC dispersions (BNB-SMC; BNB-treated using the acoustic/hydrodynamic cavitation system) were done in duplicates and the retentate and permeate samples were collected and stored for further analysis. The rheological measurements of the SMC dispersions in phase-II were carried out according to the same method as descried in phase-I. Other techniques used for characterizations of C-and BNB-SMC dispersions were not repeated in phase-II because similar model SMC dispersions were used in phase-II as well. The membrane performance in phase-II was carried out using the same methods described in phase-I.

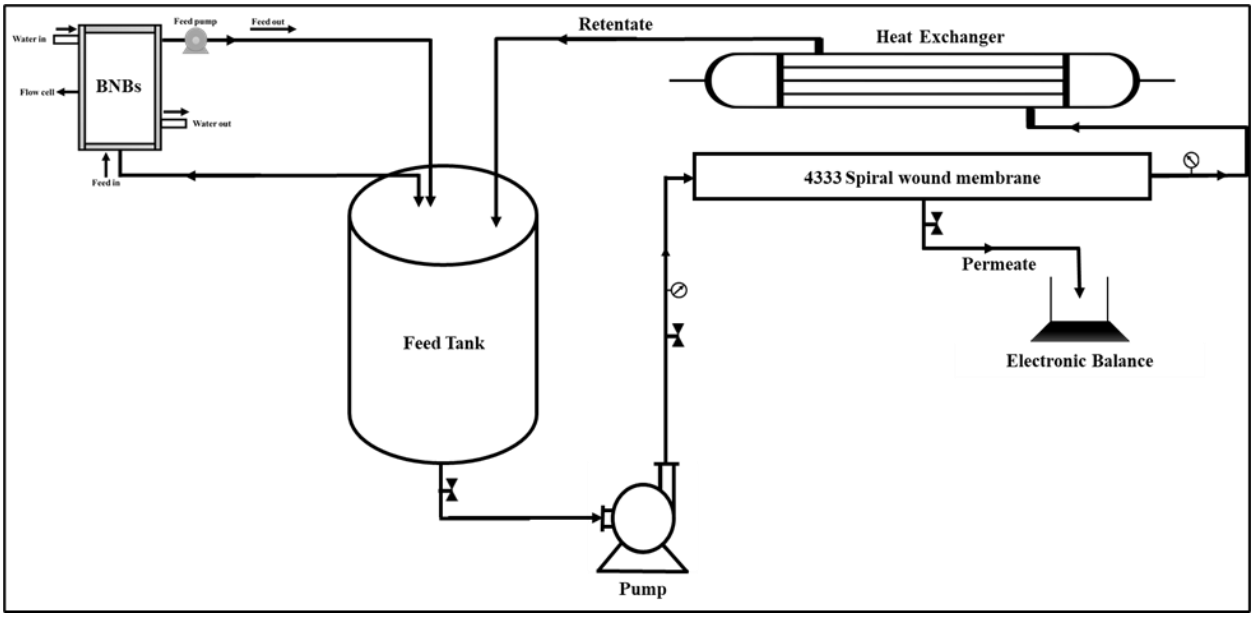

Figure 6.2 Schematic of pilot ultrafiltration unit, housing one spiral-wound element (4333 module-940 mm long and 109 mm in diameter) along with the bulk nanobubble treatment set-up.

Statistical Analysis

Repeated measures were done on the permeation flux measurements. The ANOVA and significance were indicated by $P < 0.05$, using the statistical software SAS and each experiment was repeated at least three times.

Results and discussion

Characterization of BNBs in water

For both the acoustic/hydrodynamic cavitation systems used in this study, the BNBs produced in water were characterized using NTA in terms of concentration and mean diameter. The NTA results showed a significant increase in BNB concentration upon the NB treatment, suggesting that the venturi injector based hydrodynamic cavitation and acoustic cavitation was efficient in generating sufficient BNBs. These results were summarized in chapters 3 and 5. Notably, BNBs generated by acoustic cavitation had a greater bubble concentration compared to that of the BNBs generated by hydrodynamic cavitation.

Characterization of the SMC dispersions: Phase I

Physicochemical analysis: The pH and conductivity of the C-and BNB-SMC dispersions did not change significantly ($p > 0.05$) upon BNB treatment. The C-and BNB-SMC dispersions had a pH value of 6.51 and 6.52, respectively. Similarly, Jambrak et al. (2008) and Yanjun et al. (2014) observed no significant changes ($p > 0.05$) between the pH of the control and sonicated samples at 20 kHz. In the present study, the conductivity of C-and BNB-SMC dispersions did not change significantly ($p > 0.05$). Arzeni et al. (2012) showed that the conductivities of soy

protein isolate, whey protein concentrate, and egg white protein solutions do not significantly change ($p > 0.05$) upon ultrasound treatment. The density of the BNB-SMC dispersions (0.99 g/cm^3) was lower when compared to C- SMC dispersions (1.14 g/cm^3). The average density of the BNB-SMC dispersions was ~15% less than C- SMC dispersions. Interestingly, Phan et al. (2021) reported no significant ($p > 0.05$) changes in densities of NB incorporated liquids (apple juice concentrate and canola oil). However, the density of the ice cream mix made with NB liquid was 0.77 g/mL, whereas density of the ice cream mix made with regular water was reported be 0.74 g/mL (Khaira et al., 2020). The surface tension of C-and BNB-SMC dispersions were 51.8 and 49.5 mN/m, respectively. The surface tensions of a liquid with dissolved gas and a pure liquid are different, according to Lubetkin (2003), and the surface tension of a liquid with dissolved gas drops markedly as the dissolved-gas concentration increases. Recently, Lee (2020) used acoustic cavitation to generate BNBs in deionized water (sonication time of 10 min at 20 kHz and 1100 W). The surface tension of deionized water declined as the dissolved-gas content increased (undersaturated deionized water: ~74 mN/m, saturated deionized water water: ~72 mN/m, and supersaturated deionized water: ~67 mN/m), suggesting the role of the generated BNBs.

Rheological measurements: Viscosity is a critical characteristic that impacts the operating efficiency, manufacturing capacity, product functioning, and final powder quality. During processing, both internal (total solids, pH) and extrinsic (shear-rate, temperature, pressure) elements have an effect on the viscosity of dairy concentrates. Indeed, controlling viscosity during the production of milk powder allows for lower energy usage and offers better product functionality. The relationship between shear rate and apparent viscosity of the C-and BNB-SMC dispersions are shown in Figure 6.3. The C-and BNB-SMC dispersions were shear-

dependent fluids with shear-thinning behavior revealed by the decrease in apparent viscosity with shear rate. The apparent viscosity of BNB-SMC dispersions decreased significantly compared with the C-SMC dispersions. The decrease in viscosity can be also attributed to the reduction in particle size and associated changes in the microstructure. In phase-I, the viscosity of C-and BNB-SMC dispersions at a shear rate of 100 s^{-1} were 9.62 and 6.06 mPa·s, respectively. This represents a net decrease of ~35% for the BNB-SMC dispersion. Similarly, the apparent viscosity decreased in phase-II C-and BNB-SMC dispersions as well, following the same trend as observed in phase-I C-and BNB-SMC dispersions. Apparent viscosity of BNB-SMC dispersions showed a significant ($P < 0.05$) decrease, and the lowest apparent viscosity (4.94 mPa·s) was observed in the SMC dispersions with acoustically generated BNBs, representing a net decrease of ~45% compared to the control. Whereas the SMC dispersions incorporated with BNBs from hydrodynamic cavitation had a viscosity of 6.65 mPa·s, represents a net decrease of ~35% compared to the control. Previously, Ashokkumar et al., 2009, Chandrapala et al., 2014, and Yanjun et al. (2014) have studied influence of ultrasound on dairy systems and noted that sonication breaks apart large aggregates leading to a decrease in particle size and a lower viscosity. Amamcharla et al. (2017) previously reported that introducing MNBs with an average diameter of 100 nm to 30 µm reduced viscosity in liquid dairy products. Similarly, Khaira et al. (2020) found that ice cream prepared with NBs had a decreased apparent viscosity (30% reduction). Li et al. (2018) previously shown a net decrease in milk protein concentrate viscosity of up to 55% by hydrodynamic cavitation. Similarly, Zisu et al. (2013) after acoustic cavitation of SMCs reported comparable viscosity decrease. Furthermore, the CO_2 MNB addition lowered the particle size of the lactose crystals by increasing the number of nuclei and reducing the amount of solute depositing on those nuclei (Adhikari et al., 2018). The

viscosity dropping effect of NB treatment for a 7-day test period (at 23 and 4ºC) in apple juice concentrate and canola oil was demonstrated by Phan et al. (2021) and it was attributed to the NB size and concentration. The authors also reported the lowering effect on viscosities with NB treatment declines over time as the size of the NBs grew larger, and the concentration of dissolved gas decreased. Previously, Marella et al. (2015) used CO_2 (2200 ppm of CO_2 injection before UF and an additional injection at a flow rate of 1.5-2 L/min during UF) and found that CO_2 injected samples had a lower viscosity (1.99 mPa s) than control samples (23.6 mPa s). Calcium and other minerals were removed during the ultrafiltration process as a result of CO_2 injection, which resulted in a lower pH and greater solubilization of colloidal calcium. Also, the lower calcium concentration resulted in lower viscosity in CO_2 injected samples, owing to a reduction in protein aggregation produced by calcium bridging. We believe that the BNBs might have persisted (assisting in lowering the viscosity) but been previously unnoticed, as BNBs were not a part of the study. In a recent study, the concentrations of bulk NB (generated by gas injection via a membrane) were reported to be stable for about a week (in DI water) before gradually decreasing over storage of 1 to 2 months (Shi et al., 2021). Therefore, the viscosity reduction as reported by Marella et al. (2015) can also be attributed in part to the presence of BNB in the MPC dispersion. These findings showed that using BNBs to lower viscosity and improve dairy fluid processing efficiency might be a feasible option. In the study of Gul et al. (2017), hydrodynamic cavitation applied through high pressure homogenization resulted in better rheological and microstructural properties in hazelnut milk. Furthermore, overall permeation fluxes were observed to increase by the BNB treatment (Table 6.1 and 6.2). This is expected because of reduced viscosities of the BNB-SMC dispersions. Previously, Shu-Sen (1988) investigated how solution viscosity influences the UF flux. Although, the connection between

UF flux and solution viscosity is known to be non-linear and dependent on solution viscosity. Moreover, low flux resulting from high viscosities may result in membrane fouling, gelation, and protein aggregation. Thus, BNB incorporation would be highly beneficial for weakening protein aggregates to reduce viscosity and aggregation, both to improve UF flux and to reduce membrane fouling.

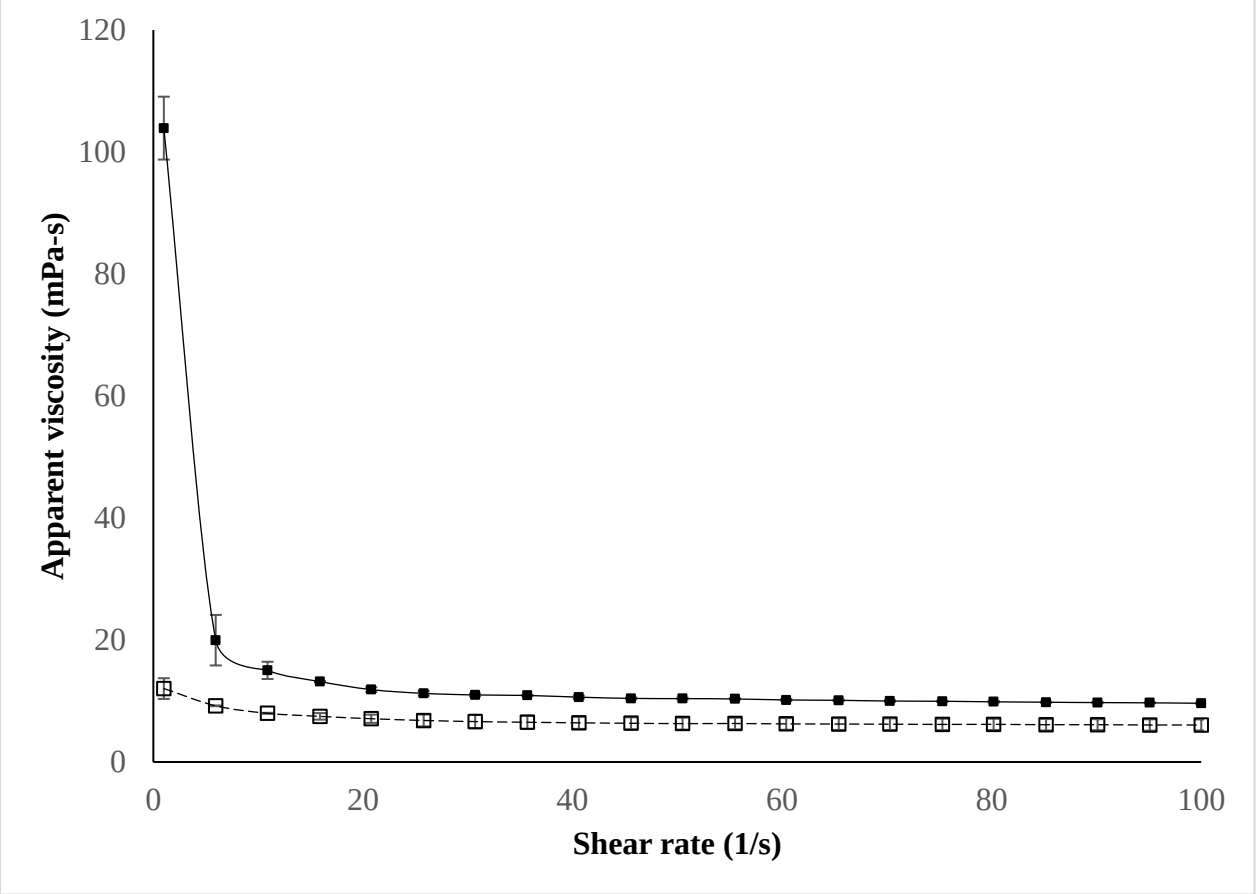

Figure 6.3 Viscosity as a function of shear rate (flow curves) for control (■) and bulk nanobubble treated (□) skim milk concentrates; n = 3. (Phase-I)

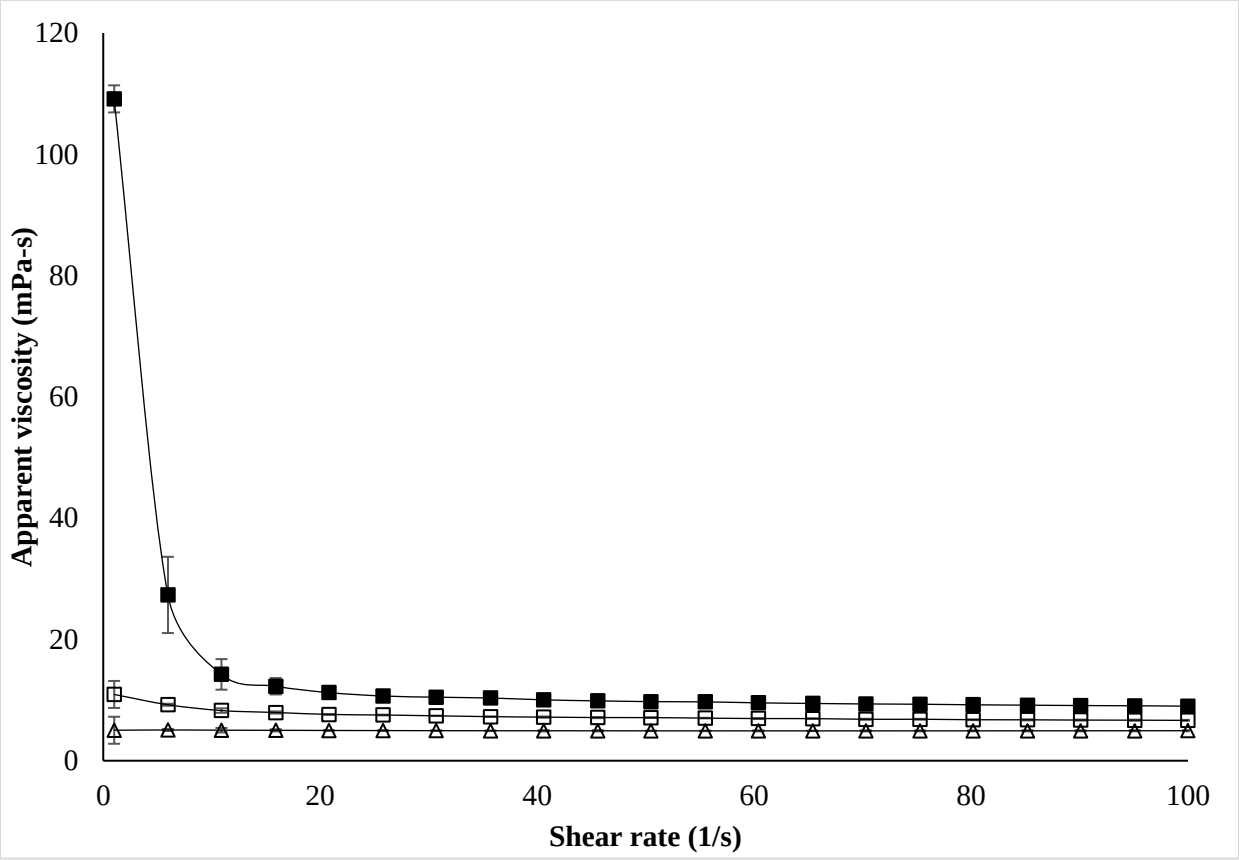

Figure 6.4 Viscosity as a function of shear rate (flow curves) for control (■), bulk nanobubbles generated by acoustic cavitation (□), and (▲) bulk nanobubbles generated by hydrodynamic cavitation skim milk concentrates; n = 2. (Phase-II)

Microstructure: The microstructure of C-and BNB-SMC dispersions after the UF run of 1 h are shown in Figures 6.4 and 6.5, respectively. The rheological characteristics of dispersions treated with BNBs clearly suggested that structural configurations had changed. CLSM and TEM were used to analyze the microstructures of C-and BNB-SMC dispersions. The CLSM did not reveal any noticeable microstructural changes upon the BNB treatment. However, the TEM micrographs of C-SMC dispersions (Figure 6.5A) revealed dense cross-linked network structural design. In contrast, less dense structure was seen in the BNB-SMC dispersion, along with thinner protein network. This can be attributed to the physical shear caused by ultrasound, which

resulted in the protein aggregates being effectively broken, thus decreasing the particle size. However, the network structure appeared more homogenous and with a higher degree of branching for the C-SMC, when the dispersions were not exposed to BNBs, which could explain the higher viscosity observed in the C-SMCs. Wang et al. (2021) showed that the shear force and turbulence generated by acoustic cavitation could cause protein dispersion, and the particle size of the complexes significantly reduced. The BNB-SMC dispersions showed a significant reduction in large aggregate formations. The structural disintegration of protein aggregates caused by bubble implosion during the hydrodynamic cavitation process might explain this. Indeed, by acting as a spatial buffer between particles in the milk system and resulting in decreased viscosity, BNB may have assisted in the prevention of protein aggregation. Previously, Babu et al. (2022) have noted noticeable microstructural changes in Greek-style yogurts upon NB treatment. Although TEM revealed a more scattered structure when the SMC system was treated with BNB, additional research is needed to determine if this is a transitory phenomenon or whether it results in a permanent viscosity decrease. Overall, the impact of BNB on the rheological characteristics of C-and BNB-SMC dispersions was clearly characterized based on structural analysis.

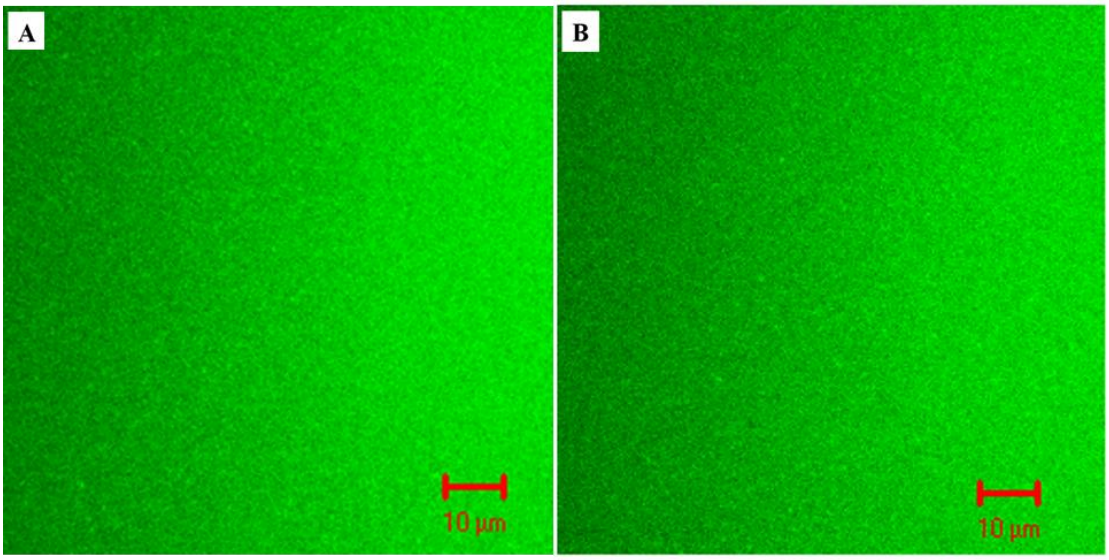

Figure 6.5 Confocal laser scanning microscopy images of control (A) and bulk nanobubble treated (B) skim milk concentrate after 60 minutes of ultrafiltration processing.

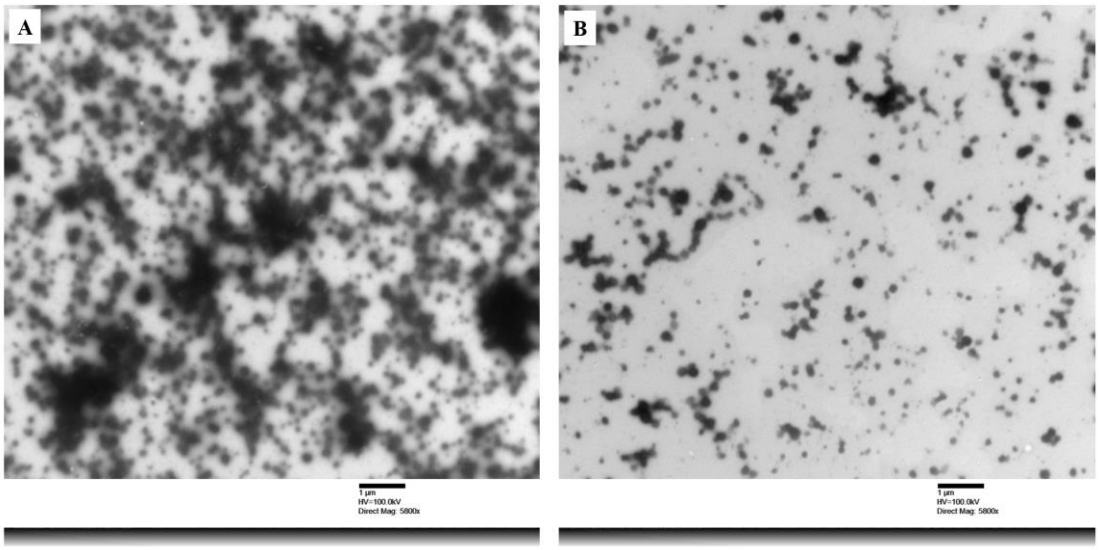

Figure 6.6 Representative transmission electron microscopy images of control (A) and bulk nanobubble treated (B) skim milk concentrate after 60 minutes of ultrafiltration processing. (Magnification and scale: 5800× and 1 µm).

Membrane performance

The effect of BNBs on the UF process was assessed in terms of permeation flux and fouling resistances. When UF was performed with the BNB incorporation, marked differences occurred in the permeation flux in the constant concentration mode. The permeation flux of the C-and BNB-SMC dispersions over a 1 h period is shown in Table 6.1. In both phase-I and phase-II, the permeation flux was significantly higher ($P < 0.05$) for BNB-SMC dispersions compared with control. In phase-I, the permeation flux after 10-mins was about ~50% higher for BNB incorporated dispersions, compared with that of the control. In phase-II, after the 1 h run period SMC dispersions with BNBs generated by acoustic cavitation had a permeation flux that was about ~38% higher for C-SMC dispersions. Whereas SMC dispersions with BNBs generated by hydrodynamic cavitation had a permeation flux that was about ~27% higher for C-SMC dispersions. In phase-I, the average permeation flux (J_{avg}) for the BNB incorporated samples were about 50% higher compared with that of the control. Similarly, for the phase-II, the J_{avg} for the BNB incorporated samples was about 30% higher compared with that of the control. Additionally, during UF process, the permeate flux for the BNB treated samples remained relatively stable for the remainder of the run time; however, relatively lower permeate flux values compared to the respective time were observed for the untreated samples. Previously, Amamcharla et al. (2017) studied the influence of MNBs on lab-scale membrane filtration system using MNBs generated by a venturi-style hydrodynamic cavitation system (air flow rate 0.01-0.02 L/min). The results demonstrated that the permeate flux of the MNB incorporated samples were always higher (~18%) than the control samples. Previously, Muthukumaran et al. (2006) used acoustic cavitation and found it was effective in improving permeate flux values by between 40-70%. The permeate flux was observed to be greater for low-frequency operation at

50 kHz compared to 1 MHz. Pore blockage, mineral precipitation, protein adsorption/ denaturation/aggregation of proteins on the surface of membrane can all contribute to the membrane fouling mechanism.

Table 6.1 Permeation flux ($kg/h \cdot m^2$) of control and bulk nanobubble treated UF runs (Phase I).

Time (min)	Control	Bulk nanobubbles generated by acoustic cavitation	Percentage change in permeation flux (%)
10	10.51 ± 0.13^{a}	16.18 ± 0.13^{b}	53.93
20	10.41 ± 0.06^{a}	15.52 ± 0.17^{b}	49.14
30	10.15 ± 0.10^{a}	15.24 ± 0.07^{b}	50.15
40	9.99 ± 0.07^{a}	15.13 ± 0.13^{b}	51.57
50	9.90 ± 0.10^{a}	14.74 ± 0.16^{b}	48.97
60	9.72 ± 0.09^{a}	14.57 ± 0.15^{b}	49.97

$^{a-b}$Mean within a row with different superscript different ($P<0.05$) n=3

Table 6.2 Permeation flux (kg/h·m^2) of control and bulk nanobubble treated UF runs (Phase-II).

Time (min)	Control	Bulk nanobubbles generated by hydrodynamic cavitation		Bulk nanobubbles generated by acoustic cavitation	
		Permeation flux (kg/h·m^2)	Percentage change in permeation flux (%)	Permeation flux (kg/h·m^2)	Percentage change in permeation flux (%)
10	7.35 ± 0.72 [a]	10.16 ± 0.08 [b]	38.21	10.19 ± 0.36 [b]	36.26
20	7.40 ± 0.01 [a]	9.80 ± 0.21 [b]	32.44	9.90 ± 0.21 [b]	33.87
30	7.22 ± 0.06 [a]	9.66 ± 0.13 [b]	33.76	9.88 ± 0.22 [b]	36.86
40	7.12 ± 0.03 [a]	9.49 ± 0.18 [b]	33.21	9.78 ± 0.15 [b]	37.30
50	7.04 ± 0.04 [a]	9.10 ± 0.27 [b]	29.30	9.70 ± 0.11 [b]	37.87
60	6.89 ± 0.03 [a]	8.81 ± 0.06 [b]	27.83	9.59 ± 0.07 [b]	39.02

[a-b]Mean within a row with different superscript different ($P<0.05$) n=2. The BNBs generated (acoustic/hydrodynamic cavitation) samples were compared to the control samples.

Figure 6.6 illustrates the potential mechanism of the BNBs on the UF membrane. Interestingly, Marella et al. (2018) noted that compared to the control samples, the J_{avg} was nearly 20% lower for CO_2 incorporated feeds. This was observed due to the presence of increased quantities of soluble minerals as a result of the lower pH caused by the injection of CO_2. The flux increase observed in this study can be linked to a substantial role played by the BNBs. Incorporating BNBs during membrane filtration in water treatment effectively prevents or reduces membrane fouling (Wu et al., 2008). Dayarathne et al. (2019) reported that MNBs increase the membrane permeability under various operational conditions. Very recently, Farid et al. (2022) have noted that when the membrane surface tested without BNBs in the feed, had significant scaling and a total flux loss within 13 h of operation. In contrast, the membrane surface examined with the BNB treatment showed only a flux decrease ~63% after 98 h. Therefore, by incorporating BNBs into the feed, the deposition on the membrane surface can be remarkably reduced. Similarly, the introduction of evenly dispersed BNBs in the SMC feed stream is expected to greatly improve the membrane performance. The presence of BNBs at the membrane surface might cause turbulence and shear pressures, thus plausibly disrupting the foulant layer, thus reducing the possibility of evidently more foulant formation on the membrane surface. Furthermore, its anticipated that any mineral precipitation could be also efficiently reduced by the significant negative charge of BNBs. Indeed, $OH^{\bullet}$ radicals are produced by collapsing cavity bubbles, which is explained elsewhere (Takahashi et al., 2007). BNBs have interior pressures that very much greater than the atmospheric pressure and when the BNBs burst, they release additional surface energy, which has the potential to convert O_2 to oxygen radicals (Zhang et al., 2022; Han et al., 2022). Similarly, Liu et al. (2014) also reported that the

water containing BNBs (NB size: ~560 nm) can produce hydroxyl radicals. It is possible that OH• radicals can break down the deposits at the membrane surface, improving the membrane performance. Additionally, membrane process performance is influenced by viscosity. Another factor potentially contributing to the increase in flux could be the viscosity reduction of SMC dispersions containing BNBs. However, it should be noted that determining the contribution of each mechanism is complex and requires further investigation. Also, the evidence of the existence, longevity, and the stability of BNBs in a complex system like dairy concentrates must be further evaluated.

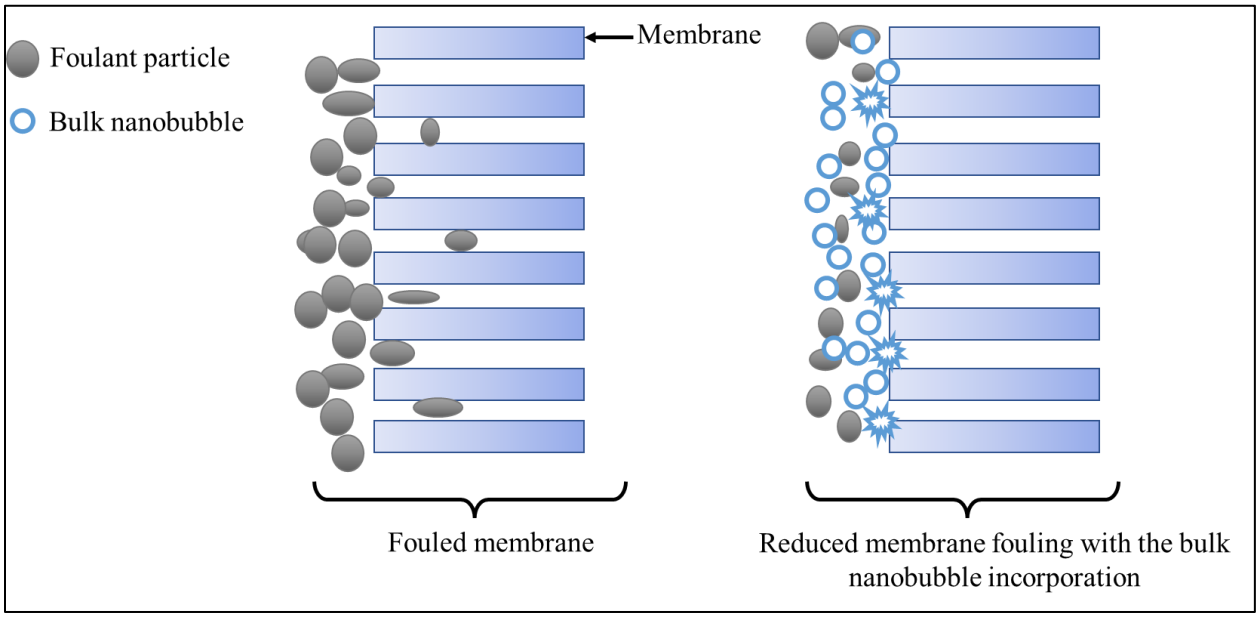

Figure 6.7 Proposed mechanism of the NBs on the ultrafiltration membrane performance

In order to elucidate the cause of the increase in flux, the behavior of the individual resistances to flow were also considered. Table 6.3 and 6.4 shows the R_m, R_{rev}, R_{irr}, and R_t for control and BNB treated samples. The R_{rev}, R_{irr}, and R_t were influenced ($P < 0.05$) by the BNB treatment. In the phase-I, the irreversible resistance was higher for the control samples than for the BNB-incorporated samplers ($29.28 \pm 1.08 \times 10^{12}$ m^{-1} vs. $17.67 \pm 1.77 \times 10^{12}$ m^{-1}). A similar trend was observed in phase-II as well. Additionally, the rate of flux decline during processing

was considerably greater for untreated samples, which was attributed to more extensive membrane fouling without the BNB treatment, as indicated by low permeability of clean water immediately after the UF processing. Overall, total resistance values were higher ($P < 0.05$) for the control and BNB treatment induced lower R_t values. Previously, Muthukumaran et al. (2005, 2006) noted that ultrasound increases the mass transfer. Liu et al. (2007) aimed to use ultrasound technology to help in membrane-based deoxidation. Under acoustic cavitation, the mass transfer performance of the submerged hollow membrane module for eliminating dissolved oxygen in water was studied and noted increased mass transfer. Muthukumaran et al. (2006) noted that membrane resistance and cake growth factors were significantly influenced by the acoustic treatment. The impact of ultrasound on flux and solute rejection in bovine serum albumin and lysozyme cross-flow UF utilizing polysulfone membrane has been investigated (Teng et al., 2006). They noted that ultrasonic irradiation enhanced not only the UF permeate flux but also the lysozyme rejection. Therefore, BNBs enhances UF process performance by reducing fouling at membrane surfaces and increasing permeate flow by promoting mass transfer. Overall, the membrane lifetime can be increases by incorporating the BNBs into the UF process, which decreases the total operation costs.

Table 6.3 Membrane performance of control and bulk nanobubble treated UF runs (Phase-I).

Sample	J_{avg} (kg/h·m^2)	Resistance (m^{-1})			
		R_m (×10^{12})	R_{irr} (×10^{12})	R_{rev} (×10^{12})	R_t (×10^{12})
Control	10.11 ± 0.31 [a]	16.09 ± 0.03 [a]	29.28 ± 1.88 [a]	5.41 ± 1.56 [a]	50.78 ± 0.02 [a]
Bulk nanobubbles generated by acoustic cavitation	15.23 ± 0.57 [b]	16.01 ± 0.05 [a]	17.67 ± 1.77 [b]	3.27 ± 1.29 [b]	36.43 ± 0.04 [b]

[a-b] Mean within a column with different superscript differ ($P<0.05$) n=3

J_{avg} = average flux (kg/h·m^2) for the entire run; R_t = total resistance (m^{-1}); R_m = membrane resistance (m^{-1}); R_{irr} = irreversible resistance (m^{-1}); R_{rev} =reversible resistance (m^{-1}).

Table 6.4 Membrane performance of control and bulk nanobubble treated UF runs (Phase-II).

Sample	J_{avg} (kg/h·m^2)	Resistance (m^{-1})			
		R_m (×10^{12})	R_{irr} (×10^{12})	R_{rev} (×10^{12})	R_t (×10^{12})
Control	7.17 ± 0.19 [a]	15.31 ± 0.02 [a]	17.84 ± 0.29 [a]	39.18 ± 0.22 [a]	72.35 ± 0.09 [a]
Bulk nanobubbles generated by hydrodynamic cavitation	9.51 ± 0.49 [b]	15.52 ± 0.05 [a]	11.55 ± 0.06 [b]	33.46 ± 0.02 [b]	60.23 ± 0.04 [b]
Bulk nanobubbles generated by acoustic cavitation	9.81 ± 0.15 [b]	15.50 ± 0.04 [a]	10.07 ± 0.09 [b]	30.08 ± 0.14 [b]	55.38 ± 0.04 [b]

[a-b] Mean within a column with different superscript differ ($P<0.05$) n=3

J_{avg} = average flux (kg/h·m^2) for the entire run; R_t = total resistance (m^{-1}); R_m = membrane resistance (m^{-1}); R_{irr} = irreversible resistance (m^{-1}); R_{rev} =reversible resistance (m^{-1}).

Membrane microstructure

The phase-I membrane performance was also monitored by the membrane microstructure imaging analysis as presented in Figure 6.8. The CLSM images indicated that the active surface of membranes operated with the BNB incorporated sample was cleaner as observed by the presence of lesser area of proteins blocking the pores and minimal fouling in the cross-sectional images. In contrast, membrane obtained after the UF with C-SMC dispersions had protein particles sticking to the surface which could not be removed by washing, and the pores might be blocked supporting the finding that increased permeate flux occurred with the BNB treatment. The CLSM was used to measure the thickness of fouled layer. It was observed that the measured thickness of membrane without BNBs (45.17 um) was notably different from the BNB-SMC (19.01 um) fouled membrane, suggesting the BNBs near the membrane surface reducing the effects of concentration polarization and membrane fouling. Indeed, the collapse of BNBs at membrane surface might have led to removal or control of the fouling layer. This increase in deposition might be caused by the protein deposits being compacted into a more densely packed layer. Moreover, the presence of BNBs near the membrane surfaces minimized the effect of concentration polarization and thus increases the mass transfer coefficient at the membrane surface as explained earlier by the mechanism of BNBs. Many researchers have previously studied the influence of ultrasound in the membrane cleaning process (Gonzalez-Avila et al., 2012: Hou et al., 2015). The BNBs acting on the membrane surface creates a physical disturbance in the membrane surface, increasing the mass transfer coefficients (Wu et al., 2015). These conditions on the introduction of BNBs in the feed stream plays a crucial role in delaying foulant formation and depositions on the membrane surface. Similar changes were anticipated in the membrane microstructure for the phase-II.

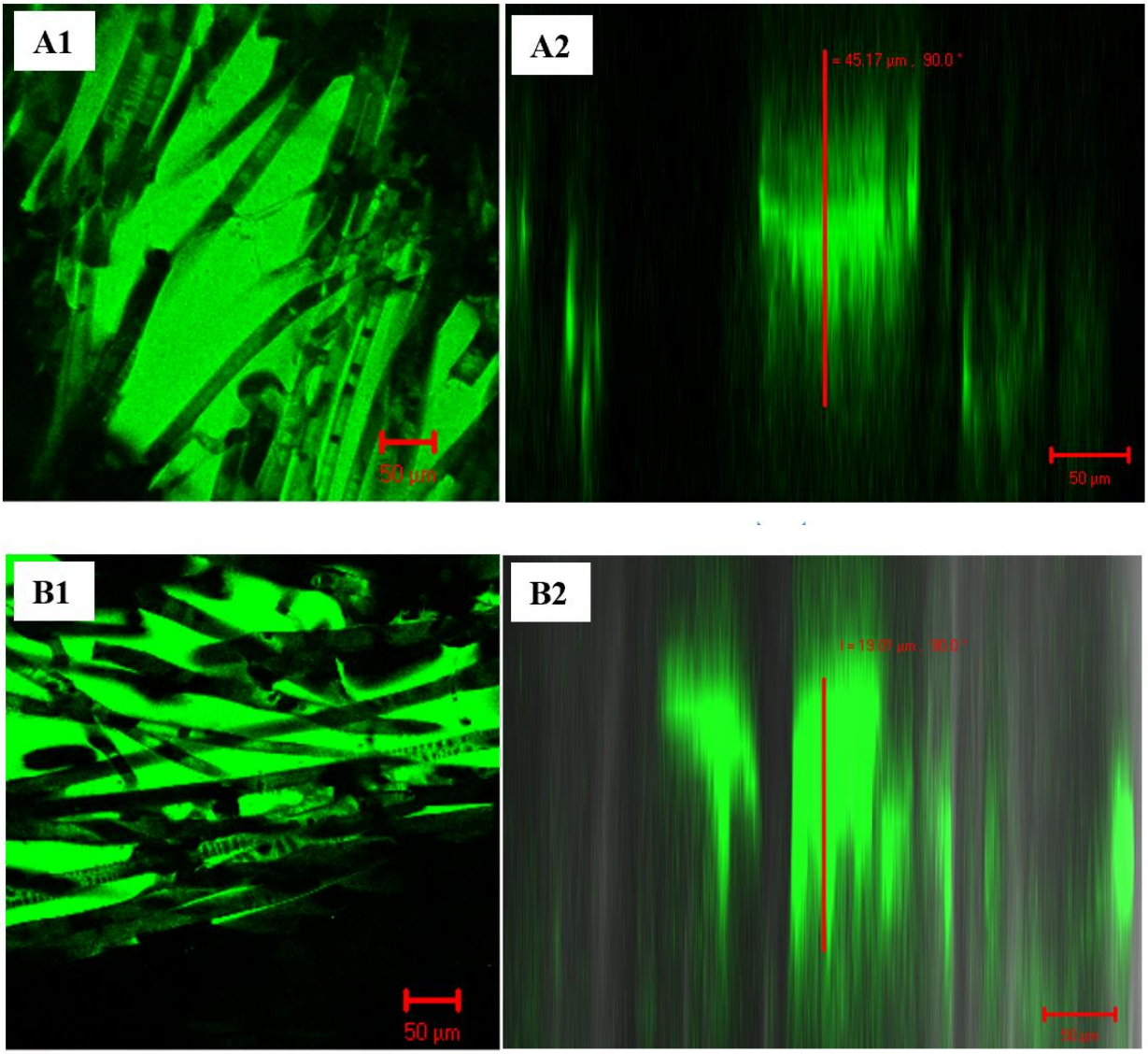

Figure 6.8 The Confocal laser scanning microscopy images of fouled membrane surface (phase I) and cross section showing thickness of fouled layer (a) control and (b) bulk nanobubble treated. Images show 3-D projection of Z-Series through microstructure of fouling film. The proteins shown in green. images of membrane**.**

Energy consumption

The energy consumption data also provides strong evidence on the effect of BNB incorporation. Figure 6.9 illustrates the electrical power usage for the processing of C-and BNB-SMC dispersions at each 10 min interval operating at 20°C. The BNB incorporation resulted in significant differences ($P < 0.05$) for the power requirements. The electrical power usage after 1 h run was about ~20% lower for BNB-SMC dispersions, compared with that of the control. This difference could be explained by the lower fluid viscosity value of BNB incorporated dispersions. The BNB incorporation is envisaged as a method of improving overall UF process efficiency. Similar results were anticipated in the energy consumption patterns for the phase-II studies.

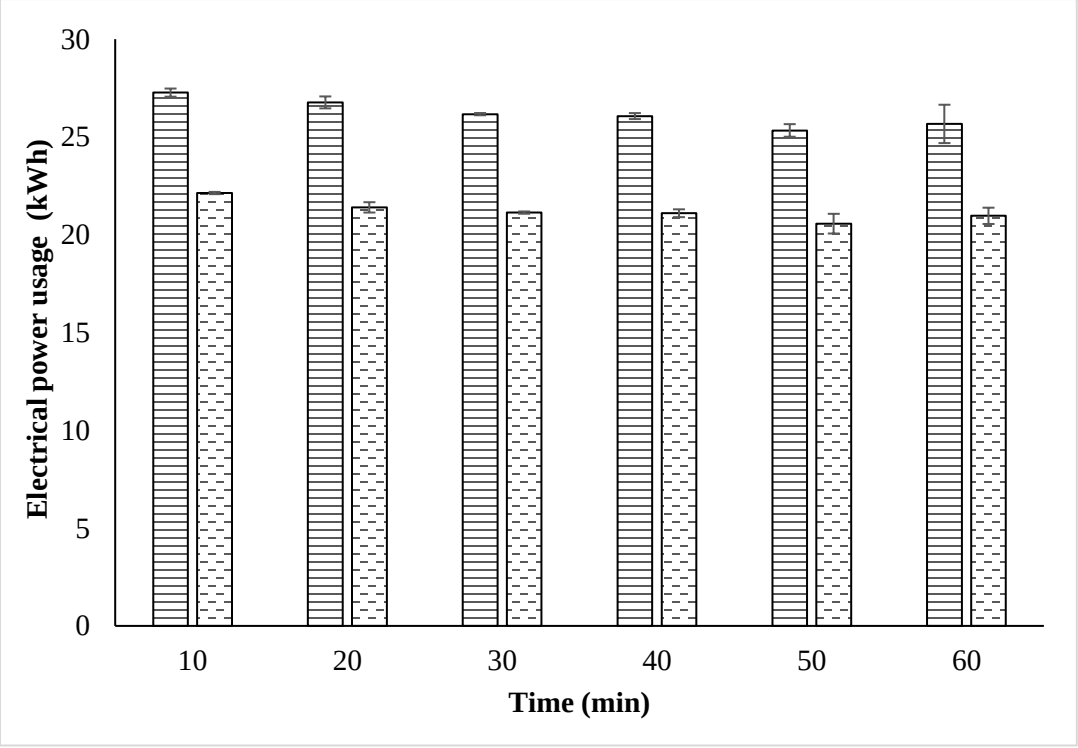

Figure 6.9 Pumping energy obtained during lab scale UF run of skim milk concentrates with bulk nanobubble (BNB) treatment (–) and without BNB treatment (--). Different letters indicate significant differences. Error bars in indicate standard deviation. n=3.

Conclusions

Reduced membrane performance represents a significant challenge hindering the effective UF processing in industrial applications. This study demonstrated the benefits of introducing BNBs into the SMC dispersions during the UF, as an eco-friendly and simple method, for alleviating flux reduction and membrane fouling associated with the UF of skim milk. Compared to the C-SMCs, introducing BNBs offered excellent permeate flux improvements at significantly lower electrical power usage. CLSM images of the fouled membranes revealed an accumulation of particles at the membrane surface and a formation of thick and denser layer on the surface of the membrane tested without BNBs in the feed, compared to those membrane tested with BNBs in the feed. Additionally, feed properties like viscosity were significantly reduced with the BNB treatment. Our findings demonstrate the advantage of introducing BNBs into the feed during the UF process and offer valuable insights for the future development of simple, eco-friendly strategies for improving membrane performance in UF processing.

References

Agarwal, A., Ng, W. J., & Liu, Y. (2011). Principle and applications of microbubble and nanobubble technology for water treatment. *Chemosphere*, *84*(9), 1175-1180.

Amamcharla, J., Li, B., & Liu, Z. (2017). Use of micro-and nano-bubbles in liquid processing. *United States*.

Arzeni, C., Martínez, K., Zema, P., Arias, A., Pérez, O. E., & Pilosof, A. M. R. (2012). Comparative study of high intensity ultrasound effects on food proteins functionality. *Journal of Food Engineering*, *108*(3), 463-472.

Ashokkumar, M., Lee, J., Zisu, B., Bhaskarcharya, R., Palmer, M., & Kentish, S. (2009). Hot topic: Sonication increases the heat stability of whey proteins. *Journal of Dairy Science*, *92*(11), 5353-5356.

Babu, K. S., Liu, D. Z., & Amamcharla, J. K. (2022). Application of Micro-and Nano-Bubbles as a Tool to Improve the Rheological and Microstructural Properties of Formulated Greek-Style Yogurts. *Foods*, *11*(4), 619.

Chandrapala, J., Martin, G. J., Kentish, S. E., & Ashokkumar, M. (2014). Dissolution and reconstitution of casein micelle containing dairy powders by high shear using ultrasonic and physical methods. *Ultrasonics sonochemistry*, *21*(5), 1658-1665.

Chen, D., Weavers, L. K., & Walker, H. W. (2006). Ultrasonic control of ceramic membrane fouling: effect of particle characteristics. *Water research*, *40*(4), 840-850.

Cui, Z., & Taha, T. (2003). Enhancement of ultrafiltration using gas sparging: a comparison of different membrane modules. *Journal of Chemical Technology & Biotechnology: International Research in Process, Environmental & Clean Technology*, *78*(2-3), 249-253.

Dayarathne, H. N. P., Jeong, S., & Jang, A. (2019). Chemical-free scale inhibition method for seawater reverse osmosis membrane process: Air micro-nano bubbles. *Desalination, 461*, 1-9.

Farid, M. U., Kharraz, J. A., Lee, C. H., Fang, J. K. H., St-Hilaire, S., & An, A. K. (2022). Nanobubble-assisted scaling inhibition in membrane distillation for the treatment of high-salinity brine. *Water Research, 209*, 117954.

Ghadimkhani, A., Zhang, W., & Marhaba, T. (2016). Ceramic membrane defouling (cleaning) by air Nano Bubbles. *Chemosphere*, *146*, 379-384.

Gonzalez-Avila, S. R., Prabowo, F., Kumar, A., & Ohl, C. D. (2012). Improved ultrasonic cleaning of membranes with tandem frequency excitation. *Journal of membrane science*, *415*, 776-783.

Gul, O., Saricaoglu, F. T., Mortas, M., Atalar, I., & Yazici, F. (2017). Effect of high pressure homogenization (HPH) on microstructure and rheological properties of hazelnut milk. *Innovative Food Science & Emerging Technologies*, *41*, 411-420.

Han, Z., Kurokawa, H., Matsui, H., He, C., Wang, K., Wei, Y., ... & Fujita, T. (2022). Stability and Free Radical Production for CO2 and H2 in Air Nanobubbles in Ethanol Aqueous Solution. *Nanomaterials*, *12*(2), 237.

Hou, D., Dai, G., Fan, H., Huang, H., & Wang, J. (2015). An ultrasonic assisted direct contact membrane distillation hybrid process for desalination. *Journal of membrane science*, *476*, 59-67.

Jadhav, A. J., & Barigou, M. (2020). Bulk nanobubbles or not nanobubbles: that is the question. *Langmuir*, *36*(7), 1699-1708.

Jambrak, A. R., Mason, T. J., Lelas, V., Herceg, Z., & Herceg, I. L. (2008). Effect of ultrasound treatment on solubility and foaming properties of whey protein suspensions. *Journal of food engineering*, *86*(2), 281-287.

Khaira, N. M., Abd Rahmana, N. A., Baharuddina, A. S., Hafidb, H. S., & Wakisakab, M. (2020). Capturing the impact of nanobubble liquid in enhancing the physical quality of ice cream. *Journal of Agricultural and Food Engineering*, *2*, 0012.

Lee, J. I., Yim, B. S., & Kim, J. M. (2020). Effect of dissolved-gas concentration on bulk nanobubbles generation using ultrasonication. *Scientific Reports*, *10*(1), 1-7.

Liu, G., Wu, Z., & Craig, V. S. (2008). Cleaning of protein-coated surfaces using nanobubbles: an investigation using a quartz crystal microbalance. *The Journal of Physical Chemistry C*, *112*(43), 16748-16753.

Liu, L., Ding, Z., Chang, L., Ma, R., & Yang, Z. (2007). Ultrasonic enhancement of membrane-based deoxygenation and simultaneous influence on polymeric hollow fiber membrane. *Separation and purification technology*, *56*(2), 133-142.

Liu, S., Oshita, S., & Makino, Y. (2014). Stimulating effect of nanobubbles on the reactive oxygen species generation inside barley seeds as studied by the microscope spectrophotometer. In *Proceedings]. Int. Conf. of Agric. Eng., Zurich* (pp. 06-10).

Lubetkin, S. D. (2003). Why is it much easier to nucleate gas bubbles than theory predicts?. *Langmuir*, *19*(7), 2575-2587.

Luo, X., Ramchandran, L., & Vasiljevic, T. (2015). Lower ultrafiltration temperature improves membrane performance and emulsifying properties of milk protein concentrates. *Dairy science & technology*, *95*(1), 15-31.

Luo, X., Vasiljevic, T., & Ramchandran, L. (2016). Effect of adjusted pH prior to ultrafiltration of skim milk on membrane performance and physical functionality of milk protein concentrate. *Journal of Dairy Science*, *99*(2), 1083-1094.

Marella, C., Salunke, P., Biswas, A. C., Kommineni, A., & Metzger, L. E. (2015). Manufacture of modified milk protein concentrate utilizing injection of carbon dioxide. *Journal of Dairy Science*, *98*(6), 3577-3589.

Méthot-Hains, S., Benoit, S., Bouchard, C., Doyen, A., Bazinet, L., & Pouliot, Y. (2016). Effect of transmembrane pressure control on energy efficiency during skim milk concentration by ultrafiltration at 10 and 50° C. *Journal of dairy science*, *99*(11), 8655-8664.

Muthukumaran, S., Kentish, S. E., Ashokkumar, M., & Stevens, G. W. (2005). Mechanisms for the ultrasonic enhancement of dairy whey ultrafiltration. *Journal of membrane science*, *258*(1-2), 106-114.

Muthukumaran, S., Kentish, S. E., Stevens, G. W., & Ashokkumar, M. (2006). Application of ultrasound in membrane separation processes: a review. *Reviews in chemical engineering*, *22*(3), 155-194.

Muthukumaran, S., Kentish, S. E., Stevens, G. W., Ashokkumar, M., & Mawson, R. (2007). The application of ultrasound to dairy ultrafiltration: the influence of operating conditions. *Journal of Food Engineering*, *81*(2), 364-373.

Olusanya, S. O., Adebayo, G. J., & Dada, A. O. (2021). Effect of Salt on the Stability of Vegetable Oil-in-Water Emulsions Stabilized by Soybean Protein and Microgel. *Journal of the Chemical Society of Pakistan*, *43*(5).

Phan, K., Truong, T., Wang, Y., & Bhandari, B. (2021). Effect of CO_2 nanobubbles incorporation on the viscosity reduction of fruit juice concentrate and vegetable oil. *International Journal of Food Science & Technology*, *56*(9), 4278-4286.

Puri, R., Singh, U., & A O'Mahony, J. (2020). Influence of processing temperature on membrane performance and characteristics of process streams generated during ultrafiltration of skim milk. *Foods*, *9*(11), 1721.

Shahraki, M. H., Maskooki, A., & Faezian, A. (2014). Effect of various sonication modes on permeation flux in cross flow ultrafiltration membrane. *Journal of Environmental Chemical Engineering*, *2*(4), 2289-2294.

Shu-Sen, W. (1988). Effect of solution viscosity on ultrafiltration flux. *Journal of membrane science*, *39*(2), 187-194.

Takahashi, M., Chiba, K., & Li, P. (2007). Free-radical generation from collapsing microbubbles in the absence of a dynamic stimulus. *The Journal of Physical Chemistry B*, *111*(6), 1343-1347.

Teng, M. Y., Lin, S. H., & Juang, R. S. (2006). Effect of ultrasound on the separation of binary protein mixtures by cross-flow ultrafiltration. *Desalination*, *200*(1-3), 280-282.

Tian, J. Y., Xu, Y. P., Chen, Z. L., Nan, J., & Li, G. B. (2010). Air bubbling for alleviating membrane fouling of immersed hollow-fiber membrane for ultrafiltration of river water. *Desalination*, *260*(1-3), 225-230.

Wang, T., Chen, X., Wang, W., Wang, L., Jiang, L., Yu, D., & Xie, F. (2021). Effect of ultrasound on the properties of rice bran protein and its chlorogenic acid complex. *Ultrasonics Sonochemistry*, *79*, 105758.

Wilson, R., S, Fazel., S. Jarrige., S. Chesters. (2013). Air bubbles enhance membrane cleaning: a future perspective. International Desalination Association World Congress on Desalination and Water Reuse.

Wu, Z., Chen, H., Dong, Y., Mao, H., Sun, J., Chen, S., ... & Hu, J. (2008). Cleaning using nanobubbles: Defouling by electrochemical generation of bubbles. *Journal of colloid and interface science*, *328*(1), 10-14.

Yanjun, S., Jianhang, C., Shuwen, Z., Hongjuan, L., Jing, L., Lu, L., ... & Jiaping, L. (2014). Effect of power ultrasound pre-treatment on the physical and functional properties of reconstituted milk protein concentrate. *Journal of Food Engineering*, *124*, 11-18.

Zhang, Z. H., Wang, S., Cheng, L., Ma, H., Gao, X., Brennan, C. S., & Yan, J. K. (2022). Micro-nano-bubble technology and its applications in food industry: A critical review. *Food Reviews International*, 1-23.

Zisu, B., Schleyer, M., & Chandrapala, J. (2013). Application of ultrasound to reduce viscosity and control the rate of age thickening of concentrated skim milk. *International Dairy Journal*, *31*(1), 41-43.

Chapter 7 - Conclusions

Different approaches have been utilized (although generally at laboratory scale) to lower the viscosity of milk protein concentrate (MPC) dispersions during processing, such as ultrasound, altering pH, cavitation, CO_2 injection, and changing the casein and whey protein ratio, etc. Changing intrinsic characteristics (such as pH and calcium content level) or using simpler process technologies is less expensive and, in more consideration, than using added processing technologies (such as extrusion-porosification), which might raise the total cost of powder manufacturing. Ultrafiltration membrane fouling is a key problem that affects the cost and efficiency of many dairy processing processes. A build-up of particles on the filtration membranes happens during the filtration of processed milk and its components, resulting in lower membrane performance and, ultimately, lower throughput in large-scale processing. The current research envisaged bulk nanobubble (NB) incorporation as a feasible substitute for other conventional techniques for viscosity reduction during processing and product performance (enhanced rehydration and bulk handling properties of the resultant NB treated MPC powders). The results demonstrated improved rheological and microstructural properties in the NB-treated dairy concentrates. This study, therefore, suggests the potential of using BNB generation by acoustic/hydrodynamic cavitation for more efficient drying of high solids milk, while improving the physicochemical and functional properties of the resultant powders. Indeed, more pilot-scale studies on a wider variety of dairy processing and products under various operating circumstances is needed to further examine the possibilities of the NB incorporation. It's also worth looking at the technological and economic benefits of implementing such tactics on product quality.

Appendix A - SAS code

Acoustic cavitation study (15 % total solids)

```
dm "output;clear;log;clear;";
options linesize=95 pagesize=65 nodate pageno=1;
data RCBD;
input Lot $ Amp VSR100 K n VF Vol pH Cond Dia Caion HCT Turbidity FI HCTA
HCTB HCTC;
cards;

1      0      65.20 224.46       0.90  0.36  0.69  4.63  6.72  1187.00
       172.93       1.21  8.94  0.347 19.18 8.27  7.08  14.97
1      50     5.66  9.52  0.04  0.52  0.58  3.83  6.72  1202.00      167.25
       1.25   8.93  0.284 19.94 7.09  7.41  15.03
1      75     6.40  9.77  0.05  0.49  0.48  3.21  6.7   1277.00      165.50
       1.23   9.29  0.26  19.45 8.22  7.28  15.28
1      90     5.66  9.52  0.05  0.50  0.46  3.08  6.67  1395.00      158.77
       1.27   8.73  0.253 19.81 8.33  7.27  14.27
2      0      69.11 225.24       0.83  0.45  0.70  4.64  6.72  1159.00
       241.20       1.15  9.03  0.345 16.50 8.21  6.74  13.24
2      50     7.37  16.55 0.09  0.42  0.50  3.35  6.71  1197.00      170.25
       1.15   8.22  0.283 17.47 7.63  7.11  12.27
2      75     6.10  8.92  0.02  0.61  0.47  3.16  6.71  1259.00      155.48
       1.21   8.43  0.265 17.86 7.00  7.40  12.68
2      90     4.55  7.76  0.03  0.59  0.42  2.82  6.68  1341.00      148.45
       1.25   8.07  0.255 18.43 6.77  6.94  12.05
;
run;
title "VSR100";
proc glimmix data=RCBD plots=studentpanel;
class Lot Amp;
model VSR100 = Amp;
random Lot; *** random blocking factor;
lsmeans Amp/pdiff adjust=tukey;
run;
title "K";
proc glimmix data=RCBD plots=studentpanel;
class Lot Amp;
model K = Amp;
random Lot; *** random blocking factor;
lsmeans Amp/pdiff adjust=tukey;
run;
title "n";
proc glimmix data=RCBD plots=studentpanel;
class Lot Amp;
model n = Amp;
random Lot; *** random blocking factor;
lsmeans Amp/pdiff adjust=tukey;
run;
title "VF";
proc glimmix data=RCBD plots=studentpanel;
class Lot Amp;
```

```
model VF = Amp;
random Lot; *** random blocking factor;
lsmeans Amp/pdiff adjust=tukey;
run;
title "Vol";
proc glimmix data=RCBD plots=studentpanel;
class Lot Amp;
model Vol = Amp;
random Lot; *** random blocking factor;
lsmeans Amp/pdiff adjust=tukey;
run;
title "pH";
proc glimmix data=RCBD plots=studentpanel;
class Lot Amp;
model pH = Amp;
random Lot; *** random blocking factor;
lsmeans Amp/pdiff adjust=tukey;
run;
title "Cond";
proc glimmix data=RCBD plots=studentpanel;
class Lot Amp;
model Cond = Amp;
random Lot; *** random blocking factor;
lsmeans Amp/pdiff adjust=tukey;
run;
title "Dia";
proc glimmix data=RCBD plots=studentpanel;
class Lot Amp;
model Dia = Amp;
random Lot; *** random blocking factor;
lsmeans Amp/pdiff adjust=tukey;
run;
title "Caion";
proc glimmix data=RCBD plots=studentpanel;
class Lot Amp;
model Caion = Amp;
random Lot; *** random blocking factor;
lsmeans Amp/pdiff adjust=tukey;
run;
title "HCT";
proc glimmix data=RCBD plots=studentpanel;
class Lot Amp;
model HCT = Amp;
random Lot; *** random blocking factor;
lsmeans Amp/pdiff adjust=tukey;
run;
title "Turbidity";
proc glimmix data=RCBD plots=studentpanel;
class Lot Amp;
model Turbidity = Amp;
random Lot; *** random blocking factor;
lsmeans Amp/pdiff adjust=tukey;
run;
title "FI";
proc glimmix data=RCBD plots=studentpanel;
class Lot Amp;
model FI = Amp;
```

```
random Lot; *** random blocking factor;
lsmeans Amp/pdiff adjust=tukey;
run;
title "HCTA";
proc glimmix data=RCBD plots=studentpanel;
class Lot Amp;
model HCTA = Amp;
random Lot; *** random blocking factor;
lsmeans Amp/pdiff adjust=tukey;
run;
title "HCTB";
proc glimmix data=RCBD plots=studentpanel;
class Lot Amp;
model HCTB = Amp;
random Lot; *** random blocking factor;
lsmeans Amp/pdiff adjust=tukey;
run;
title "HCTC";
proc glimmix data=RCBD plots=studentpanel;
class Lot Amp;
model HCTC = Amp;
random Lot; *** random blocking factor;
lsmeans Amp/pdiff adjust=tukey;
run;
```

For all experiments comparing control and bulk nanobubble incorporated samples (example viscosity)

```
data onet;
input Lot$ Type$ Viscosity;
datalines;

1 C 137.30
1 T 48.17
2 C 138.01
2 T 43.61

;
run;

proc print data=onet;
run;

proc glimmix data=onet;
* GLIMMIX for everything else;
class Type;
model Viscosity = Type/solution;
lsmeans Type/ pdiff adjust=tukey cl plot=meanplot(ascending cl);
output out=residuals residual=residual predicted=predicted;
run;
```

Permeation flux measurements

```
data storage;
input Lot trt $ Time Flux;
datalines;
1 C 10 9.19
1 C 20 9.11
1 C 30 8.84
1 C 40 8.73
1 C 50 8.66
1 C 60 8.53
1 T 10 14.05
1 T 20 13.46
1 T 30 13.26
1 T 40 13.25
1 T 50 12.74
1 T 60 12.61
2 C 10 9.08
2 C 20 9.05
2 C 30 8.81
2 C 40 8.67
2 C 50 8.56
2 C 60 8.40
2 T 10 14.31
2 T 20 13.78
2 T 30 13.40
2 T 40 13.38
2 T 50 13.06
2 T 60 12.91
3 C 10 9.34
3 C 20 9.17
3 C 30 9.00
3 C 40 8.82
3 C 50 8.77
3 C 60 8.58
3 T 10 14.14
3 T 20 13.52
3 T 30 13.35
3 T 40 13.12
3 T 50 12.91
3 T 60 12.75
;
proc print data=storage;
run;
proc mixed data=storage;
class trt time;
model Flux= trt time trt*time/ddfm= satterth;
lsmeans trt/pdiff adjust=bon;
lsmeans time/pdiff adjust=bon;
lsmeans trt*time/pdiff adjust=bon;
run;
```